

Martin Birkelund Pedersen

Assessing the Influence of Injection Temperature and Filter-Cake Build-Up on Fracture Development and Injectivity in High-Pressure Water Injection Wells:

A REVEAL simulation study

Master's thesis in Petroleum Engineering

Supervisor: Milan Stanko

June 2023

Martin Birkelund Pedersen

Assessing the Influence of Injection Temperature and Filter-Cake Build-Up on Fracture Development and Injectivity in High-Pressure Water Injection Wells:

A REVEAL simulation study

Master's thesis in Petroleum Engineering
Supervisor: Milan Stanko
June 2023

Norwegian University of Science and Technology
Faculty of Engineering
Department of Geoscience and Petroleum



Norwegian University of
Science and Technology

Abstract

This Master's thesis investigates the influence of varying injection temperatures and filter-cake accumulation on high-pressure water injectors at the Ivar Aasen field, focusing on fracture initiation, propagation, and their subsequent impact on injectivity. Collaborating with Aker BP, sector models were created using the IPM-based REVEAL 10 software, and simulations were conducted on the sector model that closely represented historical injection data at average injection temperatures. The primary injection wells considered were D-1, D-2, D-3, and D-5, with D-3 being selected as the candidate for further study.

To address complications with fracture calculations in REVEAL 10 caused by issues regarding wellhead pressure constraints and inactive cells near completions, the D-3 sector model underwent modifications, including a new schedule with fixed historical wellhead pressure. This allowed for more reliable simulations and was employed in the main temperature sensitivity study. The study encompassed two types of injection schedules: with and without pre-existing fractures. The goal was to examine the effects of injection temperature, pressure, and filter-cake buildup on fracture development and injectivity.

Key findings include a non-linear relationship between injection temperature and fracture size, indicating that sensitivity analysis may not yield linear output responses due to the complex nature of fracture calculations and real-life phenomena in highly heterogeneous reservoirs. A simple thermal fracture model demonstrated a linear relationship between fracture area, leak-off coefficient, and center width at different bottomhole temperatures, showcasing the impact of lower temperatures on viscosity, leak-off, in-situ fracture pressures, and resulting fracture sizes in a homogeneous reservoir. The effect of thermo-elastic stress reduction on fracture initiation was found to be time-dependent and dependent on operational conditions, with warmer injection temperatures leading to earlier fracture initiation when the water injection is conducted within a relatively short timeframe at a pore-pressure that exceeds the minimum in-situ stress.

Colder injection temperatures resulted in larger fracture areas for scenarios without pre-existing fractures, while warmer injection temperatures led to higher cumulative water injection and lower final injectivity index. The relationship between fracturing and injectivity at different injection temperatures was identified as case-dependent, influenced by injection pressure and temperature control. Short periods of seawater injection proved favorable for fracture development and injectivity index for cases without pre-existing fractures, while the opposite was observed for cases with pre-existing fractures. If a period of high pressure water injection and intentional fracturing is needed for the D-3 well, utilizing "warm" produced water for pressurization will therefore result in a more extensive fracture propagation and a higher final injectivity index.

The simulation results using a filter-cake model emphasized the importance of fracture development in maintaining injectivity in the Skagerak 2 formation. Periodic fracture propagation and temporary increases in injectivity were possible with the presence of fractures, countering the decline in injectivity caused by pore plugging. The study also highlighted the significance of filter-cake build-up and its cyclic occurrence, recommending the use of seawater injection to reduce suspended solids and associated filter-cake accumulation. Recommendations for further work include modeling the influence of oil in injected water and the effect of injection temperature on wettability in REVEAL, using the developed sector models. A study examining the pressure drop across the completion perforations for injection well D-3 is also recommended, to verify the influence of water viscosity on perforation pressure drop and fracture propagation.

Sammendrag

Denne masteroppgaven undersøker innvirkningen av varierende injeksjonstemperaturer og opphopning av filterkake på høytrykksvanninjektorer på Ivar Aasen-feltet, med fokus på sprekkeinitiering, sprekkeutvikling og deres påfølgende innvirkning på injektivitet. I samarbeid med Aker BP ble sektormodeller opprettet ved hjelp av IPM-basert REVEAL 10 programvare, og simuleringer ble utført på sektormodellen som representerte historiske injeksjonsdata ved gjennomsnittlige injeksjonstemperaturer. De primære injeksjonsbrønnene som ble vurdert, var D-1, D-2, D-3 og D-5, der D-3 ble valgt som kandidat for videre studier.

For å håndtere komplikasjoner med sprekkeberegninger i REVEAL 10, forårsaket av problemer knyttet til begrensninger i brønntopstrykk og inaktive celler nær kompletteringene, ble D-3 sektormodellen modifisert, inkludert en ny plan med fastsatt historisk brønntopstrykk. Dette muliggjorde mer pålitelige simuleringer og ble brukt i hovedstudien om temperaturfølsomhet. Studien omfattet to typer injeksjonsplaner: med og uten eksisterende sprekker. Målet var å undersøke effekten av injeksjonstemperatur, trykk og filterkakeoppbygging på sprekkeutvikling og injektivitet.

Viktige funn inkluderer en ikke-lineær sammenheng mellom injeksjonstemperatur og sprekkestørrelse, noe som indikerer at sensitivitetsanalyse ikke nødvendigvis vil gi lineære resultater på grunn av kompleksiteten i sprekkeberegninger og virkelighetsfenomener i sterkt heterogene reservoarer. En enkel termisk sprekke-modell viste en lineær sammenheng mellom sprekkeområde, lekkasje-koeffisient og sentral bredde ved forskjellige bunnhullstemperaturer, noe som viser betydningen av lavere temperaturer for viskositet, lekkasje, in situ sprekke-trykk og resulterende sprekkestørrelser i et homogent reservoar. Effekten av reduksjon av termoelastisk spenningspåkjenning på sprekkeinitiering viste seg å være tidavhengig og avhengig av operative forhold, der varmere injeksjonstemperaturer førte til tidligere sprekkeinitiering når vanninjeksjonen utføres innenfor en relativt kort tidsramme ved poretrykk som overstiger minimums-in situ-spenningsnivå.

Kaldere injeksjonstemperaturer resulterte i større sprekkeområder for scenarier uten eksisterende sprekker, mens varmere injeksjonstemperaturer førte til høyere kumulativ vanninjeksjon og lavere endelig injektivitetsindeks. Sammenhengen mellom sprekking og injektivitet ved ulike injeksjonstemperaturer ble identifisert som avhengig av scenariet og påvirket av injeksjonstrykk og temperaturkontroll. Korte perioder med sjøvannsinjeksjon viste seg å være gunstig for sprekkeutvikling og injektivitetsindeks for scenarier uten eksisterende sprekker, mens det motsatte ble observert for scenarier med eksisterende sprekker. Hvis det er behov for en periode med høytrykksvanninjeksjon og bevisst sprekking i brønn D-3, vil bruk av ”varmt” produsert vann for trykksetting resultere i en mer omfattende sprekkeutvikling og høyere endelig injektivitetsindeks.

Simuleringsresultatene ved bruk av en filterkakemodell understreket betydningen av sprekkeutvikling for å opprettholde injektivitet i Skagerak 2-formasjonen. Periodisk sprekkeutvikling og midlertidige økninger i injektivitet var mulig med tilstedeværelse av sprekker, noe som motvirket nedgangen i injektivitet forårsaket av poretilstopping. Studien påpekte også betydningen av filterkakeoppbygging og dens sykliske forekomst, og anbefalte bruk av sjøvannsinjeksjon for å redusere suspenderte partikler og den tilhørende oppbyggingen av filterkake. Anbefalinger for videre arbeid inkluderer modellering av påvirkningen av olje i injisert vann og effekten av injeksjonstemperatur på våthet i REVEAL ved hjelp av de utviklede sektormodellene. Det anbefales også en studie som undersøker trykkfallet over kompletteringsperforasjonene for injeksjonsbrønn D-3.

Acknowledgement

This thesis has been completed as part of the course, TPG4920 - Petroleum Engineering, Master Thesis.

I would like to express my gratitude to my supervisor, Milan Stanko. I would also like to express my sincere appreciation to Aker BP for granting me the opportunity to undertake this study on their behalf. I am thankful to the individuals at Aker BP who offered valuable insights and guidance during the course of this work. Lastly, I extend my gratitude to Steve Todman at Petroleum Experts for his assistance and support.

Table of Contents

1	Introduction	1
2	Background and motivation	2
2.1	Thesis objectives	2
2.2	Overview of the thesis structure	3
3	Previous work	3
4	The Ivar Aasen field	4
4.1	Overview of the Ivar Aasen field	4
4.2	Geology and reservoir quality	5
4.3	Production and injection history	6
5	Water injection	9
5.1	Description of water injection and its purpose in reservoir management . . .	9
5.2	Factors influencing injectivity	10
5.3	Impact of fracturing on injectivity	12
6	Hydraulic fracturing	13
6.1	Definition of hydraulic fracturing	13
6.2	Rock mechanical properties	14
6.3	In-situ stresses	15
6.4	Fracture initiation and propagation	17
6.5	Poro- and thermoelastic coefficient	18
6.6	Effect of injection temperature on fracturing	19
6.7	Effect of filter-cake build-up on fracturing	21
7	REVEAL	22
7.1	Introduction to REVEAL	22
7.2	The finite-element thermal fracture model in Reveal	22
7.2.1	Iterative Fracture Calculation Process	24
7.3	Filter-cake model	26
7.4	Perforation pressure drop	26

7.5	Inactive zones	27
8	Simulation study	28
8.1	Sector modelling	28
8.2	Fullfield model	28
8.3	Methodology for creating the sector models	29
8.4	Overview of simulation scenarios	36
8.5	Assumptions	37
8.6	Input data	38
8.7	Constraint violation and inactive cells	39
9	Results and analysis	41
9.1	Thermo-elastic stress reduction potential	41
9.1.1	Manual calculation	41
9.2	Effect of injection temperature variation on historical fracture development	43
9.2.1	S1	43
9.3	Effect of injection temperature variation on fracture development - Simple thermal fracture model	47
9.3.1	S2	47
9.4	Effect of injection temperature variation on fracture development and injectivity index	48
9.4.1	S3	48
9.4.2	S4	51
9.5	The effect of injection temperature variation on fracture development during short intentional fracturing period, comparing pre-existing fracture and no pre-existing fracture scenarios	53
9.5.1	S5	53
9.5.2	S6	57
9.5.3	S7	58
9.6	The effect of filter-cake build up on fracture development and injectivity . .	60
9.6.1	S8	60
10	Conclusion	63
11	Further work	64

Bibliography	65
Appendix	68
A CPI-log for injection well D-3 (Skagerak 2 formation)	68
B Sector model - Guide	69
C 3D visualisation of sector models	72
D Water viscosity	76
E Simple thermal fracture model	77
F Formulas/input data for thermo-elastic stress reduction calculation	78

List of Figures

1	Ivar Aasen location map and infrastructure. Location map (left) and infrastructure (right) [4].	4
2	Overview of chrono/lithostratigraphy, grain size, depositional environment, connectivity and reservoir quality for the different reservoir zones at the Ivar Aasen field [5].	5
3	Production trends for oil rate, water-cut and gas-oil ratio [5].	6
4	Daily injection temperature data from prod. start-up to present day [5]. . .	7
5	4D pressure effects from injectors during the period 2013-2021 [5].	8
6	Schematic for improved sweep of low permeability zone due to skin, induced by injectivity of low quality water, in a two-permeability-zone reservoir [13].	11
7	Images of imbibition rate of water in tight cores: (a) Core without fractures, (b) core with fractures [17].	13
8	Hooke's law: Stress-strain relationship [18]	14
9	Effect of wellbore direction on hydraulic fractures propagation. Well A: Longitudinal fracture, Well B: Transverse fracture [22]	16
10	Total fracture surface area, showing a 20 % higher value for Case 1 than for the base case [30].	20
11	Diagram of relationships in REVEAL thermal fracture model [37].	23
12	3D visualisation of the the Ivar Aasen field REVEAL model (x4 Z-scaling).	29
13	Injection well D-1: BHP for updated full-field model in REVEAL 10 (Blue) and "original" full-field model in Reveal 9.5 (Red).	30
14	3D visualisation of the near well-bore cross section for injection well D-1. . .	31
15	3D visualisation of the near well-bore cross section for injection well D-3. . .	31
16	Bottom-hole pressure (BHP) and liquid rate at 90 and 9.5 °C, from PROSPER lift-curve (VLP).	32
17	Bottom-hole temperate (BHT) and liquid rate at 10 different injection temperatures, from PROSPER lift-curve (VLP).	33
18	Injection well D-3: BHP for the time varying BC sector model (blue) and original full-field model in REVEAL 9.5 (red).	34
19	Injection well D-3: Injection rate for the fixed WHP/constant-BC sector model (blue) and historical injection rate (red).	35
20	Numerical instability for injection well D-1 (BHP).	40
21	Thermo-elastic stress reduction at different injection temperatures for D3 formation - Graph.	42
22	S1: BHP and fracture size for the average injection temperature.	44

23	S1: 3D visualisation of final fracture size and thermo-elastic stress reduction.	44
24	S1: Fracture area at different injection temperatures, for fracture seed 1, 4 and 5.	45
25	S1: Fracture area for fracture seed 1, and historical schedule.	46
26	S2: Fracture area, maximum leak-off coefficient and center width at different bottomhole temperatures - Simple thermal fracture model.	47
27	S3: BHP and injectivity index for initial injection temperature = 8,48 and 90 °C	49
28	S3: Fracture area for initial injection temperature = 8, 48 and 90 °C (fracture seed 1)	50
29	S3: Cell pressure (38.66.64) at initial injection temperature = 8 and 90 °C .	50
30	S4: Injectivity index for initial injection temperature = 8,48 and 90 °C . . .	52
31	S4: Fracture area for initial injection temperature = 8, 48 and 90 °C (fracture seed 1)	52
32	S5: BHP and BHT for simulation run with historical schedule, and prediction run with short high pressure injection period	54
33	S5: Total fracture area, final injectivity index and pre-existing fracture area for simulation runs with initial injection temperature = 8, 30, 48 and 90 °C	55
34	S5: Tubing pressures, reservoir pressure and water injection rate - initial injection temperature = 8 °C	55
35	S5: Tubing pressures, reservoir pressure and water injection rate - initial injection temperature = 90 °C	56
36	S6: Fracture area for initial injection temperature = 8 and 90 °C (fracture seed 1 and 5)	57
37	S7: Fracture area for initial injection temperature = 8, 48 and 90 °C (fracture seed 1)	58
38	S7: Injectivity index for initial injection temperature = 8, 48 and 90 °C . .	59
39	S8: Injectivity index for simulation run with filter-cake model - with/without fracture calculation, and fracture area (fracture seed 4)	61
40	S8: Water injected [Sm ³ /day] for injection temperature of 48 °C, 48 + 2.5°C/0.5year, and 48 + 5 °C/0.5 year	61
41	Sector model for injection well D-1, constant pressure BC.	72
42	Sector model for injection well D-1, time-varying BC.	72
43	Sector model for injection well D-2, constant pressure BC.	73
44	Sector model for injection well D-2, time-varying BC.	73
45	Sector model for injection well D-3, constant pressure BC.	74

46	Sector model for injection well D-3, time-varying BC.	74
47	Sector model for injection well D-5, constant pressure BC.	75
48	Sector model for injection well D-5, time-varying BC.	75
49	Water viscosity as a function of temperaute, from thermal PVT table. . . .	76
50	Simple thermal fracture model.	77
51	Cross-section simple thermal fracture model.	77

List of Tables

1	Stress properties - Skagerak 2 formation.	38
2	Fracture seed status and default values.	38
3	Completion perforation input data.	38
4	Thermo-elastic stress reduction at different injection temperatures for D3 formation - Table.	41
5	S3: Initiation status, total fracture area, cumulative water injected and final injectivity index for initial injection temperature = 8, 48 and 90 °C	49

1 Introduction

This Master's thesis results from a collaborative effort with Aker BP. The primary focus of the thesis was to assess the influence of varying injection temperatures and filter-cake accumulation on high-pressure water injectors at the Ivar Aasen field, with a specific emphasis on fracture initiation and propagation and the subsequent effect on injectivity. Sector models were created utilizing the IPM-based REVEAL 10 software, and simulations were run on the sector model with the most accurate representation of historical injection data using the average injection temperature. The full-field model was developed based on a previous Reveal study on water injection at the Ivar Aasen field. The high-pressure injection wells at the Ivar Aasen field are injection well D-1, D-2, D-3, and D5.

After developing the sector models, injection well D-3 was selected as the best candidate for this study. Unlike the other injection wells, the reservoir grid contained no inactive cells near the completions. These no-flow zones were demonstrated in the bottom-hole pressure matching process to create difficulties with fracture calculations in REVEAL 10 due to an issue with the wellhead pressure constraints used in the historical schedule. Due to this issue, the D-3 sector model was modified with a new schedule where a fixed historical wellhead pressure was used to control the injection. The modified schedule allowed for more reliable simulations, and was used for the main temperature sensitivity study. The fixed rate schedule, from the full-field model, was used in the first initial temperature study.

The first initial temperature sensitivity study was performed with five different injection temperatures ranging from 90 °C to 8 °C. The study investigated how this temperature range would affect the historic injection and fracture dimensions. The second initial study was performed on a simple thermal fracture model, developed with approximately the same reservoir depth and rock stress properties used for the sector model. This simple model was given a constant permeability throughout the different cells and was controlled with a constant wellhead pressure. This approach was used to better understand how fracture calculations are affected by constant input data in a homogeneous reservoir, compared to the first initial study, which consists of a heterogeneous reservoir that experiences rapid changes in injection rate and pressure.

The main temperature sensitivity study was performed by creating different simulation scenarios, controlling the injection well at different constant fixed wellhead pressures, using a range of temperatures between 90 °C and 8 °C. The simulations were performed based on two different types of injection schedules: with and without pre-existing fractures. The scenarios with no pre-existing fractures were given a schedule starting at the initial reservoir conditions. The scenarios with pre-existing fractures were scheduled in prediction mode, using the last WHP value at 01.12.2022, and the fracture dimensions developed from the history-matched run at the average injection temperature of 48 °C. The scenarios were developed to compare the influence of injection temperature at different operational conditions and different fracturing stages. The goal was to investigate how the change in pressure, temperature, and water quality affects fracture development and injectivity. A more detailed explanation of the different simulation runs is given in chapter [8].

This report encompasses the findings of the Reveal simulations, accompanied by an evaluation of their practical significance and a review of relevant theory concerning water injection and fracturing. Ultimately, conclusions are drawn based on these findings, and recommendations for further work are provided.

2 Background and motivation

The Ivar Aasen field employs pressure maintenance via fracture injection as its primary drainage strategy. It utilizes water injection at a pressure exceeding the minimum horizontal stress at the base caprock. Verifying safe injection with regards to out-of-zone injection is, therefore, a continuous task. In relation to this, the creation of sector models for injection wells is a point of interest for Aker BP, as it allows for quicker analysis of the injectors based on changes in the reservoir or operating conditions.

A noticeable change in operating conditions at the Ivar Aasen field is the slowly increasing temperature of the produced water that gets re-injected into the reservoir due to the increased water cut. There will be a time in the future when the cooling of the re-injected water by seawater gets limited due to a finite capacity on the topside process facilities. As the topside equipment processing produced water has a maximum operating temperature of 90 °C, there may be a need for installing a heat exchanger to reduce the temperature in the future. This makes the analysis on how "cold" and "warm" injection temperature affects the fracture development and the efficiency of the water injection another point of interest for Aker BP. An increase in re-injected produced water will also increase the concentration of solid particles. How this will affect injection, together with the increased injection temperature, is also of interest. Further analysis will create more knowledge on the topic to better assist in how they should run the injectors. An insight into the REVEAL software and fracture development at different operating conditions will provide Aker BP with helpful knowledge and enable them to simulate different scenarios and devise optimal strategies for injection control at the Ivar Aasen field. As a part of intentional fracturing to increase injectivity, as performed twice earlier for the D-3 injection well, a temperature sensitivity study will give an insight into what injection temperature to apply for optimal fracturing/injection. The study will also look at the effect of short periods of cold water injection (seawater) and the effect of filter-cake build up.

2.1 Thesis objectives

- Procure knowledge on the REVEAL software, and create injection sector models based on the full-field model of Ivar Aasen.
- Investigate the effect of injection temperature on fracture development and injectivity at different operating conditions and scenarios.
- Evaluate the impact of increasing injection temperature and filter-cake build-up on fracturing and injectivity.
- Give a recommendation on future injection strategy, for optimal water injection.
- Ensuring safe injection with regards to out-of-zone fracturing and injection.

2.2 Overview of the thesis structure

This Master's thesis is structured to provide a brief introduction to the Ivar Aasen field. Following this, the thesis presents a literature study that reviews relevant theories on water injection, fracture initiation and propagation, and previous studies related to the thesis topic. Subsequently, a chapter explains the numerical fracture calculation in Reveal and its finite-element thermal fracture model. Another chapter describes the simulation study performed in Reveal, including the methodology used to create the sector models and the different simulation runs with their respective objectives. Finally, the thesis presents the results of the simulation studies, followed by an analysis and discussion that compares the findings with the literature study. The conclusion summarizes the main contributions of the thesis.

As a comment on the figures in the thesis, small text may occur in some of them. However, the resolution of the pictures is high enough for the reader to zoom in and see the details more clearly.

3 Previous work

In order to provide a comprehensive understanding of the subject matter explored in this master thesis, it is essential to note that a related investigation was conducted in a related specialization report titled 'Investigating Out-of-Zone Injection and Hydraulic Fracturing in Overburden Shale Formation: A Reveal Study', where the potential for out-of-zone injection caused by a leak in the 13 3/8" casing shoe was thoroughly examined [1]. The study's primary objective was to assess the integrity of the secondary formation exposed to injection pressure by investigating the fracturing process and determining the extent of out-of-zone injection [1].

The report provided an overview of the background and significance of out-of-zone injection and an introduction to the Reveal software tool utilized for modeling and analyzing the potential leakage. Additionally, it investigated various aspects of fracture mechanics and their correlation to the modeling of hydraulic fractures [1].

The key findings of the report revolved around the REVEAL sector model, which was constructed based on the full-field REVEAL model of the Ivar Aasen field, used to create sector models in this thesis. Through simulations conducted under pessimistic and optimistic scenarios following casing shoe leakage, the study demonstrated a low risk of out-of-zone injection reaching the surface in situations where hydraulic fractures developed. It was determined that a highly permeable overburden formation called Heimdal effectively prevented fracture initiation and propagation by reducing pressure in the annulus. Based on these findings, it was concluded that there was no need for counteractive measures to prevent overburden fracture development. The report also highlighted the importance of parameters such as the degree of leakage at the casing shoe, shale permeability, and the reaction time from the discovery of the leakage to well shut-in, as they significantly influenced hydraulic fracture initiation and propagation in the overburden shale formation. The correlation between fracture dimensions and Young's modulus/Poisson's ratio was also investigated through sensitivity analysis [1].

Considering the relevance of the specialization report to the current research, it is recommended that interested readers refer to the report for further insights into the investigation of out-of-zone injection in Reveal.

4 The Ivar Aasen field

4.1 Overview of the Ivar Aasen field

Ivar Aasen is a oil field discovered in 2008 and is located at the Utsira Height at block 16/1, in the northern part of the North sea. The field is about 7 X 7 km in size and has a estimated oil reserve of 200 million barrels, and started production on December 24th, 2016 [2]. The development of the field was coordinated with the development of the Edvard Gried Field, located ten kilometers southeast from Ivar Aasen. The wellstream undergoes first stage processing carried out on the Ivar Aasen platform, before being transported to the Edvard Gried for further processing[3]. Since production start up, additional producers and injectors have been drilled. As per 2023, the field consists of 12 production wells, and 8 injection wells giving the field a current average daily production 4500 Sm³/d of oil, and 2000 Sm³/day of gas. The daily production is on the Ivar Aasen platform is controlled by a onshore control room located in Trondheim, as the first field to do so on the Norwegian continental shelf. Future plans for the Ivar Aasen platform is to increase total production by having the Hanz and Lille Prinsen field to be tied-back to Ivar Aasen[2]. Ivar Aasen field installation, platform and pipelines are found in Figure [1].

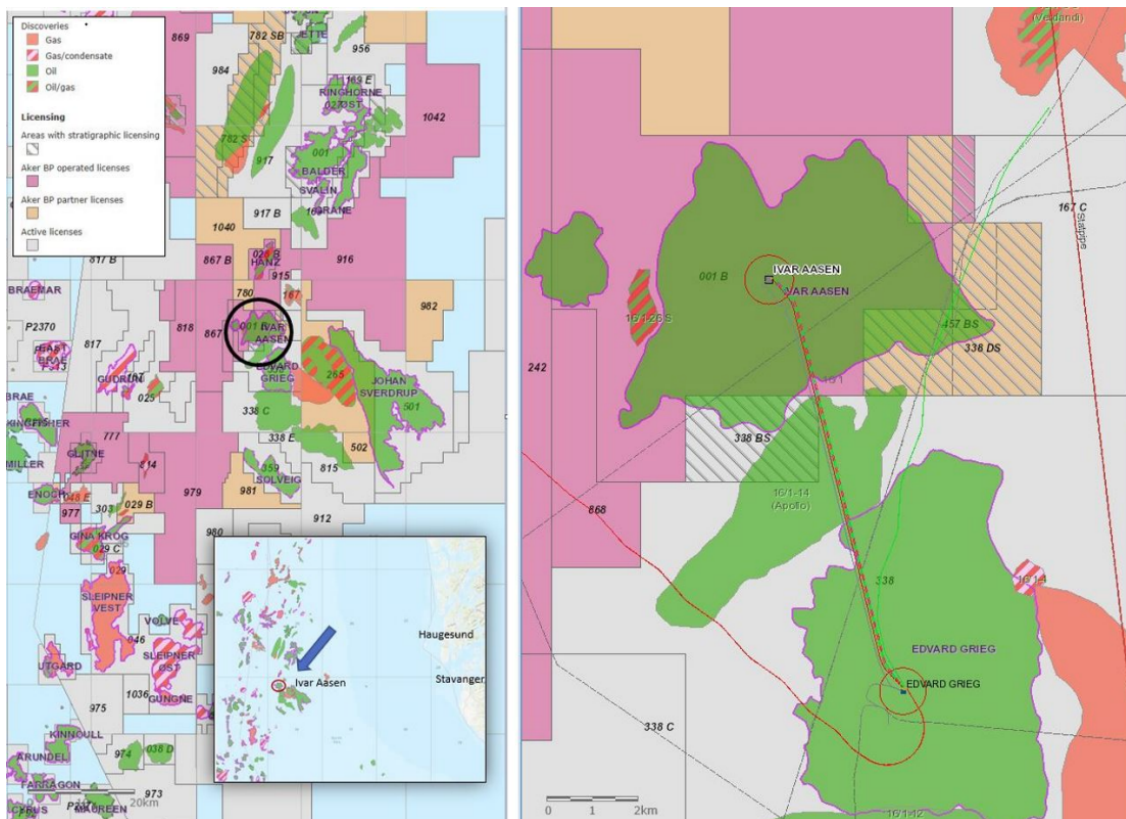


Figure 1: Ivar Aasen location map and infrastructure. Location map (left) and infrastructure (right) [4].

4.2 Geology and reservoir quality

The Ivar Aasen reservoir comprises fluvial sandstone from the Late Triassic and Middle Jurassic period. It exhibits a high degree of faulting and encompasses formations with diverse reservoir quality, resulting in a heterogeneous and complex geological system. The horizontal stresses in the formation exhibit a relatively equal magnitude, leading to the assumption of isotropic horizontal stress conditions. The stress state is determined to be a normal fault environment based on the minimum, maximum, and vertical stress magnitudes. As a result, fractures are expected to be vertical [5].

The field's high complexity and the uncertainty associated with geological interpretations present significant challenges in modeling the reservoir behavior. Figure [2] shows the reservoir quality for the different reservoir layers. The injection target is located in the challenging Skagerak 2 formation [4]. A snapshot of the CPI (Computer Processed Interpretation) for the Skagerak 2 formation for the D-3 injection well is given in Appendix [A], which illustrates the challenge related to injection with regards to the degree of permeability heterogeneity [5].

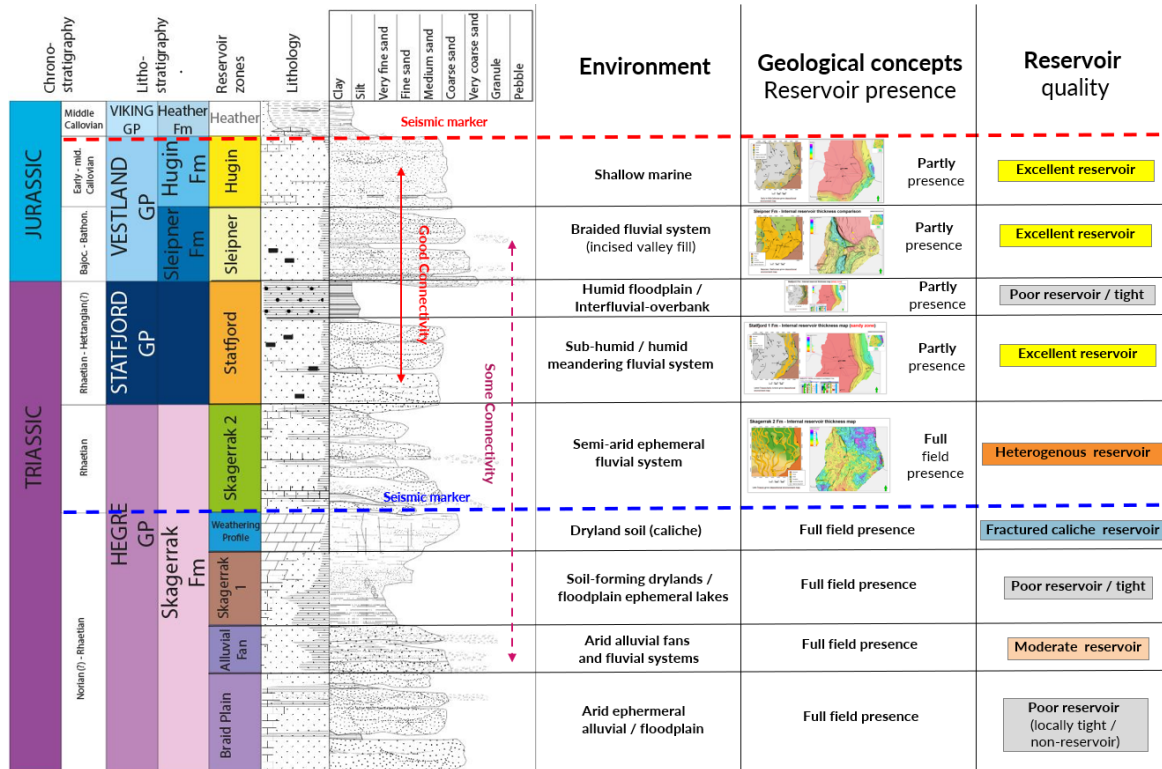


Figure 2: Overview of chrono/lithostratigraphy, grain size, depositional environment, connectivity and reservoir quality for the different reservoir zones at the Ivar Aasen field [5].

4.3 Production and injection history

The production strategy at Ivar Aasen relies on pressure depletion with water injection to maintain reservoir pressure. Gas lift is also employed in all production wells to prevent liquid loading. Figure [3] illustrates the production trends, including total oil rate, water-cut, and gas-oil ratio, from the initial production phase to the present. The graphs indicate that the plateau production phase has concluded, and the overall production is experiencing a rapid decline. As the reservoir pressure has decreased, there has been a gradual increase in the gas-oil ratio. Furthermore, water breakthrough has occurred, leading to a progressive rise in the water cut within the well stream. The presence of water tracers in most producers confirms the reason behind the increase in water-cut, attributing it to water breakthroughs.

To counteract the decline in production, several campaigns focused on increased oil recovery (IOR) has been undertaken, involving the drilling of new production and injection wells. Hybrid injection wells have recently been drilled and integrated into production before transitioning to the injection phase.

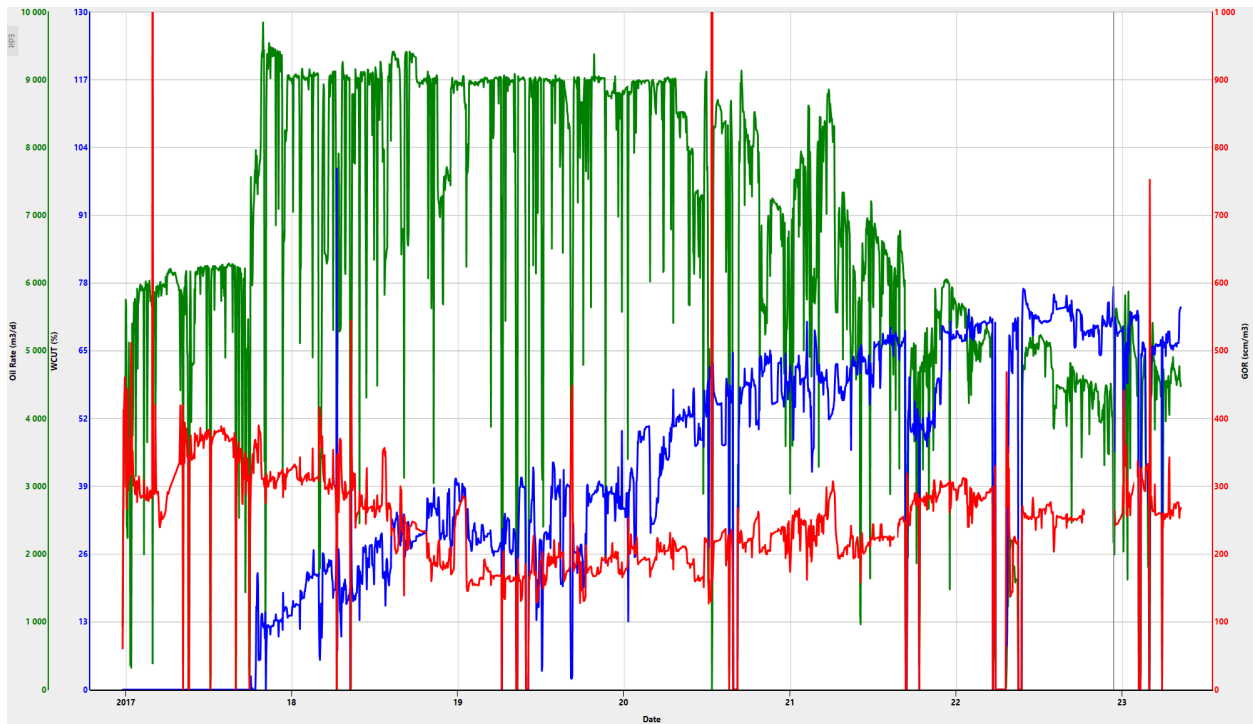


Figure 3: Production trends for oil rate, water-cut and gas-oil ratio [5].

The water injected into the reservoir for pressure support, consists of a mix between "warm" produced water and "cold" seawater. The temperature of injection water is therefore proportional to the temperature of produced water, if seawater is assumed to be constant.

To address the rising water production and the associated increase on injection temperature, various measures have been implemented, including the selective plugging of oil producing wells exposed to areas high water content and periodic shut-in of oil wells that produce excessive amounts of water. These actions have had a noticeable impact on stabilizing the increase in total water-cut during the later stages of production.

The overall trend of water-cut and injection temperature is increasing, and is expected to do so in the future. As the process facilities has a limited capacity, the volume of seawater injected subsequent cooling of produced water needs to be reduced, contributing to the injection temperature increase. This will also contribute to a increase in solids particles and oil residue being re-injected into the reservoir, resulting in a higher rate of filter-cake build up.

Figure [4] illustrates the daily average injection temperature data on the mixture of produced water and seawater, measured downstream the injection pump at Ivar Aasen between the start of production until present day.

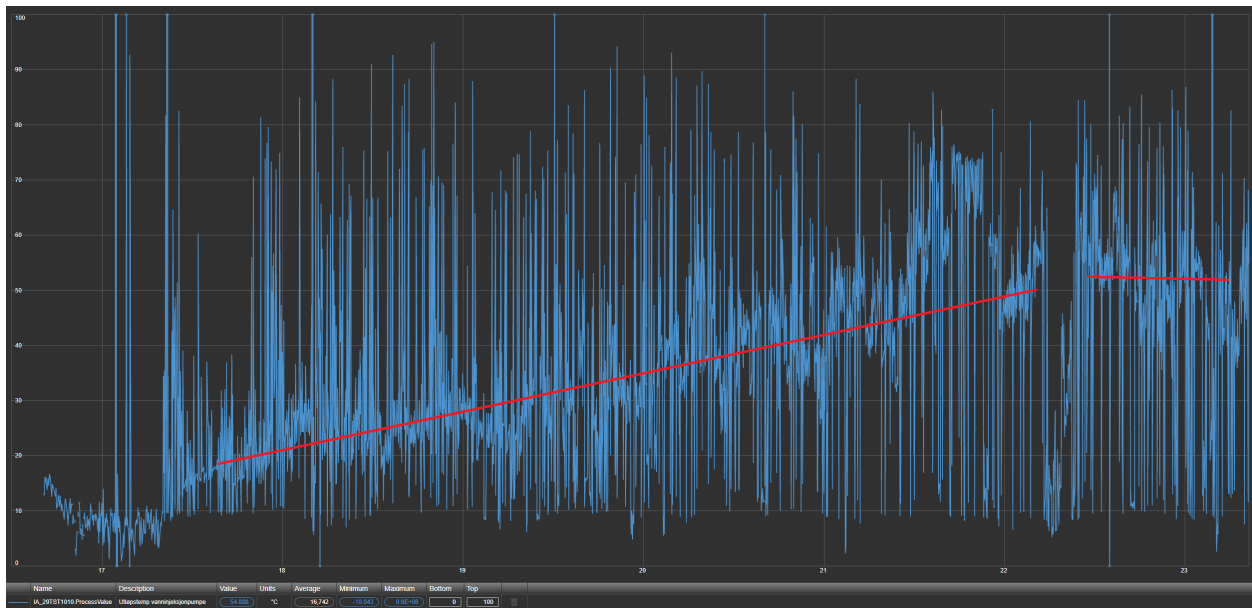


Figure 4: Daily injection temperature data from prod. start-up to present day [5].

Figure [5] shows the effect on pressure support from the injectors between period 2013-2021. This 4D data plays a important role in the Reveal modeling of injector sector models, aiding in the determination on placement of surrounding boundary blocks.

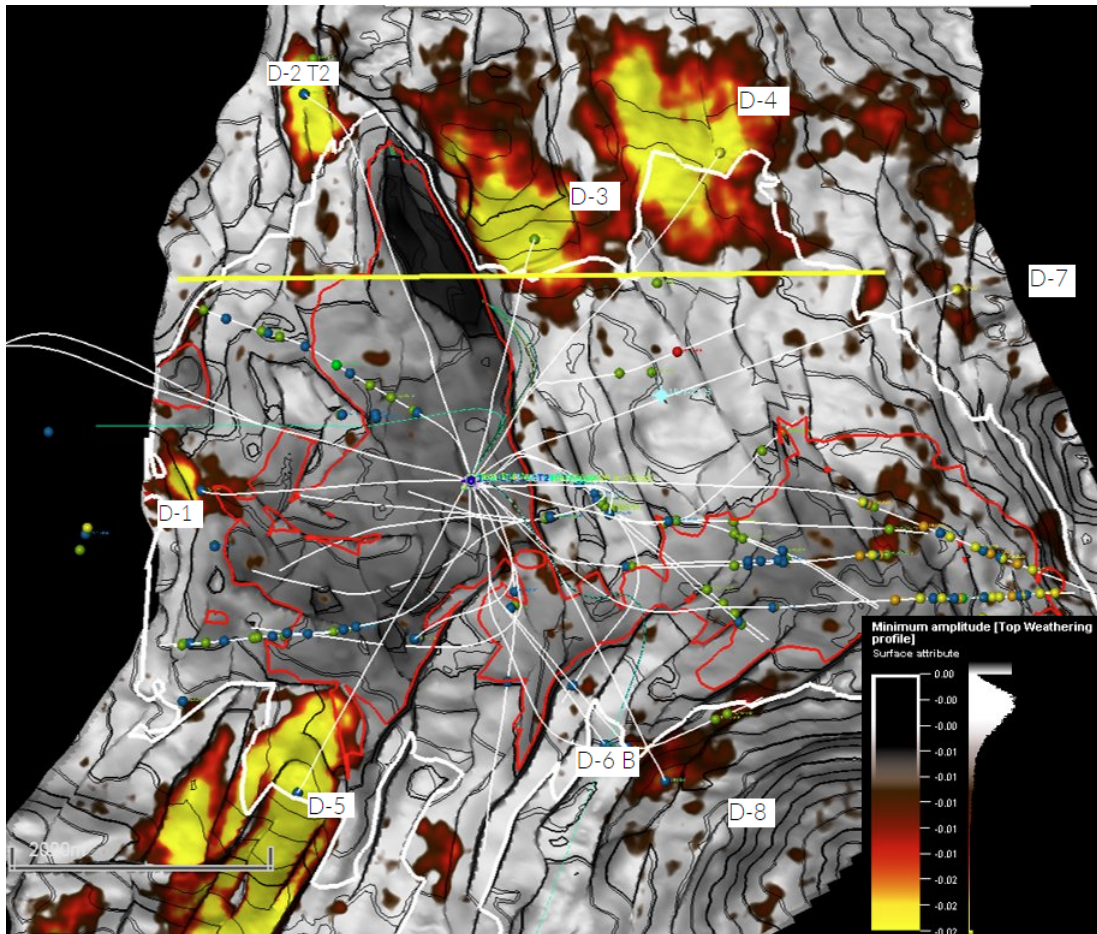


Figure 5: 4D pressure effects from injectors during the period 2013-2021 [5].

5 Water injection

5.1 Description of water injection and its purpose in reservoir management

During oil and gas production from hydrocarbon fields, it is common to encounter formation water. Over time, the volume of produced water increases as the reservoir's pressure declines. Managing this formation water becomes a concern due to environmental considerations and government regulations regarding its disposal. After undergoing topside processing, the produced formation water holds no commercial value except for its potential to be re-injected into the reservoir for pressure maintenance and water displacement. This cost-effective approach and its economic benefits make water re-injection one of the most widely used techniques for enhancing oil recovery [6].

Produced water is most often for offshore fields mixed with seawater for injection. Mixing seawater with formation water during injection is a practical solution to ensure an adequate water supply, optimize reservoir conditions, and enhance oil recovery efforts. Seawater has no concentration of oil droplets and a considerably lower amount of suspended solid particles compared to produced water, which can affect the fluid interaction with the reservoir rock and potentially improve oil recovery efficiency.

The general expression for the ultimate oil recovery factor for a field utilizing water injection is given in equation (1). This term consists of the product of displacement efficiency, areal sweep efficiency, and vertical sweep efficiency. Displacement efficiency (E_D) is the fraction of movable oil displaced from the swept zone at any given time or pore volume injected. Areal sweep efficiency (E_A) accounts for the coverage of the reservoir area by the injected water, while vertical sweep efficiency (E_V) considers the efficiency of water movement throughout the reservoir volume. The principal factors determining these sweep efficiencies include the water-flood pattern, reservoir heterogeneity, oil-water mobility ratio, injection pattern, and injected water volume[7].

$$RF = E_D E_A E_V \quad (1)$$

Oil-water mobility plays an important role in water injection and sweep efficiencies. The mobility ratio is in turn, dependent on rock/fluid properties as relative permeability and fluid viscosity [8]. The relative permeability (k_r) represents the ability of the rock formation to transmit fluid flow, while viscosity (μ) characterizes the resistance to flow. The water-oil mobility ratio is defined as the mobility of the displacing fluid (λ_D) behind the displacement front divided by the mobility of the displacing fluid (λ_d) ahead of the front, where the mobility ratio greater than 1 is considered to be unfavorably compared to a ratio less than 1. A formula for the mobility ratio of water to oil in water displacement is shown in equation (2) [9].

$$M_{w,o} = \frac{(\lambda_w)_{sor}}{(\lambda_o)_{swc}} = \frac{k_{rw}/\mu_w}{k_{ro}/\mu_o} \quad (2)$$

A high oil-water mobility ratio can cause poor displacement and sweep efficiency leading to an early breakthrough of injected water in the producers. Enhanced oil recovery (EOR) methods are designed to decrease this value, thus delaying water breakthrough and increasing sweep efficiency. Examples of EOR methods are polymer solutions to in-

crease injection water viscosity and thermal methods by increasing injection temperature and reducing oil viscosity. In addition to reducing viscosity, an increase in temperature also affects the interaction between the fluid and the rock formation, specifically the relative permeability. The relative permeability is influenced by wettability, which can be transitioned to a more favorable water-wet state by reducing the interfacial tension (IFT). This reduces oil adhesion to the rock surfaces and enhances water displacement of the oil phase [10].

In a study on the temperature effect on heavy-oil recovery by imbibition in fractured reservoirs, Tayfun Babadagli (1996) investigated the effects of temperature on the efficiency of the capillary imbibition mechanism. The study concluded that the increase in temperature resulted in a decrease in oil viscosity and interfacial tension between oil and brine. The reduction in oil viscosity was the significant factor increasing the capillary imbibition rate. The IFT reduction had a smaller but observable influence. The reduction of residual oil, was however contributed to the IFT reduction [11].

5.2 Factors influencing injectivity

Injectivity is defined as the ratio of the injection rate divided by the pressure difference between formation pressure and bottom-hole pressure, as shown in equation (3) [12]. While sweep efficiencies refer to the effectiveness of fluid displacement in the reservoir, the closely linked injectivity term refers to a well's ability to inject fluids at a desired rate without experiencing excessive pressure build-up. It is a measure of the capability of a well to inject fluids into a porous and permeable formation.

$$J = \frac{q}{(P_{BH} - P_f)} \quad (3)$$

The relationship between the two terms can be explained by discussing the reservoir physics of the interaction between injectivity and water displacement. Considering a horizontal injector and producer in a heterogeneous reservoir, low injectivity may benefit the ultimate oil recovery before water break-through. This is the case when water with a high concentration of solid particles induces formation damage in the form of filter-cake build-up, increasing sweep efficiency and reducing the amount of water injected. Several EOR methods are based on this scenario by inducing formation damage by plugging swept areas and redirecting the injected water into unswept areas. Figure [6] shows a schematic of a reservoir with a high and low permeable zone, with two horizontal wells. The main portion of the injected water passes via the well sections in the highly permeable zone, creating resistance to the flow of water. This delays the waterfront and increases the sweep efficiency [13].

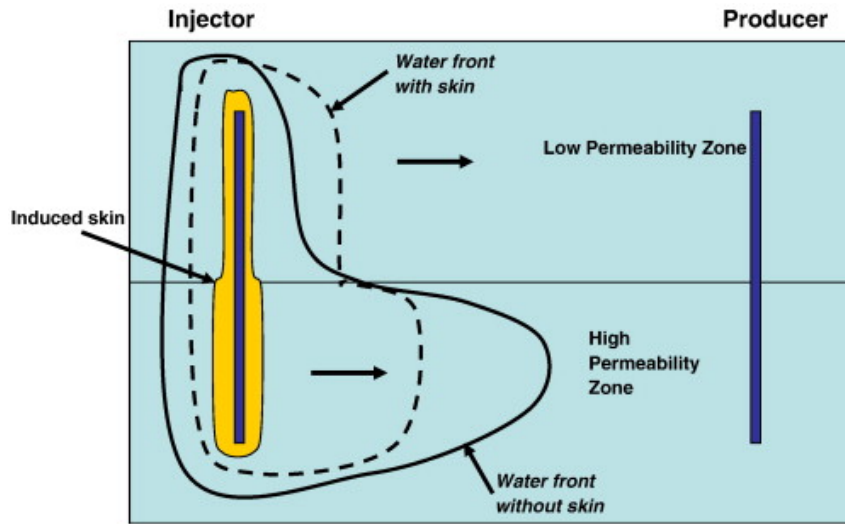


Figure 6: Schematic for improved sweep of low permeability zone due to skin, induced by injectivity of low quality water, in a two-permeability-zone reservoir [13].

High injectivity is, however, generally beneficial after water breakthrough to ensure the sufficient injection of volumes for maintaining reservoir pressure and ensuring a high sweep efficiency. Improving injectivity in a non-damaged reservoir focuses on maximizing the fluid flow rate and penetration into the reservoir by altering the factors provided in equation (3). Improved injectivity can be achieved by increasing the mobility of injection water through an increase in injection temperature. Increasing temperature reduces the water viscosity and the flow resistance through the rock formation. Increased temperature will also reduce the interfacial tension, resulting in a higher relative permeability. Filter-cake build-up will, on the other hand, increase the flow resistance through the rock formation and is not beneficial for improving injectivity. Mixing seawater into the injection water can reduce the solids and oil-droplet concentration and the subsequent filter-cake build-up.

An increase in injection temperature will, on the other hand, affect fracture initiation and propagation, which is a critical element for injectivity in a heterogeneous reservoir. A reservoir under fracture conditions introduces new influencing factors that all interact with each other. The primary influencing factors that affect injectivity for a fracturing reservoir are [14]:

- Plugging of solid particles and/or oil droplets
- Stress alteration caused by poro-elastic and thermo-elastic effects
- Opening/closure of fractures
- Fracture containment in the target zone and out-of-zone fracture growth
- Operational conditions
- Injection rate changes and associated pressure transient effect
- Distributions of injected fluid or cross flow among multiple layers

5.3 Impact of fracturing on injectivity

Injecting water into a reservoir above the fracturing pressures is often performed to increase injectivity in heterogeneous and low-permeability reservoirs. The development of fractures can either be done on intention or by accident when in-situ reservoir stress is significantly reduced due to the thermal effects of cold injection water. A more detailed explanation of this topic is discussed in chapter [6.5]. The primary benefit of fracture injection is to enhance injectivity, allowing for greater tolerance to poor water quality and associated filter-cake build up [15]. The disadvantage of fracturing is that it can reduce the sweep efficiency, depending on the size and direction of the fracture growth. The elevated pressure can also induce unwanted fracture growth, leading to out-of-zone injection, potentially affecting the effectiveness of the entire injection operation. Out-of-zone injection is identified with an increase in injection rate and a reduction of bottom-hole pressure [1]. This will register as an increase in injectivity, even if the water is injected out-of-zone. The complexity of fractures, including their dimensions and network connectivity, affects injectivity. Together with the other influencing factors mentioned in the previous sub-chapter, it increases the difficulty in predicting the isolated effect of fracturing in a reservoir and the optimal degree of fracturing for a specific reservoir without results from a simulation study.

6 Hydraulic fracturing

6.1 Definition of hydraulic fracturing

Water injection in reservoirs with low permeability and a high degree of heterogeneity often requires a high injection pressure above the minimum in-situ stress to maintain sufficient injectivity. Hydraulic fracturing is, therefore, an integrated part of water injection in unconventional reservoirs and involves pumping fluid from a well into the rock formation under high pressure to fracture the reservoir. The flow rate is maintained at a level high enough for the fluid pressure to overcome the minimum in-situ stress to the degree that splits the rock and propagates the fracture. The fracture will propagate in a complex stress field near the injection well-bore and continue to grow in the direction of least resistance [16].

The development of fractures creates channels with high conductivity for which fluid may flow, and the propagation of fractures increases the area of exposed formation rock, which, together with the high conductivity channels, may increase the injectivity and sweep efficiency. Hydraulic fracturing involves various complex physical processes, including fluid-rock interactions and fluid leak-off into the formation, rock deformation induced by fluid pressure in a high confining stress area, and fracture propagation [16].

The advantage of fracturing may be visualized by comparing the water imbibition rate in a low permeable core with and without a developed fracture. Figure [7] shows that the imbibition process in the tight core with fractures is significantly faster than in the core without fractures. In the absence of fractures, water slowly imbibes into the core matrix from the bottom. However, in the presence of fractures, water rapidly enters the fractures before gradually spreading into the surrounding matrix along the fracture pathways. The fractures within tight cores significantly increase the contact areas between water and the core matrix, improving the imbibition rate. When the cores are initially saturated with oil, the imbibition effect in the fractured cores leads to a higher oil production rate [17].

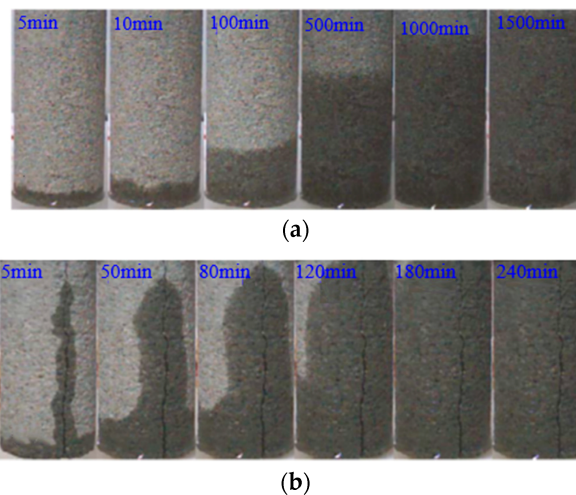


Figure 7: Images of imbibition rate of water in tight cores: (a) Core without fractures, (b) core with fractures [17].

6.2 Rock mechanical properties

Hooke's law is used to describe the relationship between stress and strain, and Young's modulus of elasticity show that the stress of an elastic body is directly proportional to the applied strain. This is visualized in the stress-strain figure [8], where the slope of the line is equal to the Young's modulus [18].

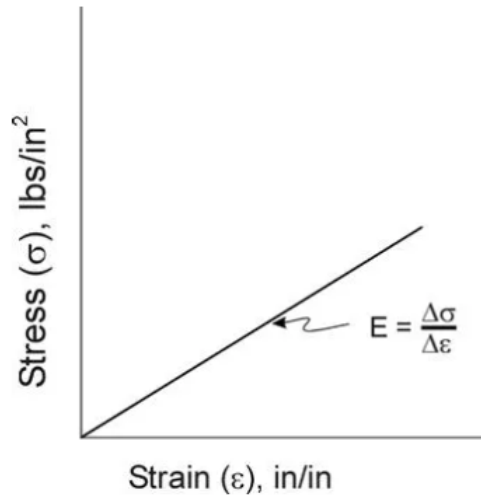


Figure 8: Hooke's law: Stress-strain relationship [18]

However, rocks are heterogeneous composites of materials containing crystals, cementing, discontinuities, and micro-cracks, leading to Hooke's law not accurately distributing the stress-strain relationship. A stress-strain diagram of a rock consists of an S-shape, divided into an elastic and plastic area [18]. The rock mechanical properties of rock can, therefore, broadly be categorized into elastic and inelastic properties. The inelastic properties are factors such as fracture gradient, fracture toughness, and formation strength, referring to the behavior of rock beyond the elastic limit. These properties are associated with permanent deformation and failure of the material. The elastic properties are interconnected, and any one of them can be expressed in terms of the other three. They are fundamental parameters used to understand the behavior of rocks under different loading conditions [19].

Elasticity is the property of matter that causes it to resist deformation in volume or shape. Hooke's law describes the behavior of elastic materials and states that for small deformations, the resulting strain is proportional to the applied stress. Depending on the mode of the acting geological force and the type of geological media the force is acting upon, three types of deformation, consisting of compressive, shear, and volumetric deformation, can result, as well as three elastic moduli that correspond to each type of deformation [19]:

- Young's modulus (E), represents the rock's resistance to deformation in under pressure.
- Shear modulus (G): represents the ratio of shearing/torsional stress to shearing strain. It characterizes a material's resistance to deformation by shear forces.

- Bulk modulus (K): is the ratio of stress to strain under hydrostatic pressure. It describes the change in volume of a material in response to applied pressure.
- An additional parameter, Poisson's ratio (ν), measures the geometric change of shape under uniaxial stress. It describes the lateral contraction or expansion of a material perpendicular to the applied force.

6.3 In-situ stresses

In the context of in-situ stresses, it is commonly observed that the two horizontal compressive stresses are not equal, leading to the identification of a maximum and minimum stress based on the orientation of the stress field. The vertical stress (σ_z) originates from the weight of the overlying rock layers, exerting pressure on the underlying formation. The horizontal stresses (σ_x, σ_y) are influenced by the poro-elastic deformation of the rocks, as well as external tectonic forces. Several factors contribute to the magnitude of the principal in-situ stresses, including the overburden weight, fluid pore pressure, porosity of the formation, and the presence of natural fractures or anomalies in the rock structure. The anisotropic in-situ stresses directly impact fracture orientation, height, width, and conductivity. Moreover, fractures will tend to propagate in a direction perpendicular to the minimum in-situ stress (minimum horizontal stress) [20]. Three different types of geological environments can be determined from the min/max horizontal stress and vertical stress magnitudes[21]:

- A normal fault environment is defined by the vertical stress being greater than the horizontal stresses ($\sigma_V \geq \sigma_{H,max} \geq \sigma_{h,min}$), where vertical fractures are the most likely to occur.
- A shear environment defined by one of the horizontal stresses being greater than the vertical stress ($\sigma_{H,max} \geq \sigma_V \geq \sigma_{h,min}$), where horizontal fractures are the most likely to occur.
- A thrust fault environment defined by the horizontal stresses being greater than the vertical stress ($\sigma_{H,max} \geq \sigma_{h,min} \geq \sigma_V$), where horizontal fractures are the most likely to occur.

There are two types of vertical fractures in a normal fault environment. These are transverse and longitudinal fractures, as seen in Figure [9]. Transverse fractures, a combination of long narrow fractures, occur when the well is drilled parallel to the minimum horizontal stress or perpendicular to the maximum horizontal stress. This orientation allows the fractures to propagate perpendicular to the minimum horizontal stress and is most often preferred as they enhance the connectivity between the wellbore and the reservoir. Longitudinal fractures are created when the well is drilled parallel to the maximum horizontal stress or perpendicular to the minimum horizontal stress. This orientation causes the fractures to propagate parallel to the minimum horizontal stress and perpendicular to the maximum horizontal stress, which is the opposite of transverse fractures[21].

Understanding the principal stresses and the geological environment to optimize hydraulic fracturing operations is essential. By considering the stress distribution and selecting the appropriate drilling direction, operators can create fractures that enhance the productivity and economic viability of heterogeneous/low permeability reservoirs in different fault environments [21].

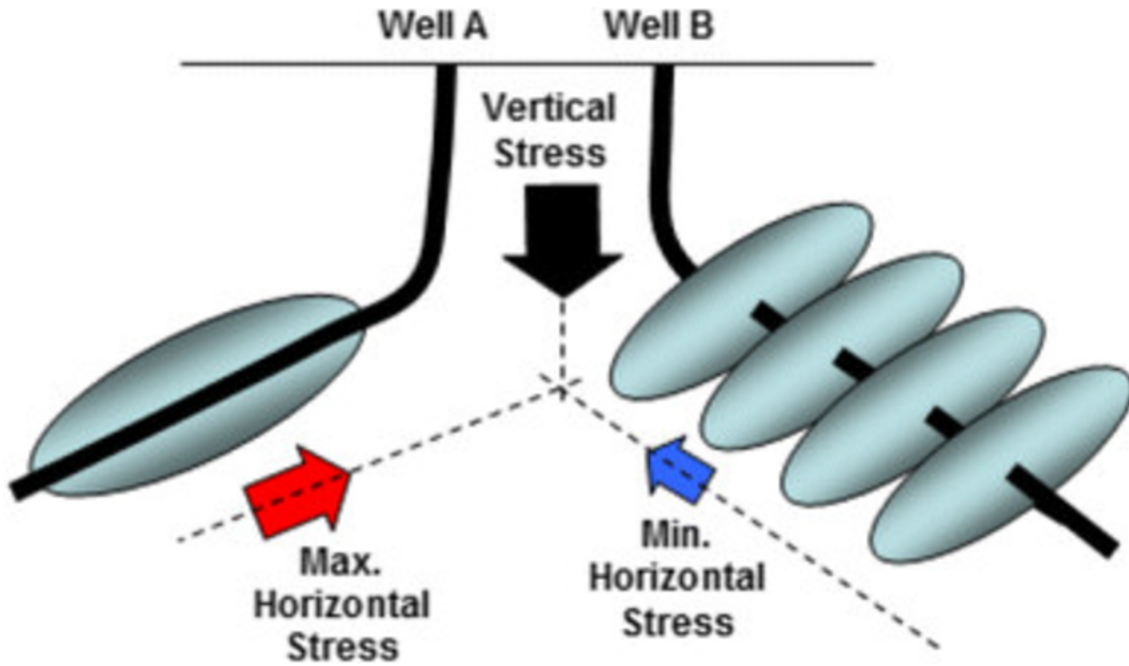


Figure 9: Effect of wellbore direction on hydraulic fractures propagation. Well A: Longitudinal fracture, Well B: Transverse fracture [22]

The estimation of the minimum horizontal stress (σ_{Hmin}), also known as fracture closure pressure, can be determined using in-situ measurements or approximated using equation (4). Equation (4) takes into account several parameters, including Poisson's ratio (ν), vertical stress (σ_v), Biot's constant (α), pore pressure (P_p), and tectonic stress ($P_{tectonic}$). These parameters significantly impact the magnitude of the horizontal stress within a formation and the pressure required to initiate a hydraulic fracture. The tectonic stress may play an important role in shaping the stress field, depending on the degree of tectonic activity [21].

$$\sigma_{Hmin} \approx \frac{\nu}{1-\nu}(\sigma_v - \alpha P_p) + \alpha P_p + P_{tectonic} \quad (4)$$

Equation (4) assumes the rock formation is isotropic and elastic, meaning the stress-strain relationship is linear. Young's modulus and Poisson's ratio are crucial in quantifying this relationship. Biot's coefficient, also known as poro-elastic constant, measures how effectively the fluid transmits pore pressure into rock grains and to what degree the pore pressure affects the in-situ stress. The Biot coefficient ranges from 0 to 1, where a value of 0 means that the pore pressure does not affect the rock mechanical properties. This means the rock can expand elastically without any resistance as pore pressure increases. At a value of 1, the pore pressure acts as a counteractive force against applied force, meaning the rock is completely rigid [18]. A rock formation with a high Biot's coefficient will therefore experience that the pore pressure significantly influences the mechanical behavior and stress distribution within the rock.

The relationship between Poisson's ratio, Young's modulus, fracture half-length, fracture width, and their impact on stress distribution and fracture growth is explored in the specialized report associated with this thesis. This analysis provides valuable insights into how these parameters influence fracture development and helps determine the minimum horizontal stress and fracture dimensions [1].

The vertical stress (σ_v), the cumulative pressure from the overburden rock layers, can be calculated using equation (5). This equation considers the formation depth (H), gravitational acceleration (g), and average formation density (ρ_{avg}). Measuring the average formation density can be challenging. However, density-logging tools are used to obtain density and fluid density measurements at specific depths, allowing for the estimation of the vertical stress gradient [21].

$$\sigma_v = \rho_{avg} \cdot g \cdot H \quad (5)$$

The maximum horizontal stress ($\sigma_{H,max}$) is more challenging to calculate and can be determined from the relationship presented by Haimson and Fairhurst (1967) for penetrating fluid (slick water) or non-penetrating fluid (gelled fluid) [23]. However, the maximum horizontal stress is often assumed to be isotropic to the minimum horizontal stress for practical computation [5].

6.4 Fracture initiation and propagation

A hydraulic fracture will initiate when the pressure experienced by the rock formation exceeds the minimum in-situ stress (minimum horizontal stress) and will continue propagating if the pressure keeps increasing. The main requirements for a hydraulic fracture initiation are the presence of a fracture seed or pre-existing damage to the rock formation that allows fluid to flow through it and create sufficient pressure to open the fracture. The main requirement for hydraulic fracture propagation is that it needs to experience a pressure that is higher than the minimum horizontal stress, which occurs when the stress intensity at the fracture tip is greater than the critical stress intensity or fracture toughness (K_{Ic}). The fracture toughness indicates a rock's strength in the presence of a pre-existing flaw and represents the additional pressure above the minimum principal stress required to propagate a fracture [1][24].

The force required to propagate fractures in a rock depends on its strength and stiffness. Among the crucial parameters influencing fracture propagation in hydraulic fracturing is the pressure of the injected fluid and its development. Several factors contribute to the pressure development in a hydraulic fracture, including the properties of the injected fluid, the geometry and orientation of existing cracks, the injection rate of the fluid, and environmental conditions like temperature and pressure. Natural fractures or other geological features can also impact pressure development [24]. A study into the relationship between the fluid leak-off into the rock formation and fracture propagation in the form of the maximum fracture half-length was performed in the specialized report associated with this thesis. It was found that rock permeability, which governs the extent of fluid leak-off into the porous rock matrix, is the most influential factor affecting pressure development and fracture development in low permeable shale [1].

Based on the energy-dissipation mechanism, fracture propagation regimes may be classified as either viscosity-dominated or toughness-dominated [25]. In the viscosity-dominated regime, the energy dissipation of pressure from the fracture to the nearby rock matrix is dominated by the flow of the viscous fluid. Whereas in the toughness-dominated regime, energy dissipated from the fracture is dominated by the creation of new fracture surfaces at the fracture tip. Based on the ability of the rock matrix to dissipate fracturing fluid, other extreme cases may also be defined called storage-dominated and leak-off-dominated. The storage-dominated regime is defined by the injected fluid remaining mainly inside the

fracture, while the leak-off dominated, is where most of the injected fluid dissipates into the surrounding rock matrix [26]. Combining these regimes results in four asymptotic regimes fundamental to understanding the hydraulic fracturing process.

Fracture development is a complex, multi-physics, multi-dimensional problem, which requires robust models that can simultaneously account for matrix and fracture deformation, fluid flow through the matrix and fractures, fluid exchange between fractures and matrix, and fracture propagation and interaction, all in a fully-coupled, three-dimensional setting [26]. To accurately capture the complex behavior of fluid-driven fractures in porous media, it is crucial to incorporate 3D fully coupled fracture calculations into simulation models that take into account the poromechanical effects of porous media deformation, the redistribution of fluid within the rock matrix, and the reduced effective stress near the fracture face.

6.5 Poro- and thermoelastic coefficient

When cold water is injected into a hot reservoir, the surrounding rock formation undergoes cooling. This rapid decrease in temperature reduces the in-situ stress components, leading to a higher probability of fracture initiation and propagation. The effect caused by a transient reservoir cooling is influenced by injection duration, which is not negligible over a timescale longer than days/months, depending on the specific reservoir. Thermal effects modify the total stress and impact the pore fluid pressure, leading to additional changes in both the stress state [27]. An increase in pressure may provide additional support to the rock cementation, making the rock stronger. This causes an increase in the stress field, resulting in a rock less liable to fracture [24]. Whether thermal effects significantly impact fracture initiation and propagation so that thermal-induced fracturing is possible depends on the thermo- and poroelastic coefficients, which can be used in fracture calculation to update the stress field based on the operational data related to pressure and temperature. Equation (6) defines the poro-elastic stress coefficient, while equation (7) defines the thermo-elastic stress coefficient. When the poro-elastic coefficient is multiplied by the variation in pore pressure, it yields the alteration in stress. Similarly, the change in temperature can be transformed into a change in stress by multiplying it with the thermo-elastic coefficient.

$$A_P = \alpha_P \frac{E}{1 - \nu}, \quad \alpha_P = \frac{(1 - \frac{C_g}{C_b})(1 - 2\nu)}{E} \quad (6)$$

where

E is Young's modulus.

ν is Poisson's ratio.

α_P is the linear poro-elastic expansion coefficient.

$(1 - \frac{C_g}{C_b})$ is known as Biot's poro-elastic coefficient (α).

$$A_T = \alpha_T \frac{E}{1 - \nu} \quad (7)$$

where

α_P is the linear thermal expansion coefficient.

6.6 Effect of injection temperature on fracturing

Scientific literature shows that temperature significantly affects the changes in rocks' mechanical properties. In addition to the change in stress field, due to thermo elastic stress effects, a change in temperature can change compressive strength and Young's modulus, affecting fracture initiation and growth. A study into how these parameters change as a function of increasing temperature showed a decrease in compressive strength and Young's modulus. These changes varied for different types of rock, depending on factors such as mineral composition, porosity, and density. It is, however, worth noting that the most essential processes that caused changes in the strength parameters of rocks occurred in the temperature range of 400 to 600 °C [28].

The extent of change in mechanical properties and thermo-elastic stress reduction is limited by the extent of the cooled area [29]. When injecting with cold water to achieve thermal induced fracturing parameters such as water viscosity, the temperature difference between injection water and reservoir rock, and the period of injection will therefore play an essential role in the temperature reduction's effect on fracture initiation and propagation.

In a recent study on enhancing the fracture growth uniformity of perforation clusters by pre-injection of cold water, J. Almarri et al. (2023) investigated how thermoelasticity impacts the uniformity of cluster stimulation and fracture initiation and growth in horizontal, multi-fractured laterals. This study utilized a fully coupled geomechanics, fracture, and reservoir simulator to investigate the impact of various fluid temperatures during the pre-treatment period. Two scenarios were simulated with and without pre-treatment by thermal cooling with cold water to visualize the effect lowering the minimum principal stress has on fracture initiation and propagation. The results, as given in Figure [10], showed that case 1 with pre-injection of cold water developed more fractures and thus a more extensive total fracture area compared to the base case without any pre-injection of cold water. The results showed that only changing the fluid temperature in the pre-treatment cooling period significantly impacted fracture propagation and improved growth uniformity [30].

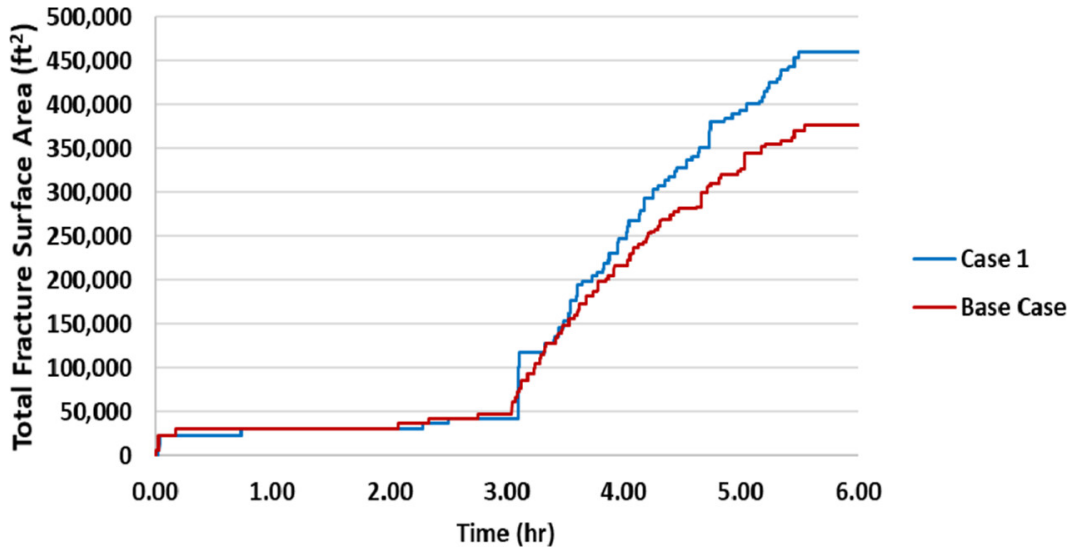


Figure 10: Total fracture surface area, showing a 20 % higher value for Case 1 than for the base case [30].

A change in injection temperature will affect the viscosity of the water injected, which is reported to impact fracture propagation significantly. In a study into transient temperature impact on deep reservoir fracture, Yu Jiang et.al (2020) investigated the temperature behavior during hydraulic fracturing, where the temperature effects on fluid viscosity and thermal stresses were included in a dynamic fracture propagation model. The fracture half-length was shown to be more significant for the isothermal fracture model than the transient heat fracture propagation model. The study results showed that hydraulic fracture propagation is decelerated with the injection of cold fracturing fluid compared to the isothermal fracture model ignoring the temperature and viscosity effects. One of the main conclusions from the report was that temperature was shown to impact different mechanisms during the hydraulic fracturing process, including the changing fluid viscosity and the formation stress distribution, and that the temperature impact is significant and cannot be ignored. The authors emphasize that although this difference may not be as significant in conventional reservoirs with lower reservoir temperatures and geothermal gradients, it must be addressed in deep reservoirs. In deep reservoirs, where the temperatures are higher, and the geothermal gradients are steeper, the difference in fracture half-length as resulted in the study may occur [31].

Another study investigating the impact of different fluid viscosities on fracture propagation revealed that high-viscosity fluids could effectively reduce the speed of hydraulic fracture propagation. This phenomenon can be attributed to the existence of a gap between the fracture tip and the front of the fracturing fluid when using high-viscosity fluids. As a result, the dominant mechanism driving propagation is the non-local effect of remote pressure [32]. In this mechanism, the propagation of the fracture is primarily driven by the pressure exerted on the fracture front by the high-viscosity fluid, which is located some distance away from the fracture tip. This can be one of the reasons why a reduction in injection temperature may cause a deceleration of fracture propagation, as mentioned above. A reduction in water viscosity also affects the water mobility and the extent of the pressurized waterfront. The two different fluid viscosities compared in the study were 1 and 1100 cP, corresponding to water (control) and glycerol, respectively.

6.7 Effect of filter-cake build-up on fracturing

The build-up of filter-cake in the near well-bore area and fracture face plays a crucial role in the propagation of fractures in low permeability reservoirs. The growth of fractures and the accumulation of filter-cake are interconnected phenomena influenced by injection pressure, changes in pore pressure, thermal stresses resulting from thermo-elastic effects, and the pressure changes caused by the build-up of particles leading to pore plugging [33].

While the presence of a thin layer of filter-cake on the fracture surface may not significantly affect the pressure-fracture opening relationship, it has a notable impact on fracture propagation. The formation of a filter-cake and the intrusion of fines into a porous rock can create less porous and permeable layers near the fracture surface. The filter-cake becomes the primary factor regulating the fluid leak-off into the surrounding rock matrix, which is a critical aspect of fracture propagation [34] [35].

7 REVEAL

7.1 Introduction to REVEAL

Information on the REVEAL software written in the specialization report related to this thesis is included below to provide a insight and introduction into the software:

REVEAL is a member of the Integrated Production Modeling (IPM) suite of specialized software developed by Petroleum Experts. It is a reservoir simulation software that enables the integration of reservoir and production studies. It is a beneficial tool that is used to bridge the gap between reservoir simulation and specialized studies such as the study of thermal and hydraulic fracturing. It can import and use existing reservoir simulation models, such as Eclipse, as a starting point for a specialized study, such as the study into fracture initiation and propagation [36].

Rock mechanical theory states that a reduction in temperature due to the injection of cold water will reduce the in-situ stress and cause a thermal fracture. Moreover, injection with a pressure that exceeds the minimum horizontal stress will cause hydraulic fractures. One of the advantages of REVEAL is the simulations of fractures and how it integrates both pressure and temperature in its calculations [36][1].

7.2 The finite-element thermal fracture model in Reveal

The finite-element thermal fracture model in REVEAL considers thermal and hydraulic injection fractures simultaneously and calculates the fracture shape, including effects of stress changes due to the injected fluids, elastic fracture opening, propagation depending on rock strength, flow within the fracture and leak-off rate balancing the well injection rate and flowing bottomhole pressure. The model investigates the possibility of fracture initiation and propagation within a coupled reservoir and well-bore system, and it couples dynamics reservoir conditions with a finite element solution of fracture mechanics and an injection well performance [1] [24].

The basic principle of the thermal fracture model is to balance:

- Flow, pressure and temperature supplied by an injection tubing.
- Rock mechanics of a fracture.
- Prevailing reservoir conditions.

The different relationships involved in the fracture model calculations, and the variables they depend is summarized in figure [11].

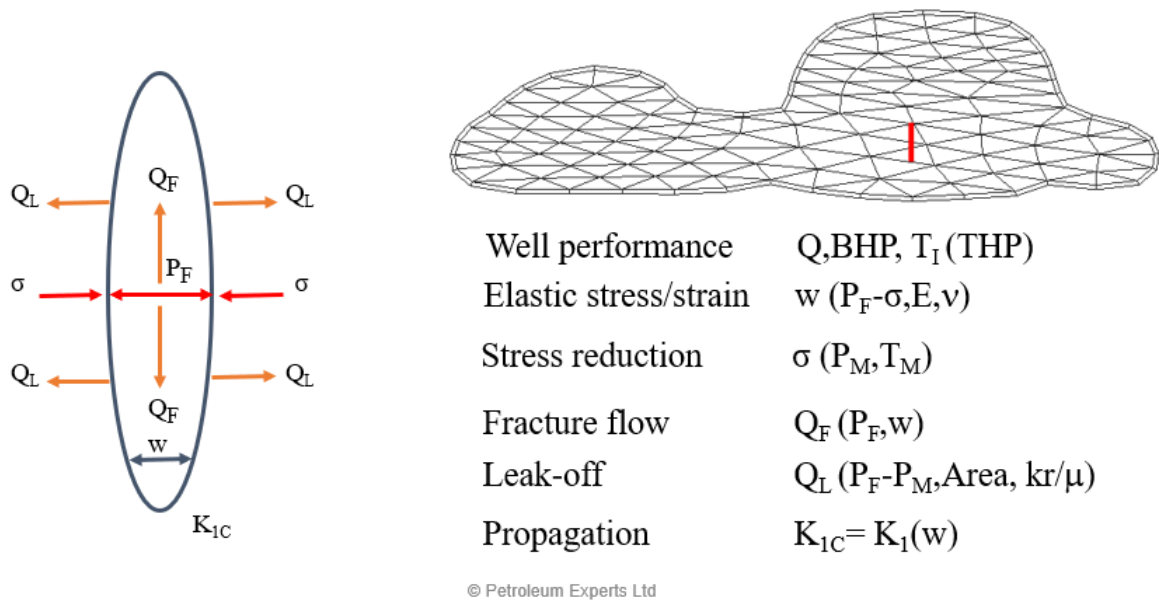


Figure 11: Diagram of relationships in REVEAL thermal fracture model [37].

Well performance:

Well performance provides the relationship between rate, pressure and temperature when controlled with a well head pressure and well head temperature, through a vertical lift-curve (VLP). It will provide information on how a change in bottomhole pressure will affect the rate, and vice versa. The lift curve will also be able to define the bottomhole temperature at given rates, which is important for the analysis of thermal induced fracturing. Using a VLP enables the coupling of a implicit well performance.

Elastic stress/strain:

As pressure is exerted within the fracture, it counteracts the stress field and promotes the opening of the fracture. This leads to the formation of a width. In essence, we utilize an elastic stress-strain model that considers the interaction between pressure, fracture, and stress, taking into account geomechanical factors such as Young's modulus and Poisson's ratio, to determine the distribution of the fracture width.

Stress reduction:

The stress present in the reservoir is influenced by the distribution of pressure and temperature within it. It is determined by the pressure and temperature conditions both within and around the fracture region or matrix.

Fracture flow:

The flow within the fracture is governed by the pressure distribution across its nodes and the width of the fracture. Additionally, conductivity models and viscosity are significant factors in this process. As the pressure gradient extends from the well through the fracture, it induces both flow and a pressure gradient within the fracture. The magnitude of the pressure gradient corresponds to the extent of the fracture opening, which is directly linked to the fracture width.

Leak-off:

Each finite element triangle within the model allows for fluid leakage into the adjacent grid blocks. This leakage is influenced by various factors, including pressure drop between the fracture and formation matrix, fracture characteristics, overlapping areas, and mobility in relation to geometric properties. During fluid flow within the fracture, the available fluid volume for propagation towards the fracture tip diminishes if leakage occurs. Consequently, the pressure at the tip decreases, leading to the closure of the fracture and hindering propagation.

Propagation:

The collective interaction of the above-mentioned relationships influences the propagation process. A specific propagation criterion is employed, which considers the fracture toughness at the fracture tip. This criterion is utilized to determine whether the fracture can sufficiently opened at the tip to enable propagation. If there is some degree of propagation, it increases fluid leakage. The increase in fluid leakage is facilitated by overlapping more grid blocks in areas where leakage can occur. This increased leakage impacts the overall flow, leading to a reduction in pressure. Consequently, the width of the fracture is also reduced. Therefore, the challenge lies in striking a balance or finding an optimal point that ensures a satisfactory compromise between propagation, leakage, flow reduction, and pressure reduction.

7.2.1 Iterative Fracture Calculation Process

The thermal fracture model uses a two-dimensional finite element grid coupled with an overall three-dimensional finite difference grid. The finite element grid, which explicitly models fluid flow and pressure drops within a fracture is characterized by triangular internal elements and quadrilateral boundary elements, where fracture width is defined. Finite element equations are combined and solved iteratively for fracture widths using the Newton-Raphson method. The width solver is supplied with a total fracture injection rate (Qf), and the shape of the fracture is iterated on until a consistent shape is found with the stress intensity at the fracture tip equal to the critical stress intensity (K_{Ic}) for the fracturing rock. The pressure at the center of the fracture (Pf) is returned, and a top level of iteration is performed to ensure that Qf and Pf are consistent with the total well rate (including flow directly from the well into the rock matrix) and the bottom hole flowing pressure (Pwf) [1] [24].

A more detailed explanation:

At each time step, which is the end of a previous time step, the pressure and temperature fields are known. This allows the model to update the stress and strain fields. The calculation is performed using the in-situ stress data defined by the user together with the poro and thermo-elastic stress coefficients.

Changes on rock volume results in stress and strain alterations in different directions. Change in rock volume are source terms on a displacement potential solution given in equation (8).

$$\nabla^2 \chi = -\frac{1-\nu}{1-\nu} (A_p \Delta P + A_T \Delta T) \quad (8)$$

From the displacement potential, any component of the stress reducing tensor may be found. The change in stress and strain perpendicular to the fracture shape (Example: Y-axis) are calculated using equation (9) and (10), respectively.

$$\sigma_{yy} = \sigma_{insitu} - \frac{E}{1 - \nu} \frac{\partial^2 \chi}{\partial y^2} - A_p \Delta P - A_T \Delta T \quad (9)$$

$$\varepsilon_y = \frac{\partial \chi}{\partial y} \quad (10)$$

The stress information from the reservoir is used as a boundary condition together with the well performance. Using these conditions, it calculates how a fracture would evolve given the current reservoir condition and well performance.

An outer loop of iterations are performed on the well performance to meet pressure and rate constraints are performed. This involves testing different rates (Q_f), and updating the fracture shape and properties to ensure the fracture flow rate and fracture pressure is consistent with the well performance. This process involves iterations on both the well performance and the fracture shape by solving two sets of coupled equations [37]:

Equation (11) is called the incompressible fluid fracture flow equation, and relates the flow through a fracture based on the pressure gradient and conductivity (permeability and width). The equation consists of the following terms: Fracture flow rate term, leak-off term, accumulation term and source term (test rate). Equation (12) is the internal pressure-width equation, where fracture pressure and width are related to the applied stress and fracture geometry.

$$- \int \frac{k}{\mu} w \nabla^2 (P - \frac{\rho h}{144}) dA + \int M (P - P_{mat}) dA + \frac{\int w dA - V_0}{\Delta t} - Q_f = 0 \quad (11)$$

where

Fracture permeability (k) is defined based on the fracture width (Parallel plate default mode)

Mobility connection factor (M) is the measure of how easily fluid can flow through a grid block that intersects a fracture.

$$(P - \sigma)(x, z) = \frac{G}{4\pi(1 - \nu)} \int \nabla \left(\frac{1}{R} \right) \nabla w' dA' \quad (12)$$

$$, R = \sqrt{(x - x')^2 + (z - z')^2}$$

where

Shear modulus (G) is the defined by Young's modulus (E) and Poisson's ratio (ν).

Within each test rate, an inner loop of iterations are performed to determine the shape of the fracture that meets the propagation criteria, as shown in equation (13) which is defined by the critical boundary width, related to K_{Ic} . An additional inner loop of iterations is also performed calculating the width and pressure at the current shape and rate. Both of the inner loops of iterations involves the coupling of equation (10) and (11).

$$w_c = \frac{3K_{Ic}(1 - \nu)}{G} \sqrt{\frac{a}{2\pi}} \quad (13)$$

The inner loops will iterate until a stable fracture shape is found, where it has propagated such that it balances the width at the tip, flow within the fracture, leak-off to the formation matrix and the opening of the fracture based on the pressure acting against the stress field. Simultaneously, the outer loop will ensure that the fracture in-situ pressure and flow is consistent with the total well rate and bottomhole pressure.

Once all the iterations have converged and we have fractures of a certain shape and size, that will be included in the next time step solve.

7.3 Filter-cake model

The filter-cake model in REVEAL accounts for the build-up of the cake with time to change the thickness/size of the filter-cake. The model have different settings, and can model internal or external filter-cake build-up with the type of filter-cake being either compressible or in-compressible. An internal filter-cake is the penetration and build-up of particles within the rock formation. In contrast, an external filter-cake is the particles that build up on the well-bore surface and/or fracture face. Compressible or in-compressible refers to whether or not the filter-cake has compressibility, i.e porosity changes with pressure [24]. The filter-cake build up can be based on produced solids such as sand, asphaltene, wax, and water chemistry minerals, with the level of concentration selected by the user.

The model performs a material balance for the filter cake using the cumulative water injected to calculate the filter-cake thickness. The skin is thereby calculated using a dynamic skin model developed to modify the injectivity into the well or fracture grid blocks as a function of the mass of filtrate that has entered the block [24].

7.4 Perforation pressure drop

In addition to a Peaceman pressure drop connection factor, connecting a well to the grid, the perforation pressure drop in the near well-bore area may be added to the model in REVEAL. This addition uses the general term as shown in equation (14), consisting of a non-Darcy and Darcy term that provides a representation of the pressure drop incorporating both linear and non-linear flow effects [24].

$$dP = 2.89137 \times 10^{-14} \rho F_t L \left(\frac{Q}{A}\right) + \frac{\mu L}{6.3266 \times 10^{-3} k} \left(\frac{Q}{A}\right) \quad (14)$$

where

Q = total volumetric rate, A = total flow area, L = damage length, ρ = density,
 μ = viscosity, k = permeability (damage perm), F_t = turbulence factor.

7.5 Inactive zones

An inactive cell is a cell that does not contribute to fluid volumes or flow in the reservoir. The reservoir simulation ECLIPSE will flag any cell with vanishing pore volume as inactive, and the user may decide to define these as inactive or not, as cells with small pore volume will contribute insignificantly to flow or production. Flagging no-flow cells as inactive is therefore generally advisable in Eclipse, as it has a positive effect on total computing time [38].

When modeling heat transfer and stress calculation within a simulator, inactive regions/cells may cause unphysical behavior near well-bore areas. Inactive cells in reservoir models imported to REVEAL, from Eclipse, are, therefore, usually assigned low values of porosity and permeability when rock mechanics are considered. Different solver options exist in REVEAL that support grids with inactive cells with regards to stress modeling through interpolation [24].

8 Simulation study

8.1 Sector modelling

Sector models represent specific sections of a field reservoir model and are helpful for simulations that do not impact the entire reservoir. These models are commonly employed for single well studies involving limited drainage, especially when a comprehensive field reservoir model is already available [39]. Implementing sector models saves time by eliminating the need to construct an entirely new model and enables faster simulations than a fullfield model. However, the user needs to make certain modifications, including incorporating boundary conditions and adjusting various settings, which can influence the accuracy of the calculations. Nonetheless, when properly executed, the resulting sector model should offer a reasonably accurate representation of the fullfield reservoir model [1].

8.2 Fullfield model

The full-field model of Ivar Aasen in REVEAL 9.5 was developed during a previous study into out-of-zone injection for all of the high pressure injection wells. The full-field model, as shown in figure [12], is based on an imported full-field ECLIPSE model (isothermal) of the Ivar Aasen field, that has been history matched up until the period of June of 2021. During the development of the REVEAL model, a history matching process was performed to validate the import and to consider thermal effects and fracture initiation and propagation [5].

The following changes were made to the model with respect to the Eclipse history import, and the history matching process:

- Isothermal PVT tables were converted to thermal PVT tables through correlation matching.
- Overburden caprock layers were added, totaling 12 layers with thicknesses of 1, 2, 5, and 9*10 meters. These layers are not hydraulically connected to the main reservoir but are thermally and geo-mechanically linked.
- Geo-mechanical properties were incorporated for all rock types, including the overburden.
- A thermal gradient of 0.01 °C/m with a reservoir temperature of 98 °C at a reference depth of 2377.6 meters was introduced.
- Permeability and transmissibility modifications were made as part of the matching process.
- Injectors were transformed from completion tables to detailed wells, for the purpose of assigning specific values for perforation permeability, length, and size.
- All bottom-hole pressure (BHP) constraints and productivity index (PI) modifiers for the injectors were eliminated. Vertical lift curves (VLP) were implemented for the wells.
- As part of the history matching process, the decision was made to control the injection wells using fixed historical injection rates. Wellhead pressure constraints were

imposed using the maximum wellhead pressure for each individual injector due to the fracture model initially yielding unrealistically high pressures during the injection period.

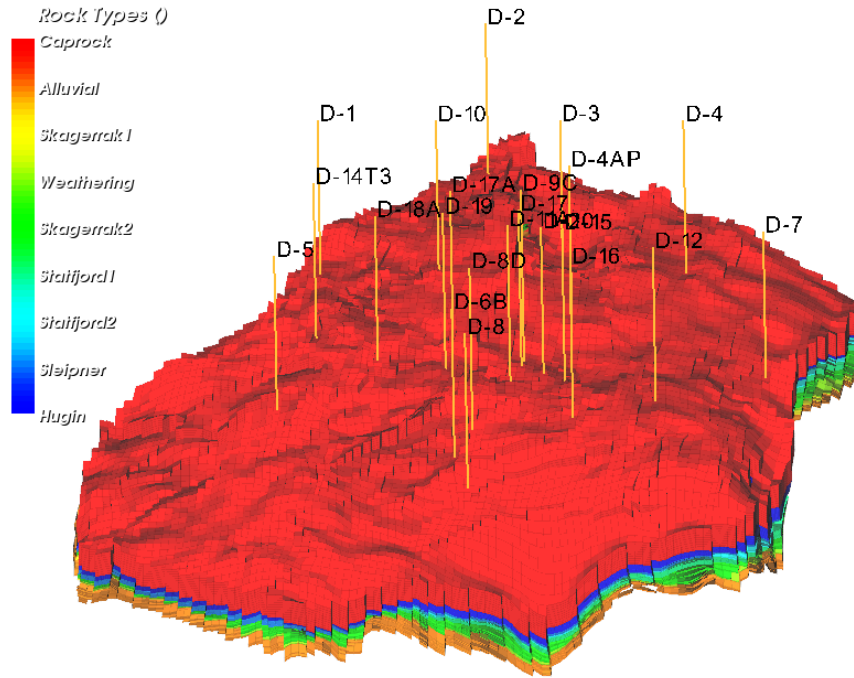


Figure 12: 3D visualisation of the the Ivar Aasen field REVEAL model (x4 Z-scaling).

8.3 Methodology for creating the sector models

The sector models for the high-pressure injection wells were developed based on the full-field REVEAL model of the Ivar Aasen field. As the new version of REVEAL became accessible for Aker BP, it was decided to use the new REVEAL 10.0 version for this study.

The process of creating sector models began by updating the schedule in the full-field model with historical injection rates to encompass the timeframe from December 24, 2021, to December 1, 2022. This update aimed to capture as much historical data as possible while avoiding major work-over periods.

The schedule update was performed by importing the new Eclipse schedule file to REVEAL. The update incorporated a 1-year period, which did not closely match the historical measured bottomhole pressure (BHP) data. The decision was made to include this period and introduce minor adjustments, if necessary. It was decided to exclude data beyond December 1, 2022, due to the introduction of new wells and the existing Eclipse model of the field becoming inaccurate beyond this point. The Eclipse schedule import consisted of making sure that the period after December 1, 2022, was deleted and that PI multipliers for the injection wells were removed, together with re-naming certain wells that did not match the names used in REVEAL.

To verify the implementation of the new schedule and that the new version of REVEAL matched the results achieved in the older version, a simulation run was performed using the average injection temperature of 48 °C. Comparing the BHP for the two versions showed

that most of the injection wells were similar to the original version. Some relatively minor differences were seen, but this was expected due to the new version having small changes implemented to the fracture calculation process. However, a significant deviation between the versions was seen for injection well D-1, as shown in figure [13]. The figure shows a high increase in BHP for the new updated full-field model in version 10.0, which resulted in unrealistic high fracture growth. This behavior is numerical instability caused by the update to how the new version of REVEAL handles the interaction between WHP constraints and inactive cells and is further explained in chapter [8.7].

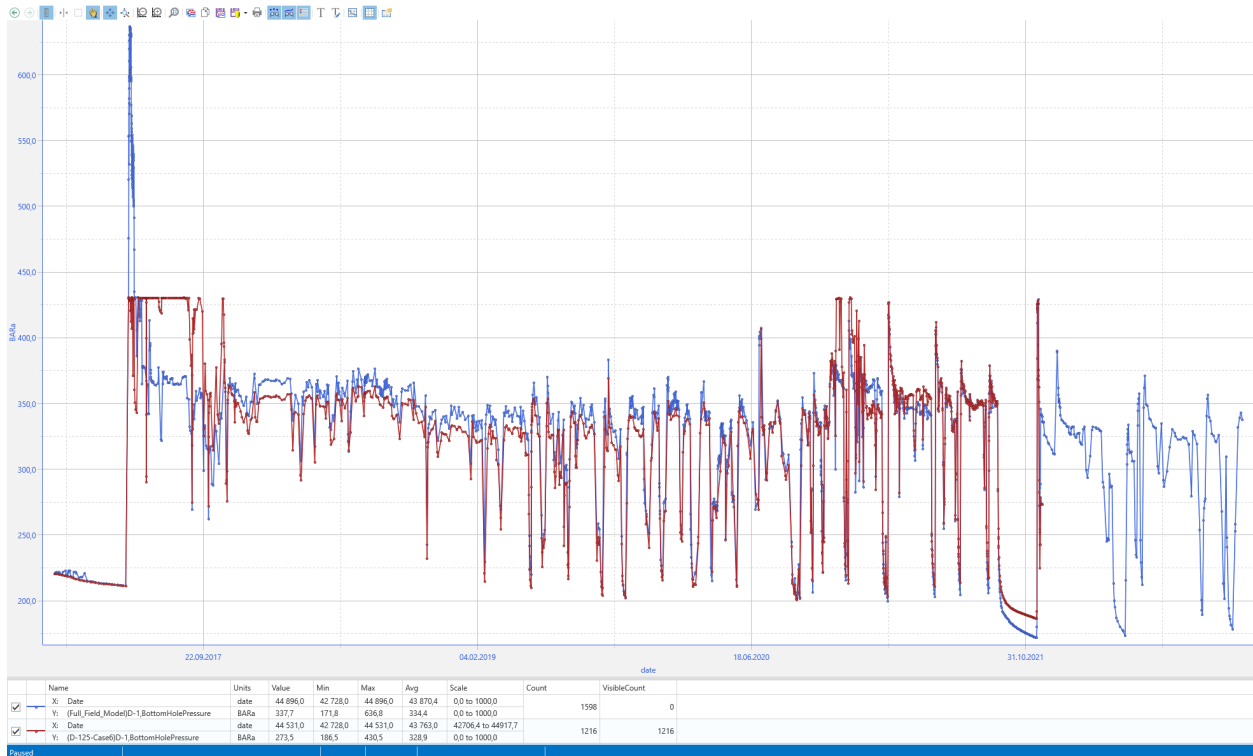


Figure 13: Injection well D-1: BHP for updated full-field model in REVEAL 10 (Blue) and "original" full-field model in Reveal 9.5 (Red).

Sector models with time-varying and constant pressure boundary conditions were developed. The sector models with time-varying boundary conditions are created in REVEAL using a special function that generates boundary conditions data for every grid block based on entered drainage regions as a function of time. The steps for how this was done can be found in the REVEAL user-guide. A guide to how the sector-models with constant pressure boundary condition was developed is given in Appendix [B]. 3D visualisation of both types of sector models for injection well D1, D2, D3 and D5 is given in Appendix [C].

Injection well D-3 was selected as the past candidate for the thesis study due to the absence of inactive cells in the near well-bore area, as opposed to injection well D1, D3, and D5. This choice was made based on the observation made for injection well D-1, showing numerical instability partially caused by the presence of inactive cells. Figure [14] and [15], show the degree of inactive cells for injection well D1, and D3, respectively. The created sector models were, despite the problem mentioned above, developed, awaiting the next REVEAL update to resolve the issue.

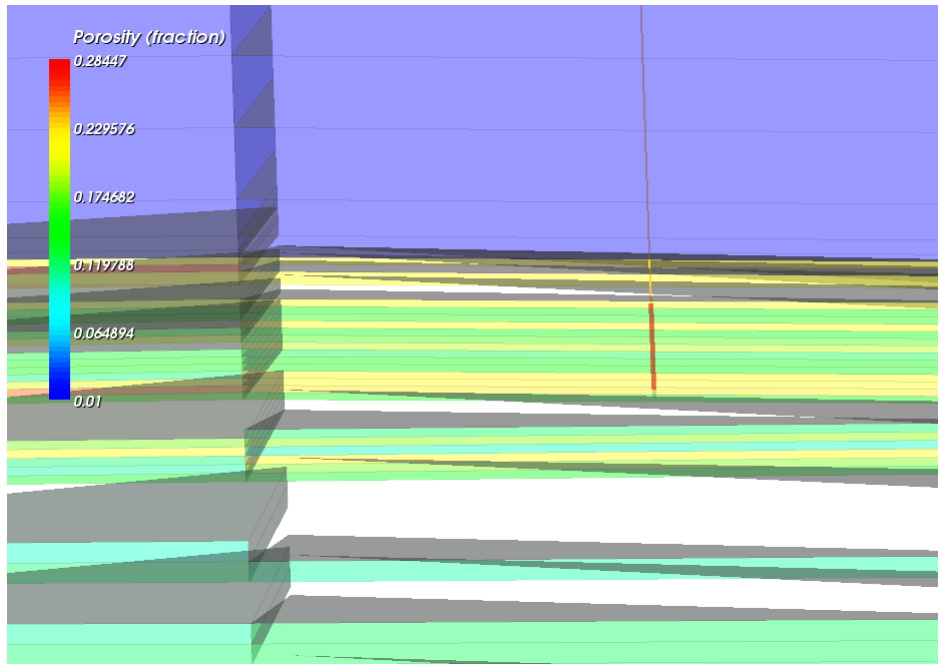


Figure 14: 3D visualisation of the near well-bore cross section for injection well D-1.

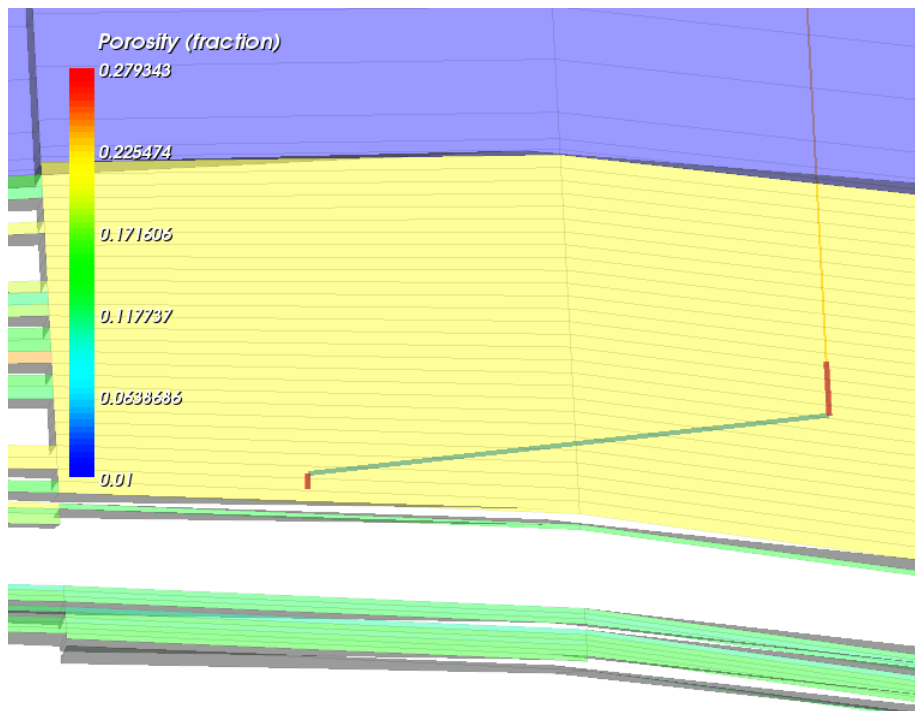


Figure 15: 3D visualisation of the near well-bore cross section for injection well D-3.

Figure [15] shows an upper and lower completion centered in each cell block. The completions are, in reality, positioned in an approximately vertical position, making the horizontal position of the lower completion inaccurate. This was done in ECLIPSE as the lower completion was partially located in the neighboring cell. The history matching process in the original full field model was performed with this configuration, and the permeability in the different Z layers is equal in both cells. Therefore, It was assumed that this would not affect the study significantly, and the position of the lower completion was left unchanged. The original distribution of fracture seeds was also kept unchanged. The distribution of 5 fracture seeds covers the different layers evenly, which was achieved using the automatic fracture seed generator in REVEAL. The fracture seeds are labeled as Fracture Seed 1, Fracture Seed 2, Fracture Seed 3, Fracture Seed 4, and Fracture Seed 5, where the numbering corresponds to increasing depth. Fracture properties used in the model are equal to the default values in REVEAL, due to a lack of data. The default values, such as fracture conductivity, represent a closed sandstone fracture with small trapped grains, which applies to the Skagerak 2 formation.

The PROSPER lift-curve (VLP) file connected to the bottomhole pressure and temperature calculations was updated. This was done by creating 20 injection temperature cases between the 0-90 °C range before importing the file to both sector models. Figure [16] illustrates the difference between bottomhole pressure at different liquid rates for a high (90 °C) and low (9.5 °C) injection temperature within the given injection temperature range. Figure [49] shows the bottomhole temperature (BHT) at different liquid rates for the ten injection temperatures within the updated range. The thermal PVT table was left unchanged, where the water viscosity as a function of temperature is given, which can be seen in Appendix [D].

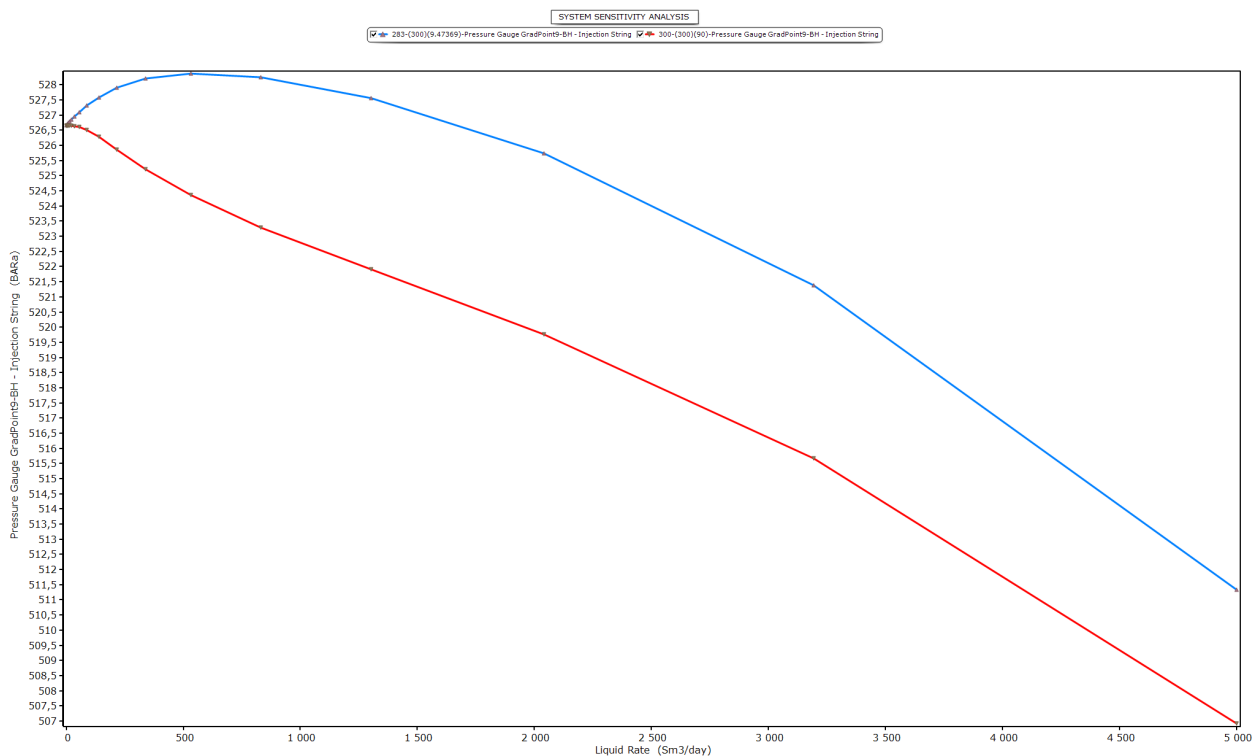


Figure 16: Bottom-hole pressure (BHP) and liquid rate at 90 and 9.5 °C, from PROSPER lift-curve (VLP).

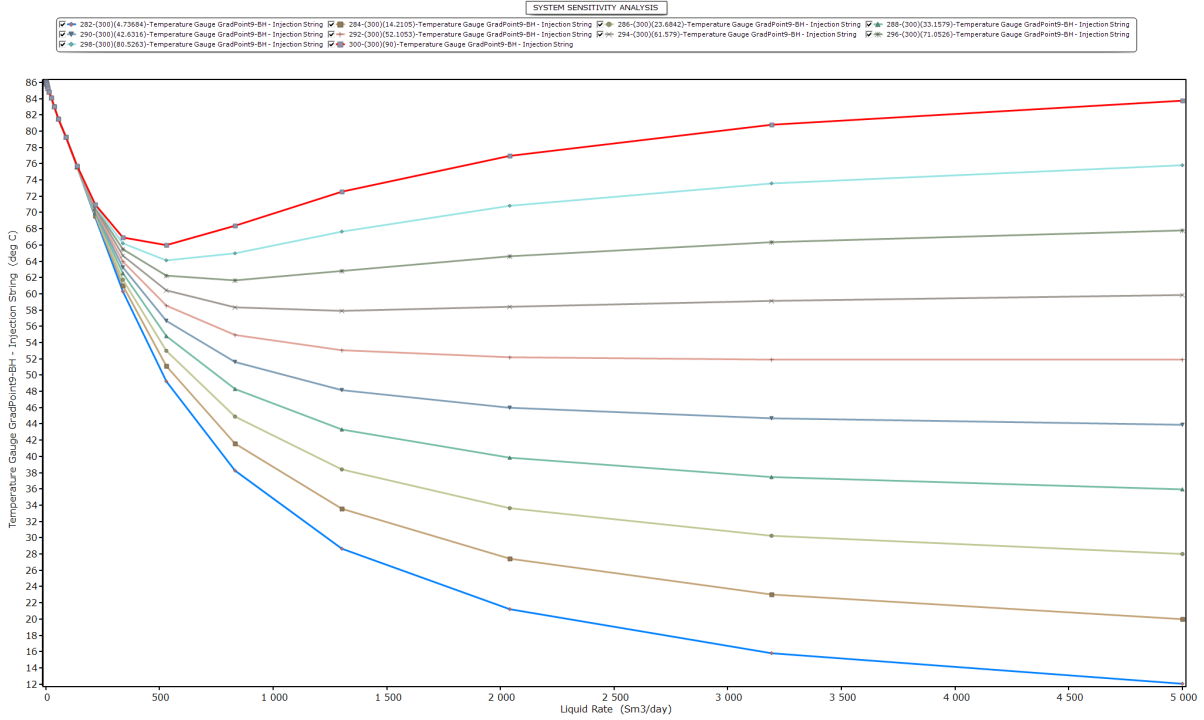


Figure 17: Bottom-hole temperate (BHT) and liquid rate at 10 different injection temperatures, from PROSPER lift-curve (VLP).

The time-varying boundary condition sector model for injection well D-3 was employed in an initial study to investigate the impact of different injection temperatures on historical fracture development(S1). This study aimed to enhance understanding of fracture initiation and propagation using the historical injection rate across temperatures between 90 and 8 °C. In figure [18], the BHP for the sector model using the average injection temperature is compared to the BHP of the original full field model. It can be observed that a deviation begins to emerge around June 1, 2021. This discrepancy could be attributed to the previously mentioned issue with WHP constraints and inactive cells. To address this, it was decided to shorten the schedule, excluding the period during which the deviation occurred. Importantly, fracture propagation did not occur after the second peak in BHP, ensuring that this decision did not impact the initial temperature study. Injection well D-3 had two periods in June of 2018 and 2019 with significantly high BHP, corresponding with the intentional hydraulic fracturing to increase injectivity. Capturing these periods was considered adequate for the initial study.

A manual calculation of the thermo-elastic stress reduction potential was performed for the Skagerak 2 formation at the injection well, highlighting the in-situ thermal stress reduction potential to be used to verify the simulation runs. The stress reduction was calculated using reservoir temperature of 98 °C against the proposed range of injection temperatures. Formulas and data used in this process are given in Appendix [F]. Another simulation scenario (S2) was performed in parallel with the initial study, using a simple thermal fracture model. The simple thermal fracture model was developed with homogeneous permeability, a single fracture seed, and similar properties to the D-3 injection well and surrounding reservoir properties. The bottom-hole temperature was controlled directly to eliminate any changes as a function of the injection rate (No VLP curve). A constant WHP was also used to reduce the number of input variables. This was done to better

understand fracture development at different operational conditions in a less complex REVEAL model. A 3D visualization of this model is given in Appendix [E].

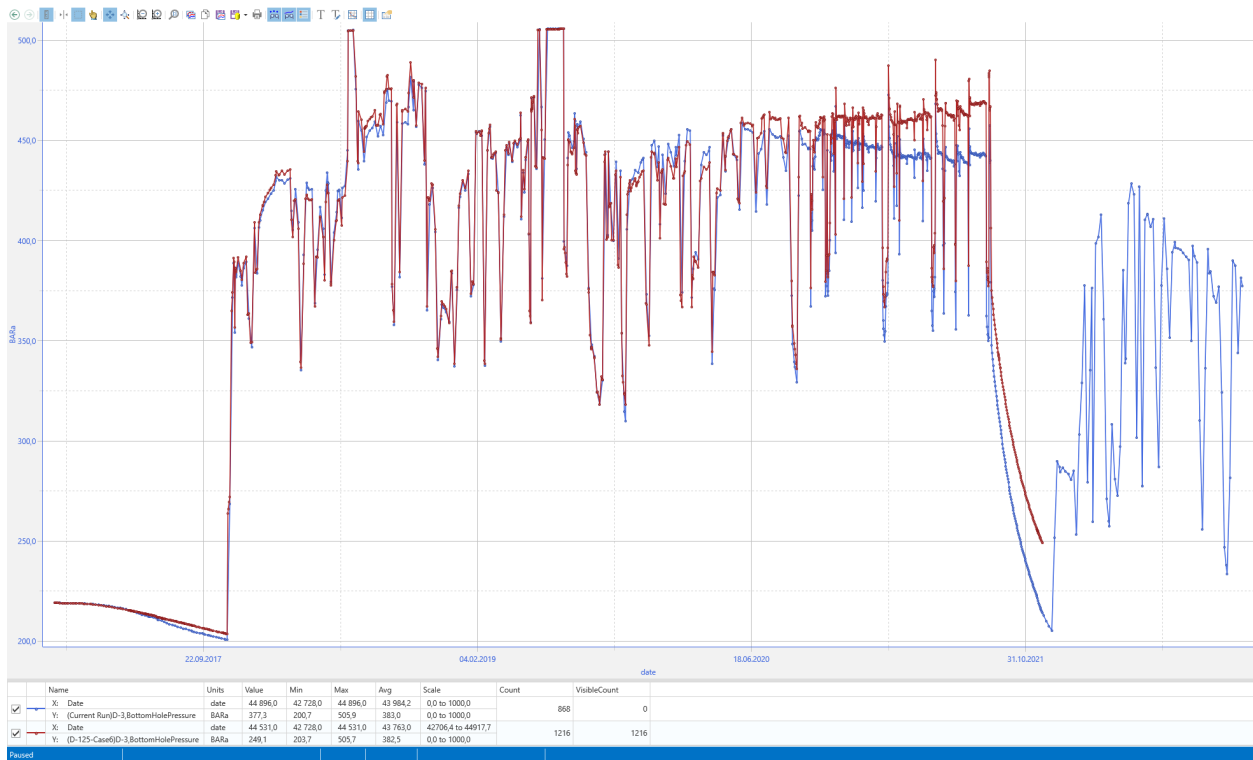


Figure 18: Injection well D-3: BHP for the time varying BC sector model (blue) and original full-field model in REVEAL 9.5 (red).

Comparing the two sector models, the decision was made to use the sector model with constant boundary conditions, as it includes the overburden rock formation. The time-varying BC sector model does not include the overburden rock formation, as the drainage region never reaches it due to the cap rock not being hydraulically connected to the reservoir. Including the cap rock allows the study of potential fracturing and OOZI in the vertical direction. Based on the issue related to the handling of inactive zones and the WHP constraints, the decision was made to control the well using fixed daily WHP, imported from measured data found in OIL FIELD MANAGER. This allows the constraint to be removed, eliminating any potential issues. It will also allow for more accurate fracture calculation, according to the REVEAL user guide, which states the calculation of fracture shape is done more accurately when dictated by a fixed WHP [24].

A new matching process was conducted, as detailed in Appendix [B]. In this process, the average injection temperature was used, with a key distinction being the injection rate as the matching parameter. Figure [19] shows the injection rate for the model against historical values. The match was considered satisfactory and showed no signs of numerical instability. BHP also had a good match, which was expected when running the well on historical wellhead pressure.

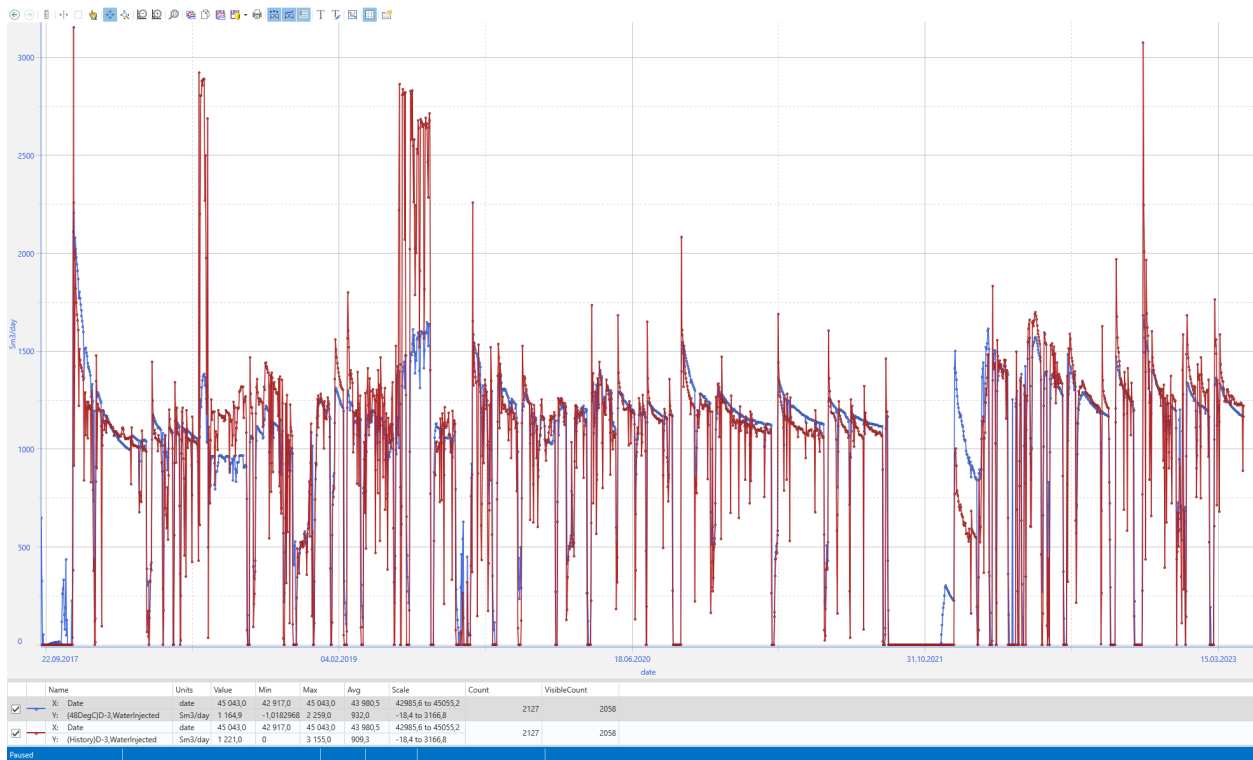


Figure 19: Injection well D-3: Injection rate for the fixed WHP/constant-BC sector model (blue) and historical injection rate (red).

A total of 6 different scenarios (S3-S8) were simulated using the constant BC sector model, either by prediction with the existing fractures from the base run or as a new schedule, at the initial reservoir conditions and no pre-existing fractures. To eliminate rapid changes in injection rate and pressure, as seen in the historical schedule, it was decided to run the simulations with fixed WHP. Doing so would reduce the number of varying input data to achieve trends that may be interpreted. The selection of different temperatures for the simulation runs varied based on the obtained results and the simulation time. The duration of injection periods at different temperatures was adjusted for the different scenarios as long as the observed trends exhibited a consistent pattern that allowed for meaningful conclusions to be drawn. An overview of the different simulation runs, and what the objectives are is provided in the next chapter.

8.4 Overview of simulation scenarios

Simulation scenario, S1:

The historical D-3 schedule up until 01.06.2021 is used together with the average injection temperature of 48 °C, to get information fracture initiation and propagation with regards to out-of-zone injection. Thereby a sensitivity analysis is performed using five injection temperatures of 8,30,50,70 and 90 °C to get results with the objective of analysing how different injection temperatures would of affected historical fracture initiation and propagation.

Simulation scenario, S2:

The simple thermal model is utilized with a schedule that injects above the in-situ minimum stress, using five different injection temperatures of 10, 30, 50, 70 and 90 °C. The objective is to analyze the effect on varying injection temperature (bottom-hole temperature) on fracture initiation and propagation, in a model consisting of a homogeneous reservoir and reduced number of variable input parameters.

Simulation scenario, S3:

The historical schedule is deleted, and replaced with a period of high pressure injection at a constant wellhead pressure of 288 bar, for a period of one year. The WHP is thereby reduced to 215 bar and injection is set back to the average injection temperature of 48 °C. The simulation starts with the initial reservoir conditions, and no pre-existing fractures. A sensitivity analyses with this new schedule is performed using three different injection temperatures of 8, 48 and 90 °C at the initial 1-year period. The objective is to analyse the effect different injection temperatures have on fracture initiation and propagation, and differences in injectivity index, under relative "extreme" operational conditions. 288 bar is the WHP used in the two intentional fracturing periods in the historic schedule, while 215 bar is the WHP before the first intentional fracturing period.

Simulation scenario, S4:

A period of pre-cooling is simulated to analyze the effect on fracture initiation and propagation, and injectivity. The BHP is set to 215 bar for 200 days, and start off with initial reservoir conditions and no pre-existing fractures. A sensitivity analysis is performed using three different injection temperatures of 8, 48 and 90 °C for the initial 20 days.

Simulation scenario, S5:

A restart file is created using the simulation run for the average injection temperature of 48 °C. A prediction schedule is developed, and a sensitivity analysis is performed at initial injection temperatures of 8, 30 48 and 90 °C. The prediction schedule consists of a 20 days period of pressurization at a WHP of 300 bar, followed by a period of 180 days at 240 bar and average injection temperature. 300 bar is used to initiate fracture propagation of the pre-existing fractures developed from the restart simulation run. Objective is to see how a new intentional fracturing period affect fracture propagation, final fracture size, and the effect on injectivity index. 240 bar is wellhead pressure used in the final stage of the historic schedule. The scenario is replicates a short period of intentional fracturing with high pressures at different injection temperature.

Simulation scenario, S6:

The scenario identical to S5, but is performed by assuming that there is no pressure drop

over the completion perforations. Perforation damage length is set to be 0 inches to achieve this. The objective is to validate the findings in S5.

Simulation scenario, S7:

Similar to S5, but without a restart file. A new schedule is developed with the same objective as S5, but with initial reservoir conditions and without pre-existing fractures. The schedule consists of a 20 day period of pressurization at a WHP of 288 bar, followed by a period of 180 days at 215 bar. A sensitivity analysis is performed using injection temperatures of 8, 48 and 90 °C in the initial 20 days pressurization period.

Simulation scenario, S7:

The restart file created in S5 is used, and a initial study on the effect of filter-cake build up is performed using a schedule consisting of a WHP of 240 bar for a period of 4 years. The scenario is simulated using a filter-cake model the average injection temperature of 48 °C, with and without fracture calculation enabled. A similar study is thereby performed using the same schedule to analyze the effect on a increasing injection temperature, with a increase of 2,5 °C/ 0.5 year and 5 °C / 0.5 year.

8.5 Assumptions

- Equal horizontal in-situ stresses are assumed, and the fracture is oriented to grow in the YZ plane.
- The position of the lower completion is considered acceptable for this study.
- Injected water is assumed to be pure, with no oil concentration. In the filter-cake simulation run, the concentration of suspended solids is set to 15 ppm, based on water samples comprising a mix of seawater and production water. This is the best approximation since no information on the filter-cake build up for injection well D-3 is available. The filter-cake build-up is assumed to be external and compressible.
- A wettability model is not utilized, and the changes in interfacial tension as a function of temperature are disregarded. This decision is based on the understanding that wettability primarily impacts sweep efficiency, while this study focuses on fracturing and injectivity in the near-wellbore area.
- The extended schedule period is deemed acceptable, considering no major workovers occurred.
- Default values for fracture properties are assumed due to the unavailability of actual data.
- The perforation data relies on information provided by the supplier. Perforation damage permeability is determined based on the dimensions and liquid rate, which is further adjusted during the history-matching process in the original full-field model. The value for perforation damage is considered to be highly uncertain. It is further assumed that the perforation pressure drop is primarily influenced by linear Darcy flow, and as a result, the turbulence factor is set to zero.
- The input data used in the original full-field simulation and the modifications made during the history-matching process are presumed to reflect reality to the best extent possible, considering the available field knowledge and information on high-pressure injection wells.

8.6 Input data

Input data for stress properties at the Skagerak 2 formation, fracture seed status and default values, and completion perforation input data is given in table [1],[2] and [3], respectively. Additional data can be accessed within the study's REVEAL files (Property of Aker BP).

Skagerak 2 formation		
Stress properties	Value	Unit
Young's modulus	8.0E+9	Pa
Poisson's Ratio	0.3	[-]
Min. Horizontal stress gradient	0.159	bar/m
Thermal expansion coefficient	1.00E-05	1/Deg C
K1C intensity	250	Psi.(ft) ^{1/2}

Table 1: Stress properties - Skagerak 2 formation.

Fracture seed parameters:	Value/status
Initial status	Closed
Orientation plane	YZ plane
Half Height Top/Bottom [m]	0.3048
Half Length [m]	0.3048
Minimum fracture conductivity [D.m]	0.3048
Closed fracture width [cm]	0.03048
Fracture topology	Variable
Double wing/single wing	Double wing

Table 2: Fracture seed status and default values.

Completion perforation data		
Parameter	Value	Unit
Flow area / length	0.74	in ² /ft
Damage length	1	inches
Damage permeability	2500	md
Turbulence factor	0	1/m

Table 3: Completion perforation input data.

8.7 Constraint violation and inactive cells

The interaction between WHP constraints and inactive cells may be the explanation for the rapid increase in BHP for D1, as previously depicted in figure [13]. The scheduled history is being run with rapid changes, controlling the injector with a fixed rate and a maximum WHP constraint.

The issue with WHP constraints can be explained by considering the early times before fractures have established:

1. Initially, the solution is obtained using the target fixed rate, leading to time step chopping to achieve a converged solution with significant pressure changes.
2. Convergence is required before checking for constraint violations, necessitating time step chopping. Besides reducing the time-step size, numerous unused solves are performed to limit excessive pressure changes.
3. The time step is decreased, resulting in large pressure changes, and subsequently detecting a constraint violation that needs to be resolved. This may involve further time step chopping to reduce all pressures and satisfy the constraint. In a few cases, as the case for injection well D-1, the solver accepts a solution despite the constraint not being fully met.

Consequently, a substantial reduction in time steps, extensive CPU cycles, and occasionally a poorly converged solution occur due to the significant pressure increase and subsequent reduction during the solution. Differences in how constraint switching is handled might be the cause of some variations in results between REVEAL 10.0 and REVEAL 9.5 [40].

In REVEAL 9.5, if a constraint is violated after convergence, the solver will be restarted with the new well constraint, repeating as necessary. This has in REVEAL 10.0 been limited to happen only twice, due to special cases involving conflicting constraints. Changing a constraint for one well can impact others, leading to incomplete or slow solves caused by cyclic constraints. The assumption was to check for well constraint violations up to two times with a re-solve, then accept the converged solution (which may still have constraint violations) and address additional conflicting constraints in the subsequent time step. Hence, the constraint violations observed in REVEAL 10.0, which were previously suspected to indicate incomplete convergence, may arise. In some cases, particularly at the start of well injection, this significantly affects the initial growth of fractures and subsequent results, especially when the fracture penetrates different layers [40]. Figure [20], shows closeup of this behavior, occurring for injection well D-1.

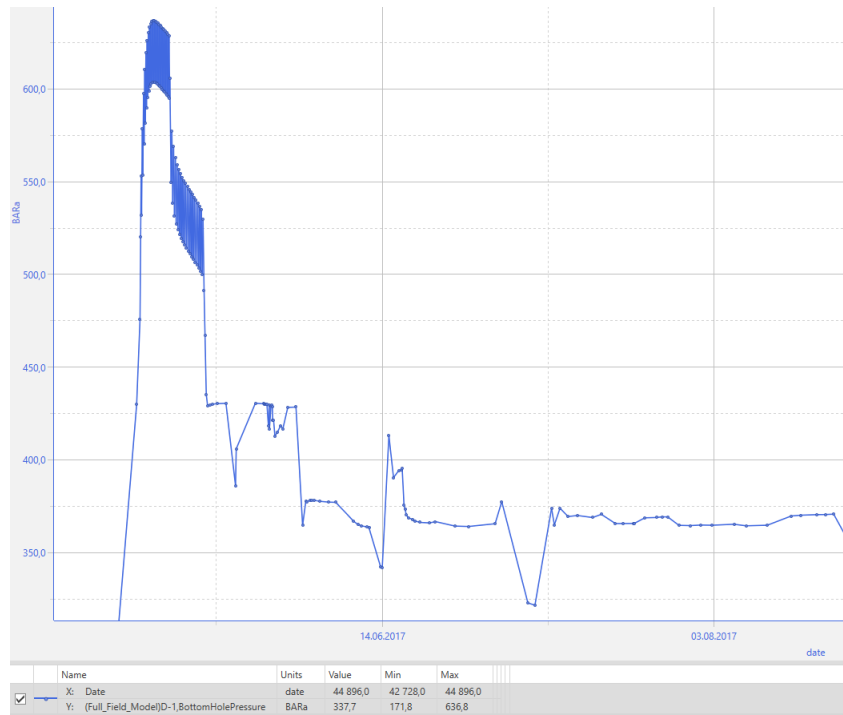


Figure 20: Numerical instability for injection well D-1 (BHP).

While it is recommended to have simulation models without "holes," it is sometimes necessary to work with the available models, as is the case for this thesis. The issue with inactive cells also contributes to the problem described above, specifically when fractures extend into inactive regions. In such cases, a fracture finite element may partially extend inside and outside an active region. Nodes within the active region correctly interpolate reservoir properties, while nodes within the inactive region have limited or zero leak-off mobility and may experience lower interpolated reservoir pressures. This leads to an artificially large leak-off rate within the finite element triangle, resulting in a reduced fracture size [40]. History matching may be improved by using these WHP constraints, but it should be noted that issues may arise as a result.

9 Results and analysis

9.1 Thermo-elastic stress reduction potential

9.1.1 Manual calculation

Table [4] and Figure [21] present the thermo-elastic stress reduction potential for the Skagerak 2 formation, considering a reservoir temperature of 98°C. The results demonstrate an increasing stress reduction as the injection temperature decreases. Specifically, lower injection temperatures exhibit a greater potential for decreasing the in-situ minimum horizontal stress than warmer injection temperatures.

The calculations were performed using various injection temperatures ranging from 8 °C to 90 °C and the reservoir temperature. It is important to note that these calculations do not account for the change in bottom-hole temperature (BHT), which represents the actual stress-reducing temperature experienced by the reservoir. The BHT value will vary for each injection temperature depending on the injection rate. The VLP curve previously shown in figure [49] illustrates this.

BHT [°C]	Δ Stress reduction [bar]	New Shmin [barg]
90	9	400
80	21	388
70	33	376
60	44	365
50	56	353
40	68	341
30	79	330
20	91	318
10	103	306
8	105	304

Table 4: Thermo-elastic stress reduction at different injection temperatures for D3 formation - Table.

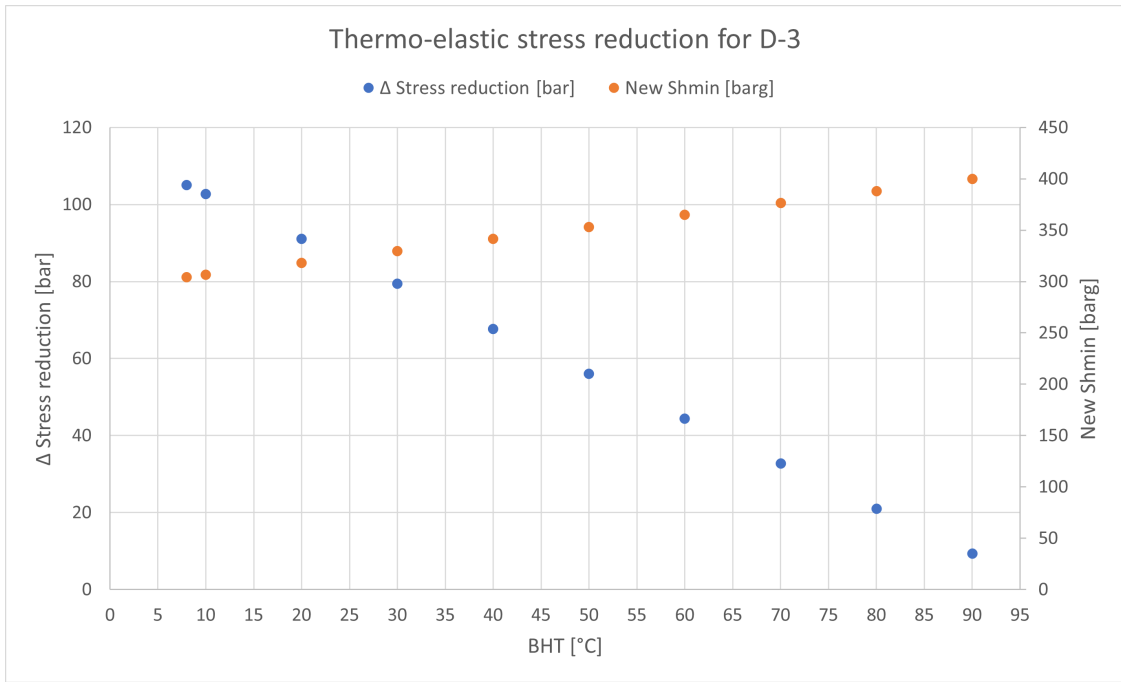


Figure 21: Thermo-elastic stress reduction at different injection temperatures for D3 formation - Graph.

9.2 Effect of injection temperature variation on historical fracture development

9.2.1 S1

Figure [22] shows the BHP and fracture area for fracture seeds 1, 4 and 5 for the average injection temperature simulation run. Figure [23] shows the 3D visualization of the final fracture sizes, with the thermo-elastic stress reduction indicated by a color bar.

The results show that fracture initiation only occurred for the mentioned fracture seeds during the two periods of intentional fracturing. It also shows the thermo-elastic stress reduction of around 50 bar near the well-bore area. The thermo-elastic stress reduction is consistent with the manual calculation shown in the previous chapter and verifies the thermal stress reduction calculations performed in the model.

The 3D visualization on 01.06.2021 shows that fracture seed 5 propagates until it reaches the no-flow impermeable inactive zone below the Skagerak 2 formation. After reaching this zone, it continues to propagate in the horizontal direction, as it cannot overcome the rock strength of the underlying Weathering Profile. The fracture will experience no leak-off into the no-flow region, increasing in-situ fracture pressure. The resulting behavior is the continuation in propagation, as long as the in-situ fracture pressure allows it. There are no indications of fracturing down and out of the Skagerak 2 formation, followed by out-of-zone injection. This observation aligns with real-world data, where no abrupt rise in injectivity or out-of-zone fractures has been registered. Fracture seed 5 initiates later than fracture seeds 1 and 4. The reason for this can be seen in the 3D visualization, where the thermo-elastic stress reduction is lower for the rock formation near the lower completion compared to the upper completion. The pressure required to initiate fracture seed 5 is, therefore, higher. The fracture seed is therefore initiated after a more extended period of "cooling" and stress reduction.

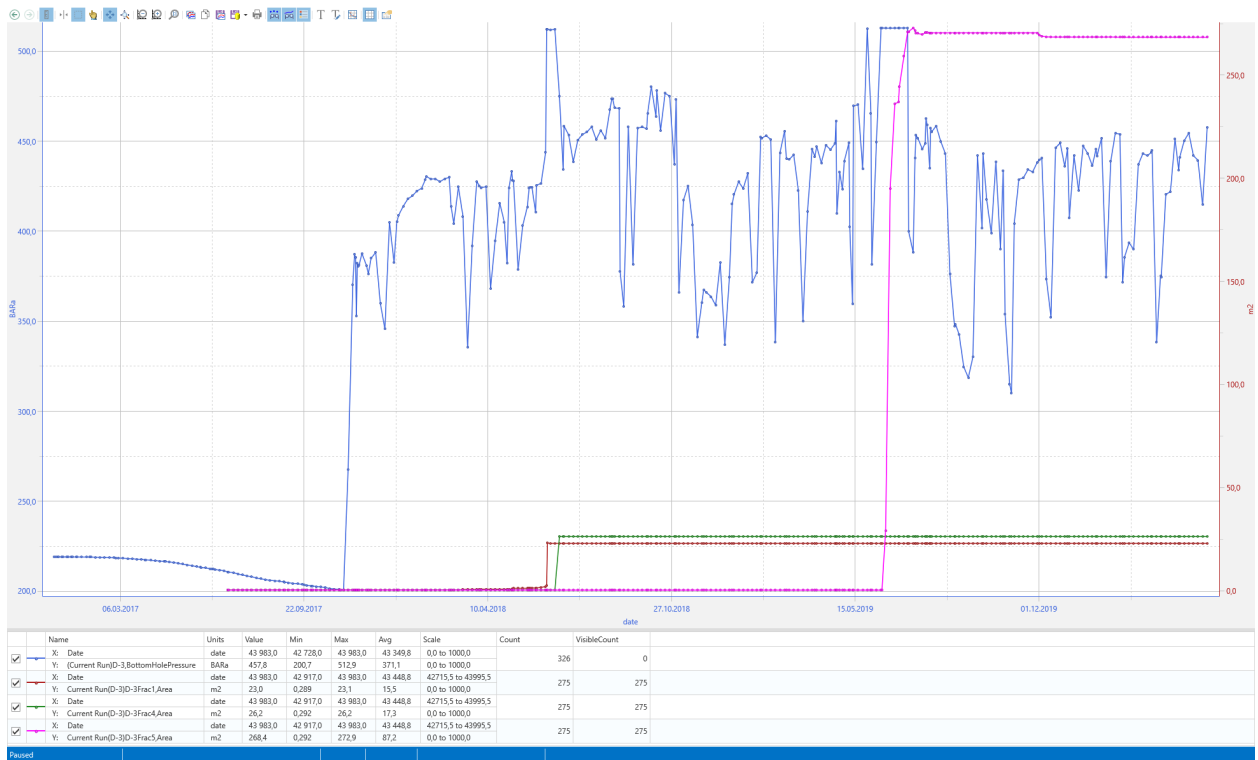


Figure 22: S1: BHP and fracture size for the average injection temperature.

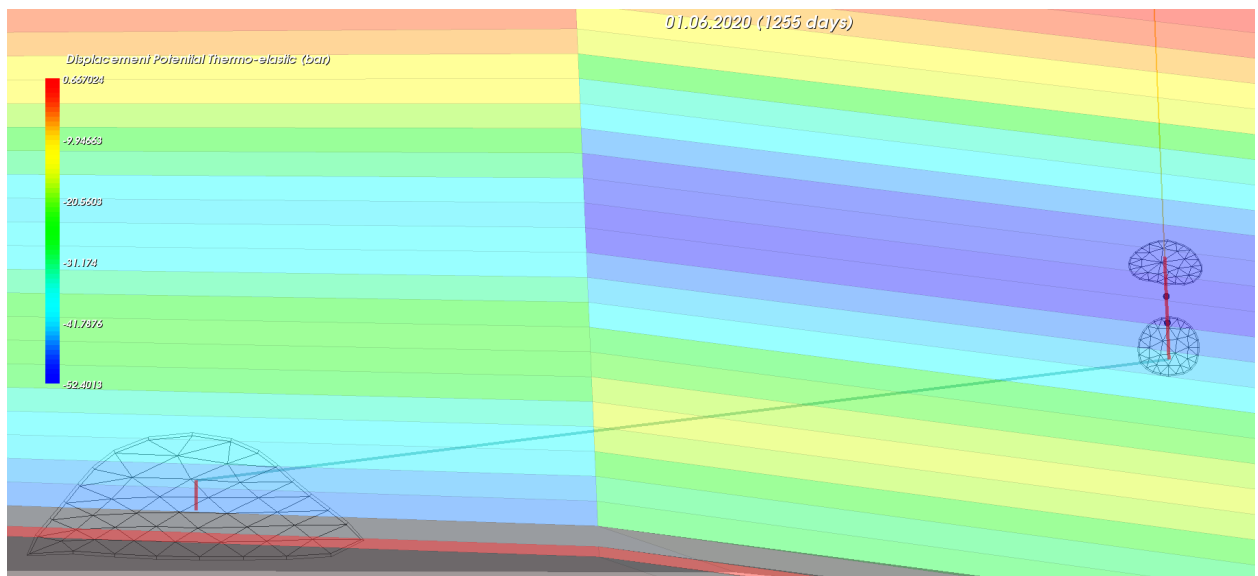


Figure 23: S1: 3D visualisation of final fracture size and thermo-elastic stress reduction.

Figure [24] show the final fracture area of fracture seeds 1, 4, and 5 for the simulation runs at different injection temperatures.

The results indicate a larger total fracture area at 8°C compared to 90°C, which is consistent with the theory of thermal induced fracturing, where the reduction in temperature reduces in-situ stress resulting in a more significant fracturing. 90 °C have a smaller total fracture area and experience no fracture initiation for fracture seed 5. This is because of the reduced thermo-elastic stress reduction. The trend between 8 °C and 90 °C is challenging to interpret. The general trend indicates that colder injection temperature increases the total fracture area. The results show that multiple fracture seeds interact and that a change in injection temperature affects the final fracture size. Results from the simulation run with an injection temperature of 8 and 90 °C are consistent with the study mentioned in chapter [6.6], where the pre-injection of cold water developed more fractures and a more extensive total fracture area. However, based on the obtained results, drawing definitive conclusions about the precise impact of injection temperature and identifying an "ideal" temperature for fracturing purposes is not possible for these simulation runs.

The non-linear behavior of the results may be due to the rapid changes in operation conditions as a consequence of controlling the well a historic schedule. A rapid change in injection pressure and rate will create rapid changes to the same parameters at the bottomhole location. Rapid changes may be a reason for the instability, together with the fact that the reservoir is highly heterogeneous.

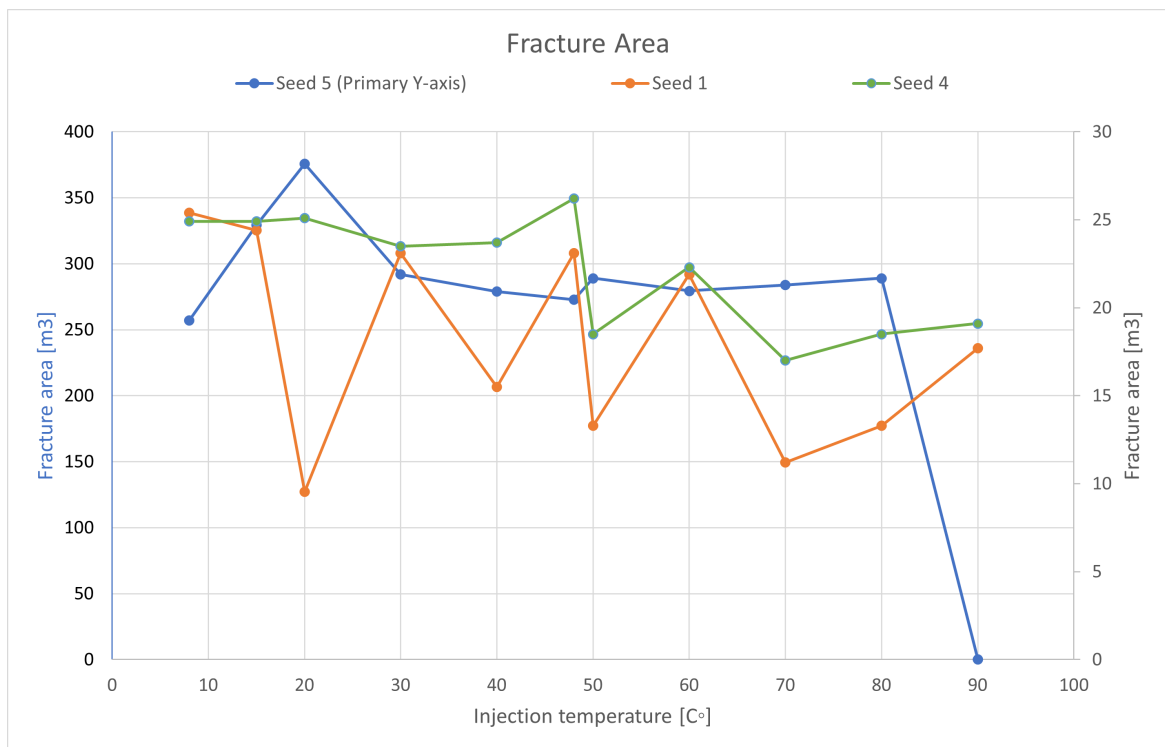


Figure 24: S1: Fracture area at different injection temperatures, for fracture seed 1, 4 and 5.

As there are two periods in the schedule with high injection pressure and rate, done intentionally to create fractures, the time at which the different simulation runs initiates fractures will affect the total fracture size. Initiation occurs earlier for the colder scenarios due to the thermo-elastic stress reduction. Different initiation times create a timeline in the schedule where the colder scenarios are exposed to the intentional high-pressure period for a more extended period. As the fractures initiate and propagate at different rates in the schedule, the degree of leak-off, a deciding factor for the final fracture size, will be different when injection pressure is at its highest. This can be a significant contributor to the achieved non-linear results. The time of initiation at different times in the historic schedule is shown in figure [25], where fracture seed 1 for different simulation runs is shown, together with the BHP for the average injection temperature run, as a reference to the historical schedule.

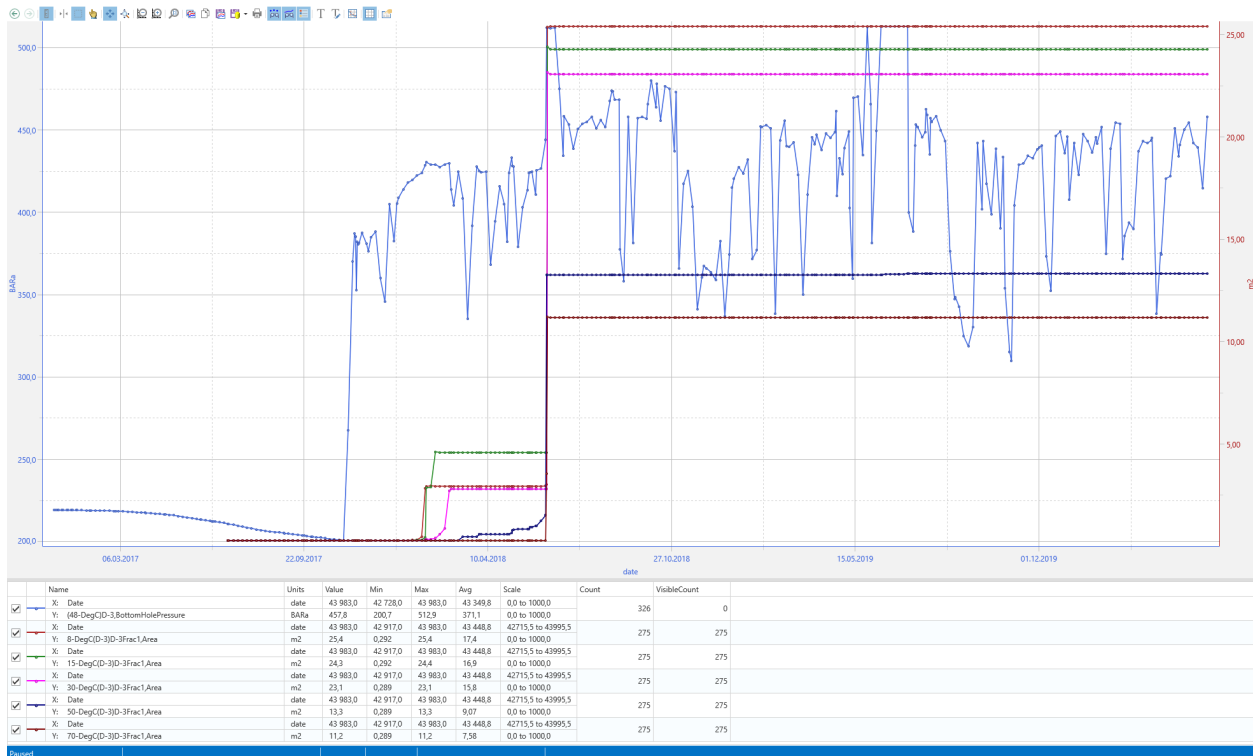


Figure 25: S1: Fracture area for fracture seed 1, and historical schedule.

The modifications made to a reservoir model in order to achieve a good history match do not guarantee that the implemented changes accurately reflect reality. Reservoir simulation inherently involves a high level of uncertainty and unknown parameters. A successful history match is determined by achieving similar values for historical bottom-hole pressure (BHP) and injection rates, which allows for an estimation of fracture development and an understanding whether fractures are contained within the reservoir. This aligns with the purpose of REVEAL, which is designed to address such questions.

Performing sensitivity analysis with a wide range of input parameters may not result in linear output responses, especially considering the non-linear nature of fracture calculations and real-life phenomena, particularly in highly heterogeneous reservoirs. REVEAL provides users with the relationship between different parameters for a given case, enabling a deeper understanding of the mechanisms governing fracture initiation and propagation under various operational conditions. This understanding can be further enhanced by us-

ing constant input data and running simulations with simple models parallel to complex sector models.

9.3 Effect of injection temperature variation on fracture development - Simple thermal fracture model

9.3.1 S2

Figure [26] show fracture area, maximum leak-off coefficient, and maximum center width for different bottomhole temperatures from the simple thermal fracture model. The results show a close to a linear relationship between fracture area, leak-off coefficient, and center width at different bottomhole temperatures. As temperature reduces, the increase in viscosity yields a lower leak-off rate to the nearby rock matrix. The reduced leak-off creates a bigger in-situ fracture pressure, which leads to a more significant fracture propagation rate. The reduction in temperature also contributes to lowering the in-situ horizontal minimum stress and contributing to the increased rate of propagation and earlier fracture initiation. The result is a bigger final fracture size for colder bottomhole (injection) temperatures. The results for this simple thermal fracture model indicate that reducing the amount of varying input data and reservoir complexity makes the relationship between temperature and fracture size more linear.

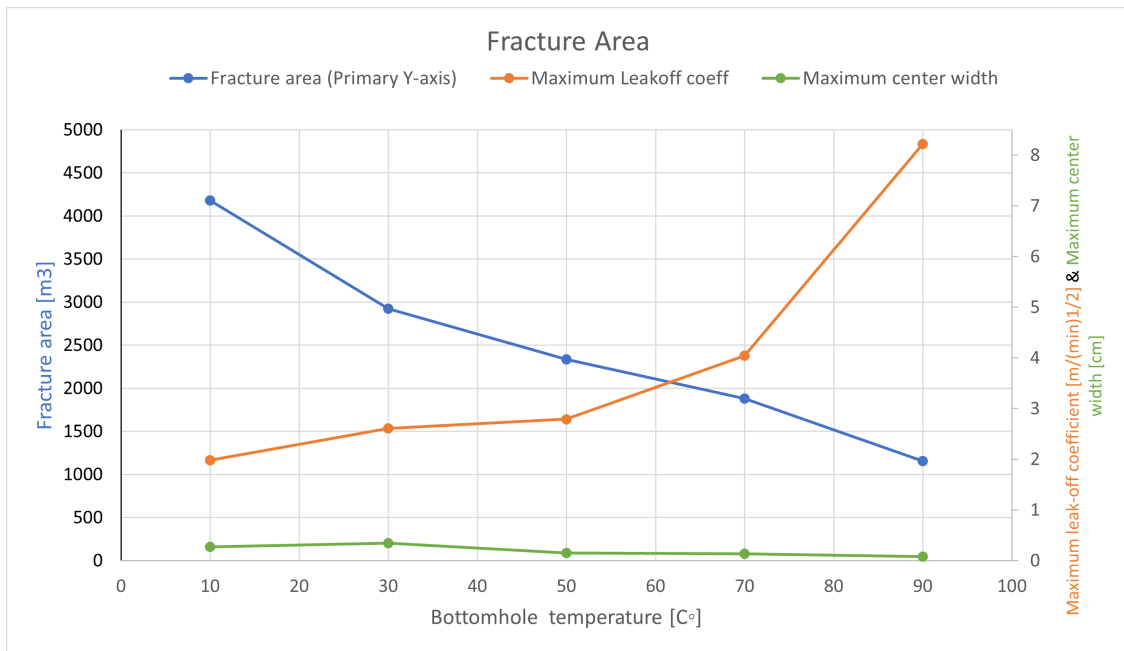


Figure 26: S2: Fracture area, maximum leak-off coefficient and center width at different bottomhole temperatures - Simple thermal fracture model.

9.4 Effect of injection temperature variation on fracture development and injectivity index

9.4.1 S3

Table [5] shows the total fracture area, cumulative water injected, and the final injectivity index (end of schedule) for the initial injection temperatures of 8, 48, and 90 °C. The results indicate a more extensive fracture area for colder injection temperatures, consistent with the theory of thermo-elastic stress reduction and the results from the previous simulation runs. Warmer injection temperature yields higher cumulative water injected and a lower final injectivity index. To better understand why this occurs, we have to look at the trends.

Figure [27] shows the BHP and injectivity index trends for injection temperatures of 8, 48, and 90 °C. The BHP trends show a higher BHP for colder injection temperatures due to the higher viscosity creating flow resistance. The injectivity trends show that a higher injection temperature gives a higher injectivity index during the initial high-pressure period. The opposite is observed after the injection pressure is reduced and the injection temperature returns to the average injection temperature. The initial instability in the injectivity curves is related to fracture initiation and changes to the fracture width during propagation.

The lower viscosity for warmer injection temperatures causes the high initial injectivity index observed in the high pressure period. Low viscosity creates a lower flow resistance, allowing for a higher water rate. This effect is initially more substantial than the effect that colder injection temperatures have on fracture area. Colder injection water creates higher viscosity and a higher flow resistance contributing to the initial "low" injectivity index. After the initial high-pressure period, the injectivity index increases to be higher for colder injection temperatures, which is consistent with the theory on fracture size and injectivity and can be attributed to the more extensive fracture areas.

Figure [28] shows the fracture area for fracture seed 1 at the three injection temperatures, indicating an earlier fracture initiation for warmer injection temperature, which is in contrast to the results achieved in S1 and S2. The early initiation for warmer injection temperatures can be attributed to the temperature effect on water mobility and the injection schedule. A higher injection temperature leads to a lower viscosity, thus, higher water mobility. This creates a more rapid pressurization of the surrounding cells in the well-bore area, as indicated in figure [29], showing the cell pressure at the cell block for fracture seed 1. Higher in-situ pressure will initially increase the minimum in-situ stress (poro-elastic stress effect) but will come to a point where the reservoir pressure exceeds the stress, and fracturing starts. A lower injection temperature gives a lower viscosity and lower water mobility, leading to a reduced area extent of the thermo-elastic stress reduction. The reduced mobility effect is amplified by the fact that the Skagerak 2 formation is highly heterogeneous, with the cell block at the fracture seed 1 location having a permeability of 52.3 mD. Therefore, the thermo-elastic stress reduction is smaller than the effect that higher injection temperature and increased mobility have on in-situ pressure. This is especially true for this simulation run, which uses an "extreme" initial pressurization period with high injection pressure for a long period (1 year). The earlier fracture initiation did not occur for warmer injection temperatures for the previous simulation runs due to the extended pre-cooling period during injection below the in-situ stress before the intentional fracturing period. It may be noted that the schedule in this simulation run is used to amplify the effect of varying injection temperature on fracture initiation and propagation

and is not representative of how the well is controlled in real life.

Injection temperature	Fracture initiation	Total fracture area	Cumulative water injected	Final injectivity
[Deg C]	Fracture seed	[m2]	[m3]	[Sm3/day/bar]
90	1,4	9.542	1.25E+06	232.0
48	1,4,5	49.11	1.22E+06	244.4
8	1,4,5	350.3	1.17E+06	255.1

Table 5: S3: Initiation status, total fracture area, cumulative water injected and final injectivity index for initial injection temperature = 8, 48 and 90 °C

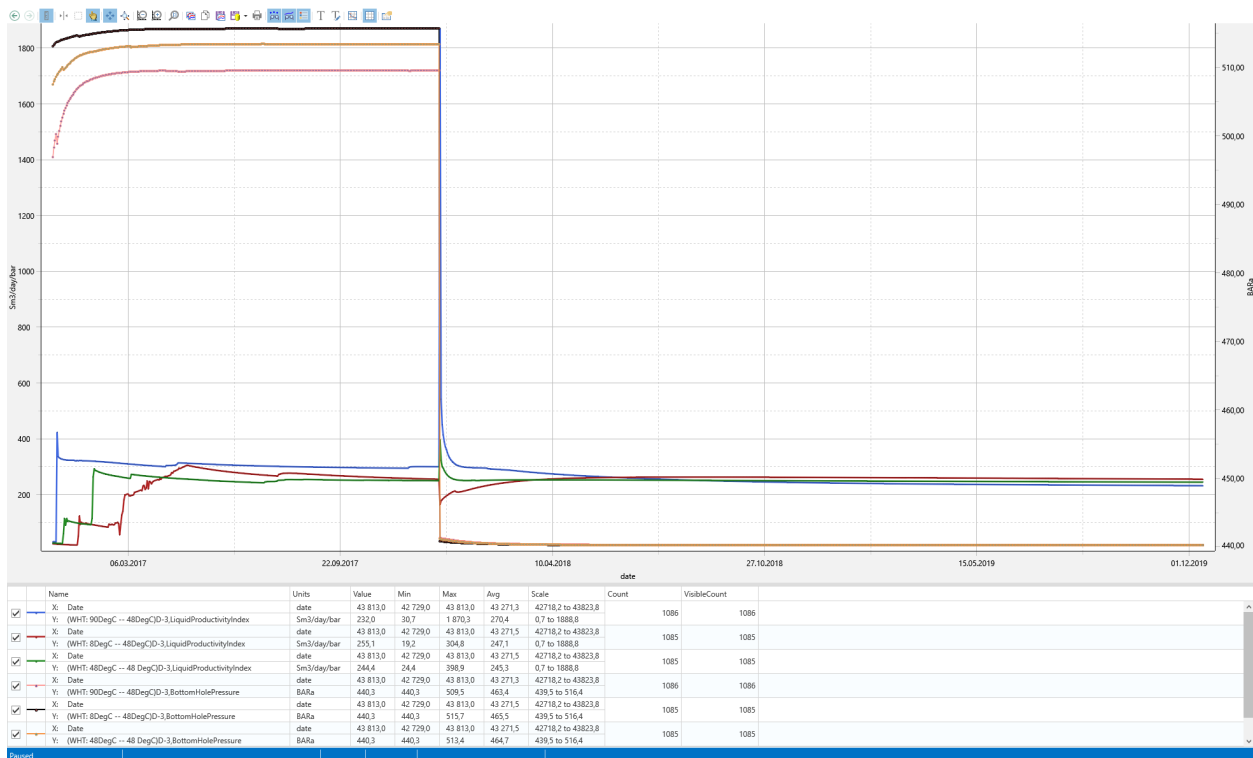


Figure 27: S3: BHP and injectivity index for initial injection temperature = 8,48 and 90 °C



Figure 28: S3: Fracture area for initial injection temperature = 8, 48 and 90 °C (fracture seed 1)

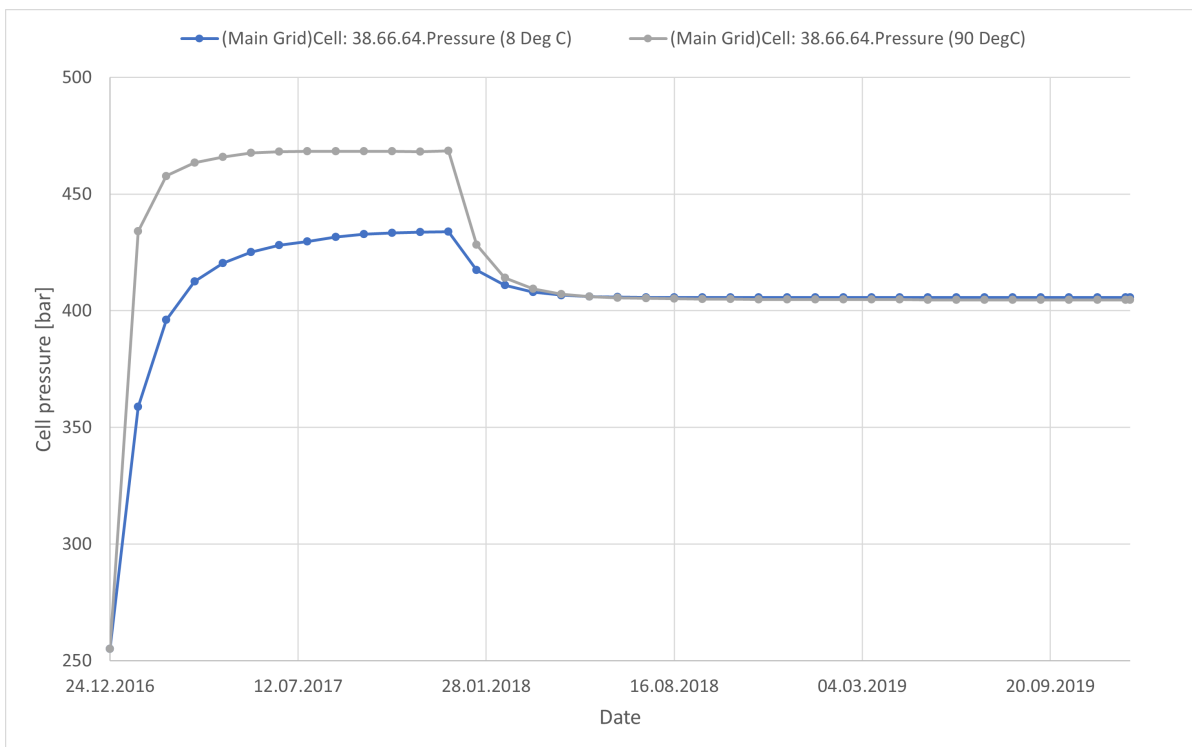


Figure 29: S3: Cell pressure (38.66.64) at initial injection temperature = 8 and 90 °C

The simulation scenario highlights the effect that temperature has on fracturing and the effect that fracturing has on injectivity. It also highlights that the relationship between fracturing and injectivity at different injection temperatures is case-dependent and strongly connected to how the injection well is controlled regarding injection pressure and temperature. The effect of thermo-elastic stress reduction could be more significant for this simulation if the reservoir temperature were higher. A higher reservoir temperature could potentially create higher injectivity for colder injection temperatures in the initial stage. The effect of thermo-elastic stress reduction could also be more extensive for a colder injection temperature if the schedule injected at a lower pressure.

The results for the simulation runs show that when the injection pressure is significantly high enough to initiate fractures, regardless of the injection temperature, a higher injection temperature will give a higher initial injectivity index. This period will contribute to higher cumulative water injected at the end of the schedule. As injection pressure is reduced and an average injection temperature is used, the injectivity will be a function of the size of the developed fractures. Comparing the results with simulations S1 and S2 shows that the thermo-elastic stress reduction and its effect on fracture initiation is time-dependent.

9.4.2 S4

Figure [30] shows the injectivity index for the initial injection temperature of 8, 48, and 90 °C. The results indicate a higher injectivity index during the initial 20-day period for higher injection temperatures caused by higher water mobility. The difference between the three injectivity trends is reduced as the injection temperature returns to the average of 48 °C. The average injection temperature continues to cool down the reservoir and reduce the in-situ stress to the point of fracture initiation. Correspondingly, the injectivity index is increased, where the simulation run with the lower initial injection temperatures has the highest injectivity index. Figure [31] shows the total fracture area for the simulation runs with initial temperatures of 8, 48, and 90 °C. A lower injection temperature reduces the in-situ stress in the initial period, leading to an earlier initiation and bigger fracture size. The relatively low injection pressure resulted in fracture seed 1 being the only seed initiated for all injection temperatures.

The results from the simulation runs show that the injection of cold water (seawater as an example) for a short period has a positive effect on the injectivity index as it accelerates fracture initiation and propagation when injecting under the minimum horizontal stress for the Skagerak 2 formation, with no pre-existing fractures. It also shows that the effect of thermo-elastic stress reduction is higher than the mobility effect for this scenario. This confirms that the relationship between fracturing and injectivity at different injection temperatures is case-dependent and strongly connected to how the injection well is controlled. The schedule in this scenario is more realistic to how the D-3 injection well was controlled at the early injection stage.

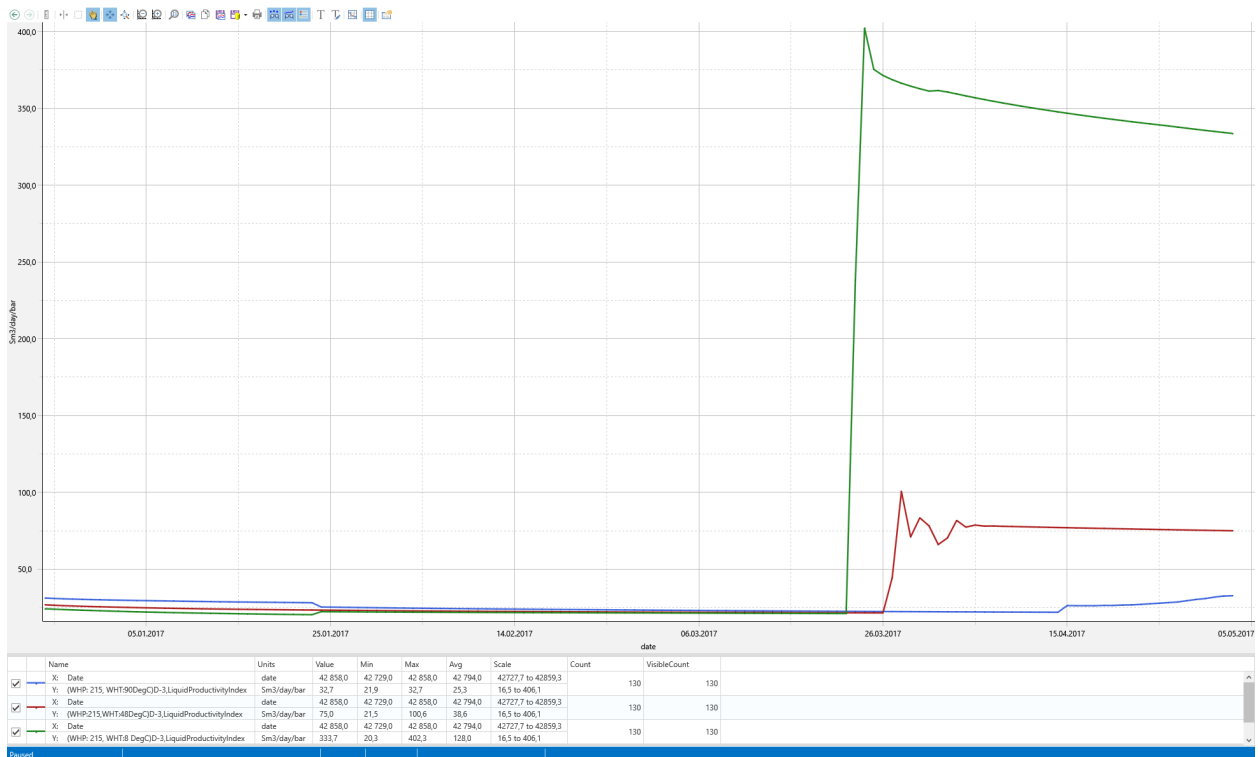


Figure 30: S4: Injectivity index for initial injection temperature = 8,48 and 90 °C

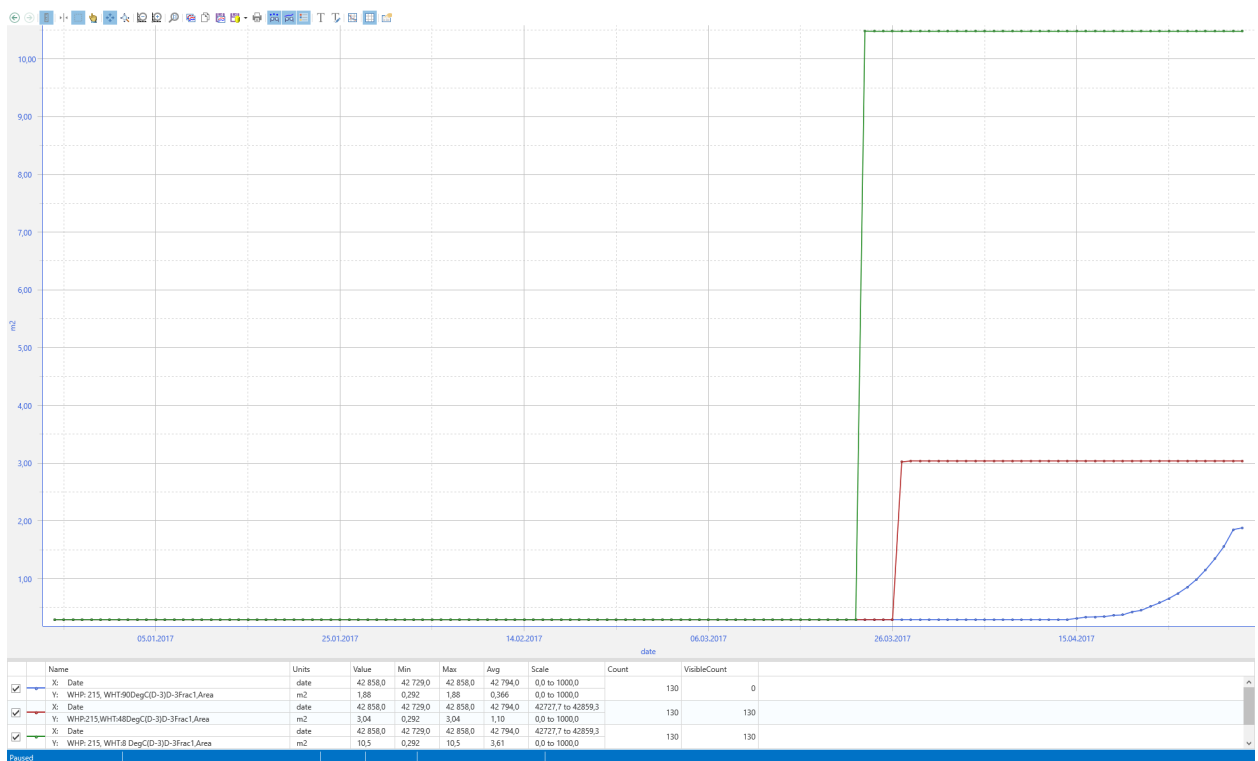


Figure 31: S4: Fracture area for initial injection temperature = 8, 48 and 90 °C (fracture seed 1)

9.5 The effect of injection temperature variation on fracture development during short intentional fracturing period, comparing pre-existing fracture and no pre-existing fracture scenarios

9.5.1 S5

Figure [32] shows the BHP and BHT for the historical simulation run using the average injection temperature and the prediction run consisting of a short intentional fracturing period at a WHP of 300 bar and injection temperature of 8 °C. The figure illustrates how scenario S5 is based on a restart file, where the reservoir and fracturing conditions from the historical run are used as a starting point. The figure shows an increase in BHT for every injector shut-in period, as the reservoir is not exposed to "cold" injection water. The increase in reservoir temperature is why injectivity may increase after shut-in due to a warmer reservoir increasing the water mobility.

Figure [33] shows the total fracture area and final injectivity index for the simulation run with initial injection temperatures of 8, 30, 48, and 90 °C during the high injection pressure period, together with the pre-existing fracture area. The figure shows an opposite relationship between fracture area and injectivity index at different injection temperatures compared to the previous simulations without pre-existing fractures. The figure shows that the injectivity index and total fracture area are reduced at lower injection temperatures.

The opposite relationship can be attributed to the reservoir having pre-existing fractures and a reservoir that has already been cooled down from the historical injection of water at 48 °C. The temperature difference between the colder injection temperatures and the reservoir is therefore reduced, reducing the effect of thermo-elastic stress reduction. The thermo-elastic stress reduction effect in the near-wellbore area at an injection temperature of 8 °C is approximately comparable to that of injecting with 90 °C under the initial reservoir conditions. Therefore, the effect will be lower than the effect that higher injection temperature and a lower viscosity have on the in-situ pressure.

Figure [34] and [35] illustrates the pressure at various depths along the tubing, accompanied by the tubing outflow pressure, reservoir pressure, and water injection rate for injection temperatures of 8 and 90 °C, respectively. The results show a higher BHP for 8 °C, which is expected due to higher viscosity. This is in accordance to figure [16], previously shown in chapter [8.3], where a lower injection temperature yields a higher BHP. A higher BHP may also be due to the fracturing and reduced propagation rate for colder temperatures. The figures show a more significant completion pressure drop between the BHP and tubing outflow pressure (named tubing inflow pressure in Reveal) for an injection temperature of 8 °C. The tubing outflow pressure is similar to the pressure experienced by the pre-existing fractures.

When a pre-existing fracture is present, the leak-off rate will be more extensive compared to a scenario with no pre-existing fractures. The presence of pre-existing fractures causes a larger water flow rate from the completion to the reservoir. A larger flow rate creates a more significant pressure drop over the completions. Completion pressure drop is driven by the perforation geometry and is a mix of Darcy and non-Darcy flow. For these wells it is assumed a Darcy dominated pressure drop characterised by effective flow area and perforation tunnel permeability and length. This pressure drop is proportional to the rate and is an important factor in determining the rate of fracture propagation. Another critical factor is the fluid viscosity. The viscosity table in Appendix [D] shows how a reduction in temperature from 90 to 8 °C yields a reduction in viscosity by a factor

of approximately 3. The Darcy term shown in chapter [7.4], shows that an increase in viscosity will increase the perforation pressure drop. The results showing a reduced fracture area for colder injection temperatures are related to an increased perforation pressure drop due to increased viscosity. An increase in perforation pressure drop reduces the in-situ fracture pressure. It affects the potential for fracture propagation when the leak-off rate is sufficient to avoid pressure build-up above the minimum horizontal stress. The above mentioned statement is valid under the assumption that the pressure drop is dominated by linear Darcy flow. Further investigation into the actual perforation pressure drop requires detailed modelling of the D-3 perforations, to validate the viscosity effect on perforation pressure drop and fracture propagation, as observed in this scenario.

After running the simulation with an initial injection temperature of 8 and 90 °C, we decided to re-run it with a 20 day shut-in period before the high pressure intentional 20-day period. The reason for this was to determine if closed pre-existing fractures would undergo the same relationship between injection temperature and fracture propagation as the pre-existing open fractures from the initial simulation run. The results were conclusive - the same relationship was achieved as in the initial run, with a higher injection temperature resulting in more extensive fracture propagation and final fracture area.

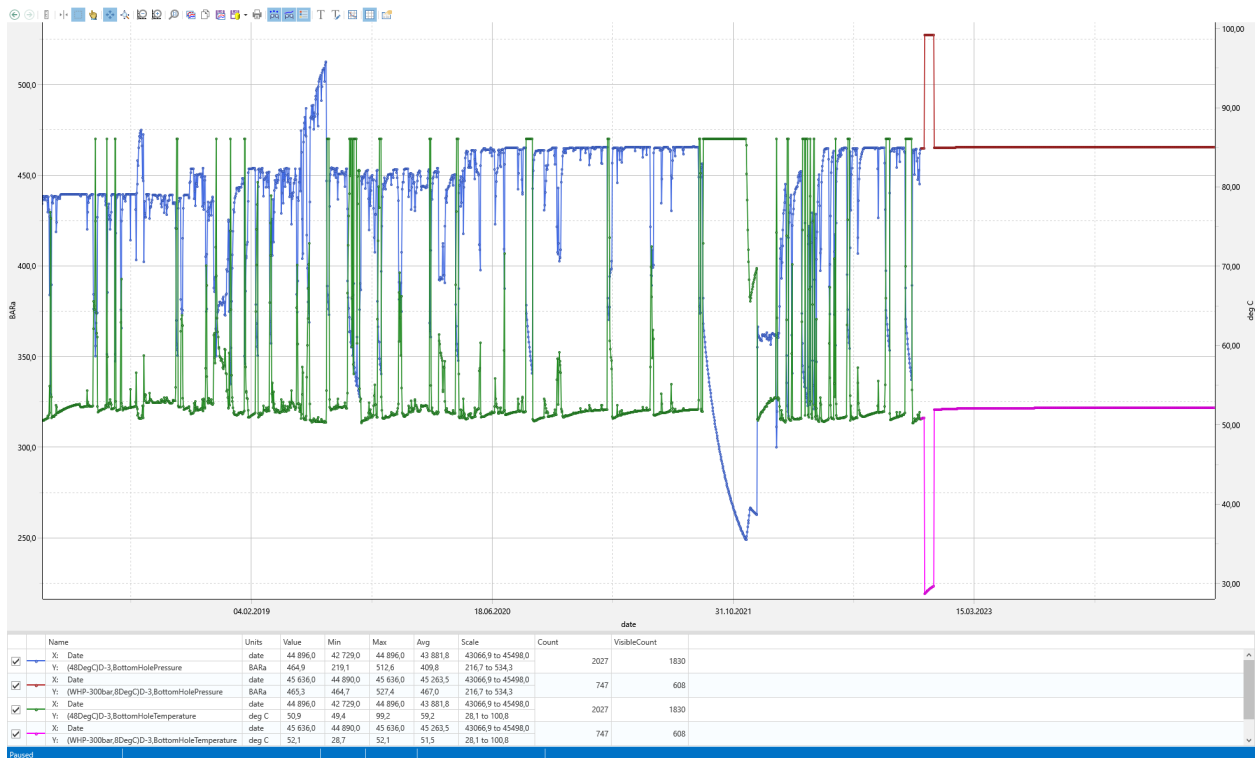


Figure 32: S5: BHP and BHT for simulation run with historical schedule, and prediction run with short high pressure injection period

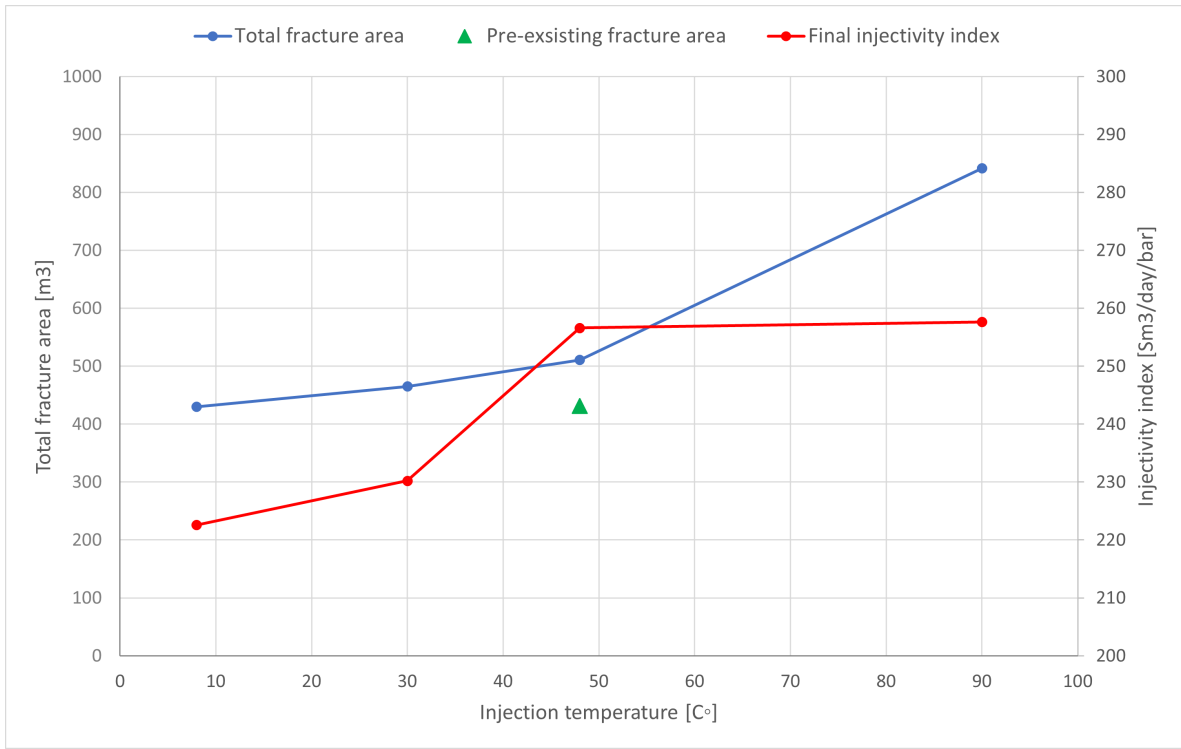


Figure 33: S5: Total fracture area, final injectivity index and pre-existing fracture area for simulation runs with initial injection temperature = 8, 30, 48 and 90 °C



Figure 34: S5: Tubing pressures, reservoir pressure and water injection rate - initial injection temperature = 8 °C

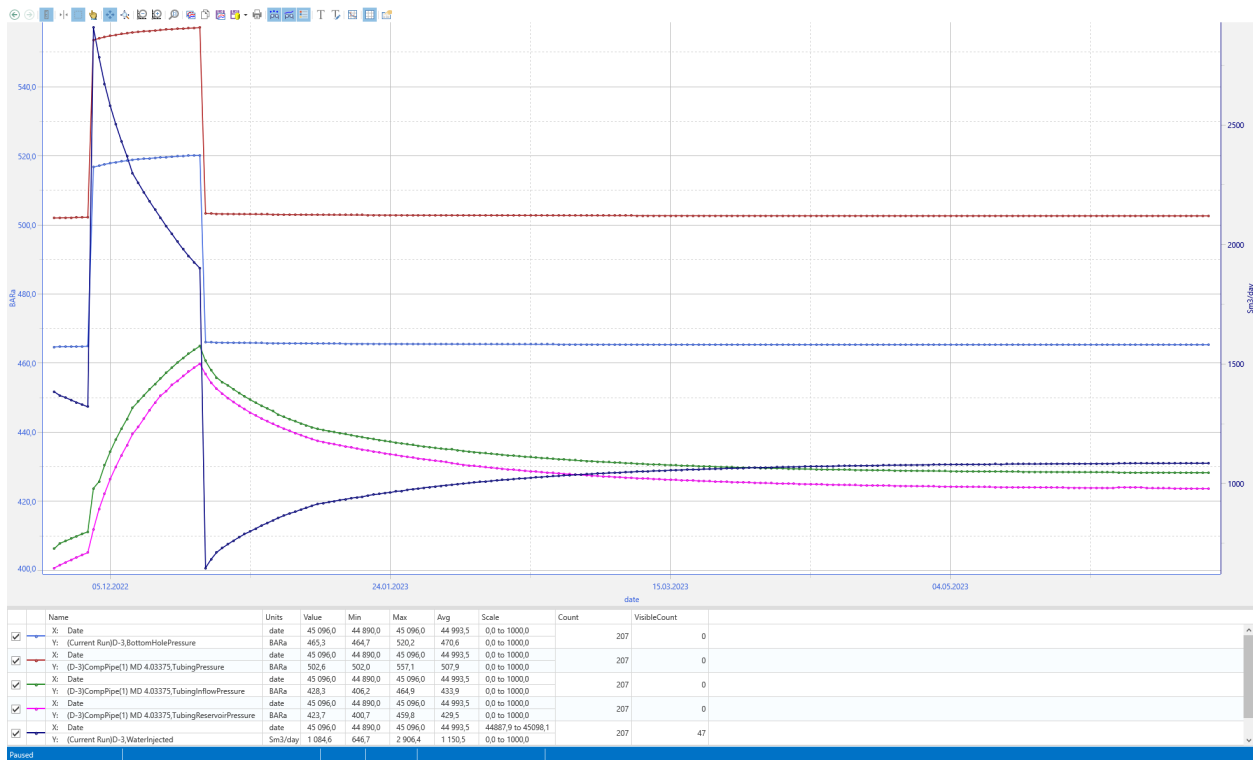


Figure 35: S5: Tubing pressures, reservoir pressure and water injection rate - initial injection temperature = 90 °C

The results obtained in this simulation scenario are similar the findings from the study conducted by Yu Juang et al., as mentioned in chapter [6.6]. The study demonstrated that temperature plays a crucial role in hydraulic fracturing, affecting various mechanisms including fluid viscosity. The study revealed that injecting cold fracturing fluid resulted in a deceleration of fracture propagation, contrasting the isothermal fracture model that neglected temperature and viscosity effects.

In chapter [6.6], reference was made to another study that explored the impact of different fluid viscosities on fracture propagation. The study revealed that the use of high viscosity fluid could result in a slowdown of fracture propagation due to the presence of a gap between the fracture tip and the front of the fracturing fluid, which may be realistic. However, it is worth noting that this phenomenon was observed specifically with glycerol, a fluid with considerably higher viscosity than the "cold" water utilized in this simulation. Furthermore, this particular phenomenon is not accounted for by REVEAL and is , therefore, irrelevant to the observations in this simulation scenario.

The findings from the results in this scenario may form a part of the explanation for the non-linear results achieved in simulation scenario S1, where there are two periods of intentional fracturing at high injection pressure, where fracture propagation of pre-existing fractures are observed. Depending on the conditions, affecting the degree of leak-off and total water rate through the completion, the viscosity effect on pressure drop over the perforations and the subsequent effect on fracture propagation may vary. Adding this with different initiation times, at different operational conditions in the historical schedule, reservoir heterogeneity and variations of bottomhole pressure and temperature at different topside pressure and rate contribute to the observed non-linear outcomes.

9.5.2 S6

Figure [36] shows the fracture area for fracture seeds 1 and 5 at initial injection temperatures of 8 and 90 °C. When the perforation pressure drop is neglected, the results show a more extensive total fracture area for colder initial injection temperatures. Results are unrelated to the actual operational conditions but confirm the findings in simulation scenario S5 and validate the effect viscosity has on perforation pressure drop and fracture propagation in a reservoir with pre-existing fractures, under the assumptions used in the simulations studies.

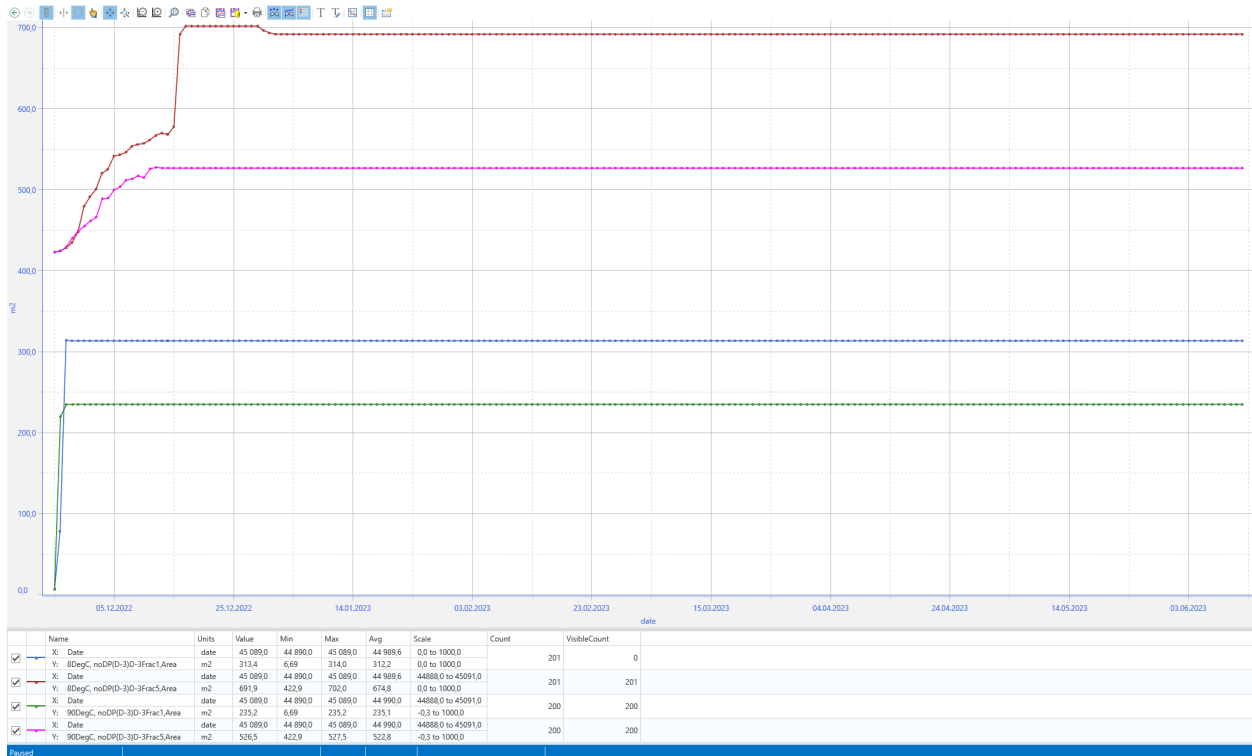


Figure 36: S6: Fracture area for initial injection temperature = 8 and 90 °C (fracture seed 1 and 5)

The damage permeability is one of the most significant uncertainties for estimating the perforation pressure drop. Quantifying the precise impact of perforation pressure drop on the propagation of pre-existing fractures is, therefore, challenging. The results from simulation scenario S5 and S6 do, however, indicate that if an intentional fracturing period is needed to increase the injectivity index in a reservoir with pre-existing fractures, a warmer injection temperature will give better fracture propagation and more extensive final fracture areas. If the decision is made to proceed with this procedure and pressurize the reservoir using seawater, produced water, or a combination of both, utilizing warmer produced water will result in a greater fracture area and higher final injectivity index. It may be worth noting that doing so will increase the risk of out-of-zone fracturing, followed by out-of-zone injection.

9.5.3 S7

Figure [37], shows the fracture area for fracture seed 1, at initial injection temperatures of 8, 48, and 90 °C. Fracture seed 1 is the only seed that experienced fracture initiation. The figure, therefore, shows the total fracture area for the different simulation runs. The results are similar to those achieved in S3, with colder injection temperature yielding a more extensive fracture area and warmer injection temperature yielding earlier fracture initiation.

Figure [38] shows the injectivity index for the initial injection temperature of 8, 48, and 90 °C. The results indicate a higher injectivity at the initial stage for warmer injection temperatures due to the injection temperature effect on water mobility. The opposite is observed for the simulation runs with initial temperatures of 8 and 90 °C after reducing the injection pressure. These observations align with the findings in S3. This is, however, not the case for the simulation run with an initial injection temperature of 48 °C, which is lower than that of the run with an initial temperature of 90 °C. The discrepancy arises from the limited propagation of the fracture area in the 48 °C run, which fails to surpass the influence of heightened water mobility observed in the 90 °C run.



Figure 37: S7: Fracture area for initial injection temperature = 8, 48 and 90 °C (fracture seed 1)



Figure 38: S7: Injectivity index for initial injection temperature = 8, 48 and 90 °C

The results show that a colder injection temperature will give a bigger total fracture area when there are no pre-existing fractures in the reservoir. This differs from the results achieved in S5, where a warmer injection temperature gives a more extensive total fracture area, when the reservoir has pre-existing fractures. As stated earlier, The effect of injection temperature on fracture initiation and propagation is case-dependent. A short period of seawater injection is favorable for fracture development and injectivity index for cases with no pre-existing fractures. The opposite is observed to be true for cases with pre-existing fractures. As pre-existing fractures are present in the D-3 well, the increase in injection water, as observed due to the increase in produced water, will be positive regarding fracture development and injectivity index.

However, it is important to note that these simulations do not account for the periodic shut-in periods in the historical schedule. During shut-in periods, fractures undergo closure, potentially affecting the extent of leak-off to the surrounding rock matrix upon resuming injection. The presence of shut-in periods may diminish the positive impact of warmer injection temperatures on fracture propagation and associated injectivity. Nevertheless, due to the relatively high injection pressure, fractures open rapidly, and the rate of leak-off returns to its pre-shut-in state swiftly. Therefore, overall, an increase in injection temperature is expected to yield more favorable results for this particular case compared to a colder injection temperature.

Parallels from the conclusions made in these simulation runs may be drawn to the other high-pressure injection wells at the Ivar Aasen field, as all inject into the same Skagerak 2 formation and have pre-existing fractures. A lower injection temperature would be ideal for potential future injection wells, starting off with no pre-existing fractures. However, the overall effect of a higher injection temperature will be positive for the total water injection at the field. If there comes a point in the future where there is necessary with

the installation of a heat ex-hanger to reduce the injection temperature, due to topside limitations. The recommendation based on the results achieved in this thesis, will be to keep the injection temperature as high as possible.

9.6 The effect of filter-cake build up on fracture development and injectivity

9.6.1 S8

Figure [39] shows the injectivity index for the simulation run with and without fracture calculation turned on, and the fracture area for fracture seed 4. Fracture seeds 1 and 5 did also propagate. Fracture seed 4 is shown as an illustration of how fracture development affects injectivity.

The results show that the simulation, run without any fracture development, quickly "dies" due to pore plugging, leading to a rapid decline in the injectivity index. The results also show that the run with fracture calculation turned on has a rapid increase in injectivity index followed by a steady decline. The rapid increase in injectivity is consistent with the rapid fracture propagation, caused by pore plugging. The decline in injectivity is counteracted by periods of fracture propagation due to pore plugging and subsequent increase in in-situ fracture pressure. This is consistent with the theory in chapter [5.3], which states that fractures increase the tolerance to poor water quality and associated filter-cake build up.

Figure [40] displays the water injected [Sm³/day] for the simulation runs with an injection temperature increase of 2.5 °C per 0.5 years and 5 °C per 0.5 years, along with the run using a constant injection temperature of 48 °C. The results show that an increase in injection temperature over time is positive for the development of the injected water rate. With the filter-cake model turned on, the degree of leak-off into the nearby rock matrix depends more on the filter-cake thickness. As stated in chapter [6.7], the filter-cake becomes the primary factor regulating the fluid leak-off, a critical aspect of fracture propagation. When the filter-cake thickness builds up to a point, the reduced leak-off and the subsequent increase in in-situ fracture pressure lead to fracture propagation, which exposes "new" rock formation. At this point, after every rapid fracture propagation, a higher injection temperature, due to a higher viscosity and water mobility, will give a temporary increase in injection rate. The filter-cake build-up mechanism, followed by pressure build-up and fracture propagation, continues in a cyclic matter, as seen in the figure.

The results show that a steady increase in injection temperature is positive regarding the water injected and injectivity of the well, as it counteracts the negative effect of filter-cake build up. As the real-life rate of filter-cake build up for the D-3 injection well is unknown, it is essential to mention that the achieved results do not accurately represent the actual conditions in the reservoir. This means that the degree of increase in water injected, as the temperature increases, will not necessarily happen at the same rate as seen in figure [40]. In addition to this, the reservoir pressure and temperature be influenced by shut-in periods and operational conditions that are not simulated in this scenario.



Figure 39: S8: Injectivity index for simulation run with filter-cake model - with/without fracture calculation, and fracture area (fracture seed 4)



Figure 40: S8: Water injected [Sm³/day] for injection temperature of 48 °C, 48 + 2.5°C/0.5year, and 48 + 5 °C/0.5 year

The increase in injection temperature is positive for the injectivity index when a filter-cake model is present in the simulation. Moreover, a higher injection temperature proves beneficial for fracture propagation and the resulting injectivity index in the Skagerak 2 formation with pre-existing fractures. If a heat exchanger is installed due to topside temperature limitations, the recommendation of keeping the injection water as warm as possible remains the same. Additionally, efforts should be made to minimize filter-cake formation by incorporating seawater into the injected water and reducing the suspended solids concentration in the injection fluid.

It is essential to highlight that none of the conducted simulations (S1, S3-S8) exhibit indications of fracturing upward through the cap-rock or out-of-zone injection from the Skagerak 2 formation. These simulations were performed under various operational conditions, including extreme scenarios, confirming the well's integrity and the safety of injection practices concerning the cap-rock. Furthermore, there is no evidence of fracturing downward through the Weathering profile, indicating the continued safety of injection operations. Nevertheless, it is crucial to acknowledge that ensuring 100 % guarantee of safe injection, free from fracturing and out-of-zone migration in the downward direction, is subject to uncertainties regarding the properties and integrity of the fractured Caliche within the Weathering profile. Operators must undertake a risk analysis to address this potential risk. The sector models developed in this thesis, insights into fracture initiation and propagation and knowledge gained from REVEAL, can aid operators in making informed decisions regarding specific issues that may arise and assist decisions for present and future injection strategies.

It is important to acknowledge that certain parameters were not considered in this thesis, which could potentially impact the results obtained. Two significant parameters include the presence of oil in the injected water and the temperature effect on wettability. These factors influence the interaction between the fluid and rock, and further investigation is recommended to model these parameters in REVEAL. This would contribute to the ongoing efforts to ensure the safety of injection operations at the Ivar Aasen field.

10 Conclusion

The aim of the study is to assess the influence of varying injection temperatures and filter-cake accumulation on high-pressure water injectors at the Ivar Aasen field, with a specific emphasis on fracture initiation and propagation and the subsequent effect on injectivity. The simulation studies have indicated the following:

- The initial temperature sensitivity study using a historical schedule showed a non-linear relationship between the injection temperature and developed fracture size. Performing sensitivity analysis with a wide range of input parameters may therefore, not result in linear output responses, especially considering the non-linear nature of fracture calculations, particularly in highly heterogeneous reservoirs
- The simple thermal fracture model demonstrated a linear relationship between fracture area, leak-off coefficient, and maximum center width at different bottomhole temperatures. Lower temperatures increased viscosity, reducing leak-off and larger in-situ fracture pressures. This, in turn, contributed to more significant fracture propagation and earlier fracture initiation, which resulted in bigger final fracture sizes. The simulation showed that reducing the number of input data and reservoir complexity made the relationship between temperature and fracture size more linear.
- Colder injection temperatures resulted in larger fracture areas for scenarios with no pre-existing fractures. Warmer injection temperatures, on the other hand, led to higher cumulative water injection and lower final injectivity index. The injectivity trends showed that higher injection temperatures initially yielded a higher injectivity index due to higher water mobility. However, colder temperatures resulted in a higher final injectivity index after reducing the injection pressure. The results emphasized that the relationship between fracturing and injectivity at different injection temperatures is case-dependent and influenced by injection pressure and temperature control.
- The impact of thermo-elastic stress reduction on fracture initiation depends on the degree of cooling and the specific operational conditions. When the water injection is conducted within a relatively short timeframe at a pore-pressure that exceeds the minimum in-situ stress, water mobility becomes the dominant factor influencing fracture initiation resulting in earlier fracture initiation for warmer injection temperatures.
- A short period of seawater injection is favorable for fracture development and injectivity index for cases with no pre-existing fractures when injecting at a pore-pressure above and below the minimum in-situ stress. The opposite is observed to be true for cases with pre-existing fractures, when perforation pressure drop is assumed to be dominated by linear Darcy-flow. As pre-existing fractures are present in the D-3 well, the increase in injection temperature, as observed due to the increase in produced water, will be positive regarding injectivity, and degree of fracture propagation at high pressure periods. If a period of high pressure injection and intentional fracturing is needed for the D-3 well, utilizing "warm" produced water for pressurization will result in a more extensive fracture propagation and a higher final injectivity index.
- Estimating the perforation pressure drop, under the assumptions made in the study, is difficult due to the uncertain nature of the damage permeability parameter. Con-

sequently, accurately quantifying the specific impact of perforation pressure drop on the propagation of pre-existing fractures presents a significant challenge.

- The simulation results using a filter-cake model demonstrated the importance of fracture development in maintaining injectivity in the Skagerak 2 formation. Without fracture development, the injectivity quickly declined due to pore plugging, while the presence of fractures allowed for periodic fracture propagation and temporary increases in injectivity. The filter-cake build up mechanism, accompanied by pressure build up and fracture propagation, occurred cyclically. Increasing injection temperature over time positively affects the injectivity index by counteracting the negative impact of filter-cake build up.
- If the installation of a heat exchanger is needed due to topside temperature limitations, the injection temperature should be kept as high as possible while minimizing filter-cake formation by incorporating seawater to reduce the concentration of suspended solids and associated filter-cake build up.
- There were no simulations with indication of fracturing through the cap-rock and the Weathering profile, followed by out-of-zone injection from the Skagerak 2 formation.

11 Further work

- The presence of oil in the injected water and the injection temperature effect on wettability may influence the fluid/rock interaction, thereby affecting the achieved results in this thesis. It is therefore a recommendation to model these parameters in REVEAL, for further investigation. The developed sector models as a part of the thesis work may be used to achieved this.
- A study into the integrity of the Weathering Profile in the near-wellbore area of injection well D-3 should be conducted to ensure safe injection with regards to out-of-zone fracturing and injection in the downwards direction from the Skagerak 2 formation.
- To validate the influence of water viscosity on perforation pressure drop and fracture propagation, a study examining the pressure drop across the completion perforations of injection well D-3 is recommended.

Bibliography

- [1] Martin Birkelund Pedersen. ‘Investigating Out-of-Zone Injection and Hydraulic Fracturing in Overburden Shale Formation: A Revealing Study.’ In: *NTNU, Department of Geoscience and Petroleum TPG4560 - Specialization report* (2022), p. 2.
- [2] Ivar Aasen. URL: <https://akerbp.com/en/asset/ivar-aasen-3/> (visited on 09/05/2023).
- [3] Ivar Aasen. URL: <https://www.norskpetroleum.no/fakta/felt/ivar-aasen/> (visited on 09/05/2023).
- [4] Aker BP. ‘Ivar Aasen Reservoir Characterization Report 2020’. In: *Aker BP’s internal documents* (2020).
- [5] Aker BP. ‘Internal’. In: (2023).
- [6] A Dandekar. *Petroleum Reservoir Rock and Fluid Properties. 2nd.* CRC Press, 2013, p. 489.
- [7] Tarek Ahmed. *Reservoir Engineering Handbook.* Elsevier Science, 2019. Chap. 14.
- [8] Mohamed Mahmoud Ibnelwaleed A. Hussein. *Fluid-Solid Interactions In Upstream Oil And Gas Applications: Volume 78 (Developments in Petroleum Science).* Elsevier Science, 2023, pp. 181–246.
- [9] J. Fanchi. *Integrated Reservoir Asset Management.* Elsevier Science, 2010. Chap. 10.7.1.
- [10] Omid Karoussi Aly A. Hamouda. ‘Effect of Temperature, Wettability and Relative Permeability on Oil Recovery from Oil-wet Chalk’. In: *Department of Petroleum Engineering, University of Stavanger, 4036 Stavanger, Norway* (2008).
- [11] Tayfun Babadagli. ‘Temperature effect on heavy-oil recovery by imbibition in fractured reservoirs’. In: *Journal of Petroleum Science and Engineering 14 (1996) 197-208* ().
- [12] Hawkins MF Craft BC. *Applied petroleum reservoir engineering.* Englewood Cliffs, NJ: Prentice-Hall Inc., 1959.
- [13] Pavel G. Bedrikovetsky et al. *Taking advantage of injectivity decline for improved recovery during waterflood with horizontal wells. Volume 78, Issue 2.* Elsevier Science, 2011. Chap. 2.
- [14] Jongsoo Hwang and Mukul Sharma. ‘Simulation of Injectivity and Fracture Containment: Water Injection in a Turbidite Reservoir, Offshore Ghana’. In: *SPE-195567-MS* (2019).
- [15] M.S.H. Bader. ‘Seawater versus produced water in oil-fields water injection operations’. In: *Elsevier Science* (2006), p. 166.
- [16] A. Shojaei and Shao. *Porous Rock Fracture Mechanics.* Elsevier Science, 2017. Chap. 6.2.
- [17] Jinjie Wang et. al. Long Yu. ‘Enhanced Tight Oil Recovery by Volume Fracturing in Chang 7 Reservoir: Experimental Study and Field Practice.’ In: *Energies* 12 (2019).
- [18] E. et.al. Donaldson. *Hydraulic Fracturing Explained.* Elsevier Science, 2014. Chap. 3.6.
- [19] *Rock mechanical properties.* URL: https://petrowiki.spe.org/Rock_mechanical_properties (visited on 15/05/2023).
- [20] C.W. Hopkins. ‘The importance of in-situ stress profiles in hydraulic fracturing applications’. In: *Society of Petroleum Engineers - 38458* (1997).
- [21] H. et.al Belyadi. *Hydraulic Fracturing in Unconventional Reservoirs.* Elsevier Science, 2019. Chap. 13.

- [22] Nick Bahrami, David Pena and Ian Lusted. ‘Well test, rate transient analysis and reservoir simulation for characterizing multi-fractured unconventional oil and gas reservoirs’. In: *Journal of Petroleum Exploration and Production Technology* 6 (Dec. 2015). DOI: 10.1007/s13202-015-0219-1.
- [23] Bezalel Haimson; Charles Fairhurst. *Initiation and Extension of Hydraulic Fractures in Rocks - SPE-1710-PA*. URL: <https://onepetro.org/spejournal/article/7/03/310/163176/Initiation-and-Extension-of-Hydraulic-Fractures-in> (visited on 16/05/2023).
- [24] *User Manual, IPM - Reveal Version 10*. Petroleum Experts Limited, 2023.
- [25] Emmanuel Detournay. ‘Propagation Regimes of Fluid-Driven Fractures in Impermeable Rocks’. In: *International Journal of Geomechanics* 4 (Mar. 2004). DOI: 10.1061/(ASCE)1532-3641(2004)4:1(35).
- [26] Saeed Salimzadeh, Adriana Paluszny and Robert W. Zimmerman. ‘Three-dimensional poroelastic effects during hydraulic fracturing in permeable rocks’. In: *International Journal of Solids and Structures* 108 (2017), pp. 153–163. ISSN: 0020-7683. DOI: <https://doi.org/10.1016/j.ijsolstr.2016.12.008>. URL: <https://www.sciencedirect.com/science/article/pii/S0020768316303754>.
- [27] Kwanghee Chun. ‘Fracture Propagation Under Poro-Thermally Induced Stress Using the Displacement Discontinuity Method’. In: *Thirty-Eighth Workshop on Geothermal Reservoir Engineering Stanford University, Stanford, California, February 11-13, 2013* 108 (2013), pp. 153–163. URL: <https://pangea.stanford.edu/ERE/pdf/IGAstandard/SGW/2013/Chun.pdf>.
- [28] Anna Sygala, Mirosława Bukowska and Tomasz Janoszek. ‘High Temperature Versus Geomechanical Parameters of Selected Rocks – The Present State of Research’. In: *Journal of Sustainable Mining* 12.4 (2013), pp. 45–51. URL: <https://www.sciencedirect.com/science/article/pii/S2300396015300689>.
- [29] Erling Fjær et al. ‘Chapter 11 - Mechanics of hydraulic fracturing’. In: *Petroleum Related Rock Mechanics*. Vol. 72. Developments in Petroleum Science. Elsevier, 2021, pp. 555–600. URL: <https://www.sciencedirect.com/science/article/pii/B9780128221952000206>.
- [30] Misfer J. Almarri et al. ‘Enhancing the Fracture Growth Uniformity of Perforation Clusters by Pre-injection of Cold Water’. In: *ACS Omega* 8.1 (2023), pp. 289–296. DOI: 10.1021/acsomega.2c04324. URL: <https://doi.org/10.1021/acsomega.2c04324>.
- [31] Eliahu Rosenthal et al. ‘Transient Temperature Impact on Deep Reservoir Fracturing’. In: *Geofluids* (2021), p. 6653442. URL: <https://doi.org/10.1155/2021/6653442>.
- [32] Kunhwi Kim et.al. ‘OUGH–RBSN simulator for hydraulic fracture propagation within fractured media: Model validations against laboratory experiments’. In: (). URL: <https://pangea.stanford.edu/ERE/pdf/IGAstandard/SGW/2013/Chun.pdf>.
- [33] K. Prasad Saripalli; Steven L. Bryant; Mukul M. Sharma. ‘Role of Fracture Face and Formation Plugging in Injection Well Fracturing and Injectivity Decline’. In: *SPE-52731-MS* (1999). DOI: <https://doi.org/10.2118/52731-MS>. URL: <https://onepetro.org/SPEHSSE/proceedings/99EPEC/All-99EPEC/SPE-52731-MS/60892>.
- [34] Ching Yew. *Mechanics of Hydraulic Fracturing*. Elsevier Science, 1997.
- [35] *An Experimental and Fundamental Interpretation of Fracturing Filter-Cake Fluid Loss*. Vol. All Days. SPE Annual Technical Conference and Exhibition. SPE-22873-MS. 1991. DOI: 10.2118/22873-MS. eprint: <https://onepetro.org/SPEATCE/proceedings-pdf/91SPE/All-91SPE/SPE-22873-MS/2002002/spe-22873-ms.pdf>. URL: <https://doi.org/10.2118/22873-MS>.




- [36] *Simulator for Specialised Reservoir Studies*. URL: <https://www.petex.com/products/ipm-suite/reveal/>.
- [37] *Internal Aker BP documents supplied by Petroleum Experts Ltd.*
- [38] Øystein Pettersen. *Basics of Reservoir Simulation With the Eclipse Reservoir Simulator - Dept. of Mathematics, Univ. of Bergen, 2006*. URL: https://portal.tpu.ru/SHARED/n/NAV281087/eng/academics/Tab/Eclipse_0.pdf (visited on 24/05/2023).
- [39] Jon Morten Ferkingstad. 'Numerical Simulation of Productivity Effects by Hydraulic Fracturing in a Low permeability Fluvial Reservoir in the North sea'. In: *UiS, Master thesis presented* (2011).
- [40] Steve Todman. 'Principle developer for REVEAL - Petroleum Experts Ltd.' In: (2023).

B Sector model - Guide

Guide to creating a Sector model in Reveal

There are two ways of creating a sector model in Reveal. The first method is a simple “manual” way of creating a block sector model, as described in this Guide. The second method uses drainage regions created by Reveal and can be performed by following instructions as given in the Reveal User-Guide (Page 433).

Step 1:

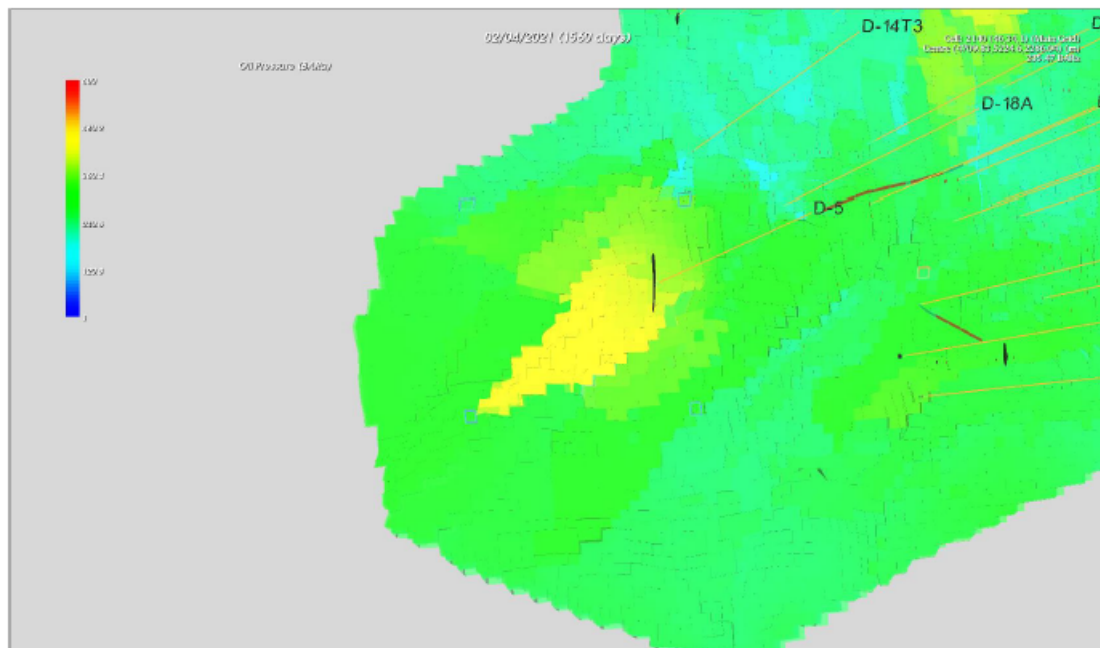
- Open the full field Reveal model, and press  to open the 3D visualisation of the saved simulation of the field. (This may take some time, and the graphics may be slow to navigate).
- Navigate the 3D model so that you are located above, looking down on your specific well as seen in the illustrative picture below (Tips for 3D navigation is given in the User-Guide, page 497).
- Select oil pressure, located on the left-hand side, as your parameter. Run the simulation using these buttons . This will allow you to observe the pressure development around your well. This will give an indication of how the sector model should look like in terms of size when considering pressure development around your well, and communication with nearby wells.
- Press  and select the corner cells you want for your sector model. Hovering over the cells will provide the X,Y,Z coordinates in the upper right hand side of the screen. Take a note of these coordinates. When selecting these, make sure that the sides of your sector model is straight. As an example, the coordinates of the selected blocks around D5, are shown in the picture below:

Upper left side: (87,41,1)

Upper right side: (69,41,1)

Lower left side: (87,23,1)

Lower right side: (69,23,1)



Step 2:

- When the coordinates from Step 1 have been noted, go to the Reservoir section of the script. (Press Navigator on the left-hand side to see the different sections of the script)

By modifying the existing porosity range, the sector model can be isolated from the rest of the field model. The porosity data for the different layers are stored as arrays within the input wizard (Interface of the script). The added overburden formations and the porosity range is written directly into the script and can be seen in the 9th line under “Section Reservoir”, as shown below in point 1) and 2). Point 3) to 6) shows the areas around the sector model that need to be “deleted”, by giving it a porosity of 0.


- Put in the coordinates for your sector model and follow the pattern between the X, Y coordinates as given in Step 1, and the porosity range 3) to 6), as shown below.

For a X-coordinate range of 87-69, you want to zero out the surrounding blocks in the X-direction 88-97 and 1-68. The same is performed for the blocks in the Y-direction.

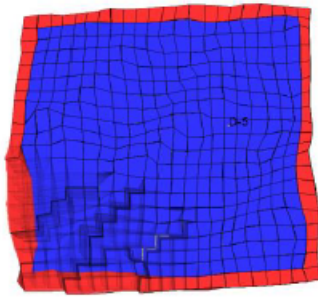
- 1) porosity range x 1 97 y 1 92 z 1 12 0.01 !fraction (*Pre-existing input)
- 2) porosity range x 1 97 y 1 92 z 5 6 0.2 !fraction (*Pre-existing input)
- 3) porosity range x 1 68 y 1 92 z 1 167 0 !fraction (*Add to script)
- 4) porosity range x 88 97 y 1 92 z 1 167 0 !fraction (*Add to script)
- 5) porosity range x 1 97 y 1 22 z 1 167 0 !fraction (*Add to script)
- 6) porosity range x 1 97 y 42 92 z 1 167 0 !fraction (*Add to script)

- Save the file before verifying the shape of your sector model by opening the initial 3D visualisation of the sector model by pressing **t=0** .

Step 3:



- Access the input Wizard by pressing  and go to Well section by pressing Well → Position on the right-hand side. Delete the wells that are not of interest, located in the well list on the left-hand side.
- Go to Control → Options and put YES for an Analytical Aquifer Model.
- Go to Aquifer → Boundary. Add a new boundary under Region list, and make it a Constant pressure boundary, in Properties.
- Using the coordinates noted in Step 1, put in the Boundary and Connection area. Example of how this should look, given the previous mentioned example, is given below:

Dir	Range
X-	(69,1,1) - (69,92,167)
X+	(87,1,1) - (87,92,167)
Y-	(1,23,1) - (97,23,167)
Y+	(1,41,1) - (97,41,167)



- Pressing the plot button allows you to verify the boundary blocks.
- Exit the Wizard by pressing Finish and save your file.

Step 3:

- Run a simulation of your sector model by pressing .
- Press  to open results from your current simulation.
- Compare the BHP of the current run with the BHP achieved in the full field model, which the sector model is based on. The goal is for these to be as similar as possible. If this is the case, congratulations! If, however, a significant difference in BHP is observed, a matching process can be performed by adding a Boundary PI.
- Stop the simulation and go to the Wizard → Aquifer → Boundary. A high PI value will be equal to constant pressure boundary. A low PI value will give the boundary a leaky pressure behavior. Changing this value and run simulations until a satisfactory match is achieved. A potential range of PI values that can be used are from 100 to 10 000.

This will be a trial-and-error process, which may take some time. There is no reason to wait until the entire simulation is finished. If a match is achieved or not will be easy to observe quite early in the simulation.

*Tips for creating a sector model, and when using Reveal in general, is to perform simulation runs for every significant modification that are being made. This makes the process of identifying potential reasons for deviation in the BHP matching process much easier.

Made by Martin Birkelund Pedersen

C 3D visualisation of sector models

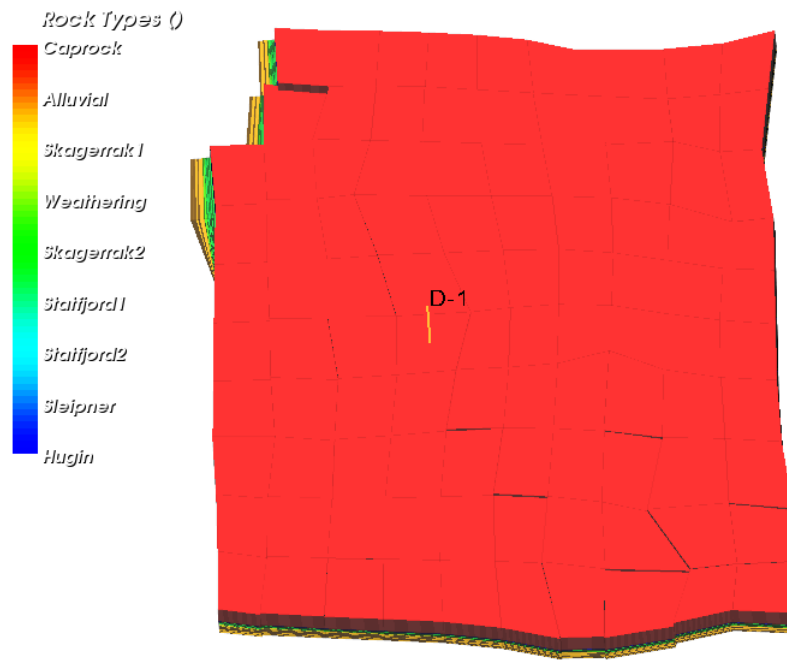


Figure 41: Sector model for injection well D-1, constant pressure BC.

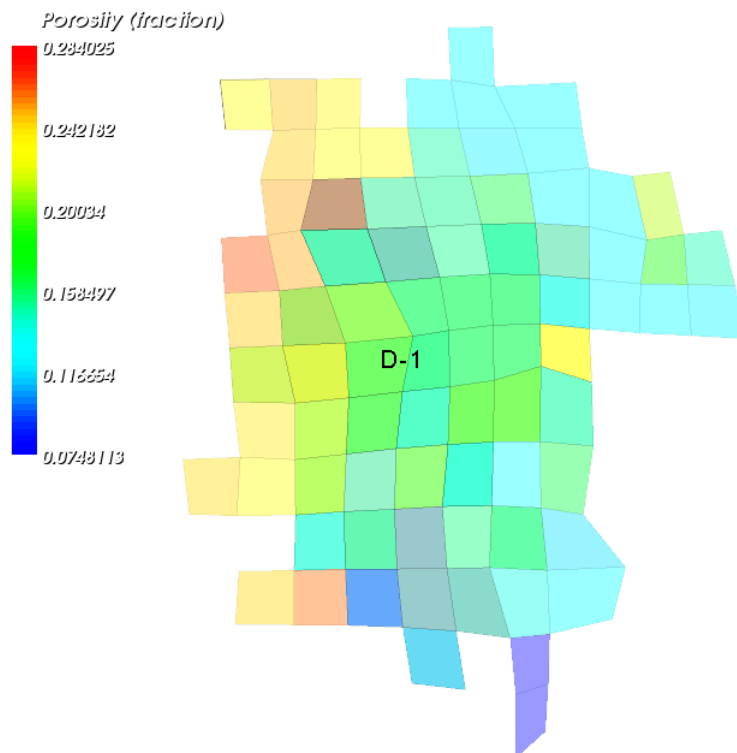


Figure 42: Sector model for injection well D-1, time-varying BC.

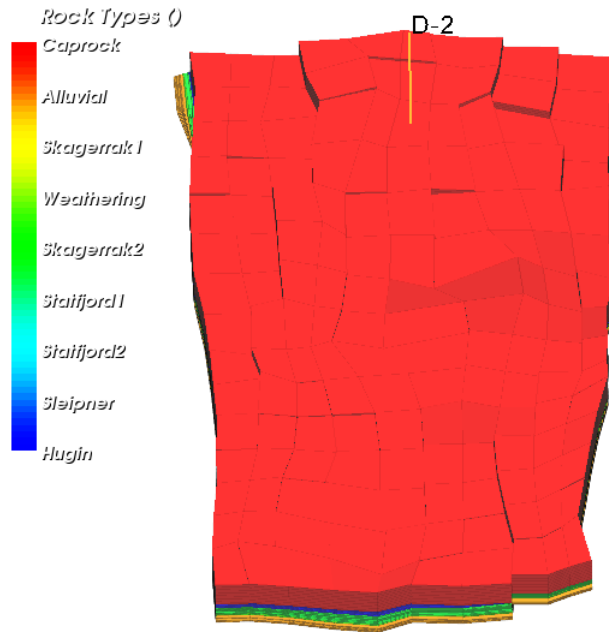


Figure 43: Sector model for injection well D-2, constant pressure BC.

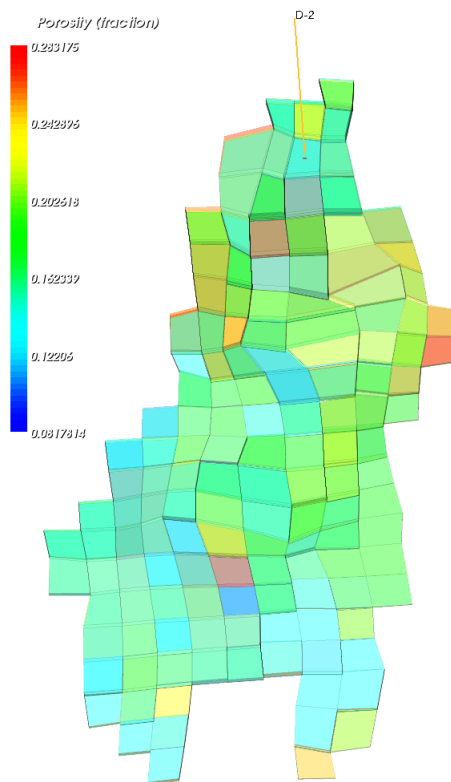


Figure 44: Sector model for injection well D-2, time-varying BC.

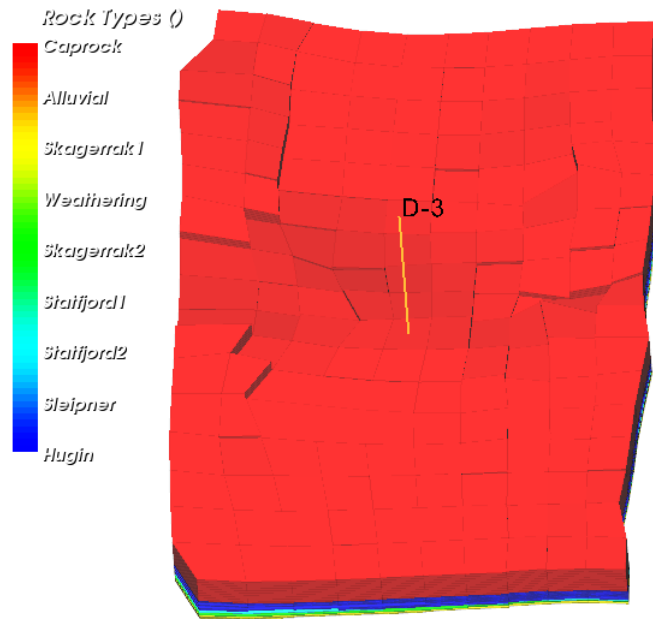


Figure 45: Sector model for injection well D-3, constant pressure BC.

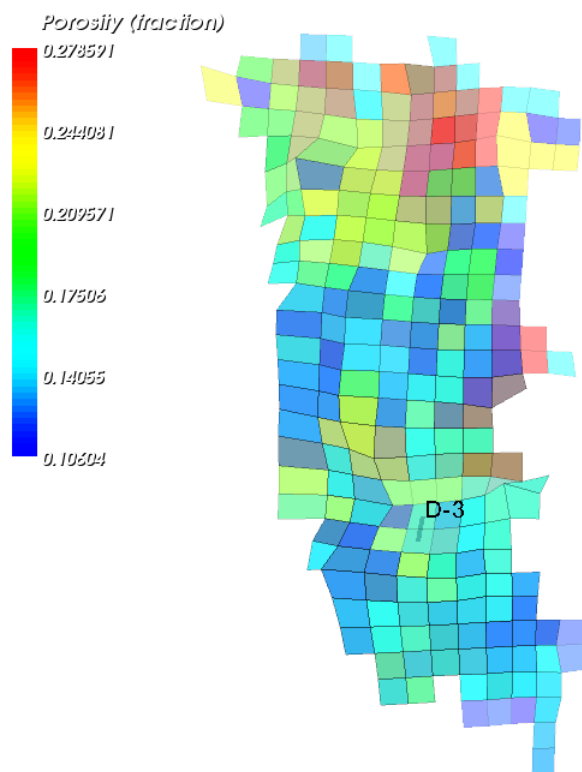


Figure 46: Sector model for injection well D-3, time-varying BC.

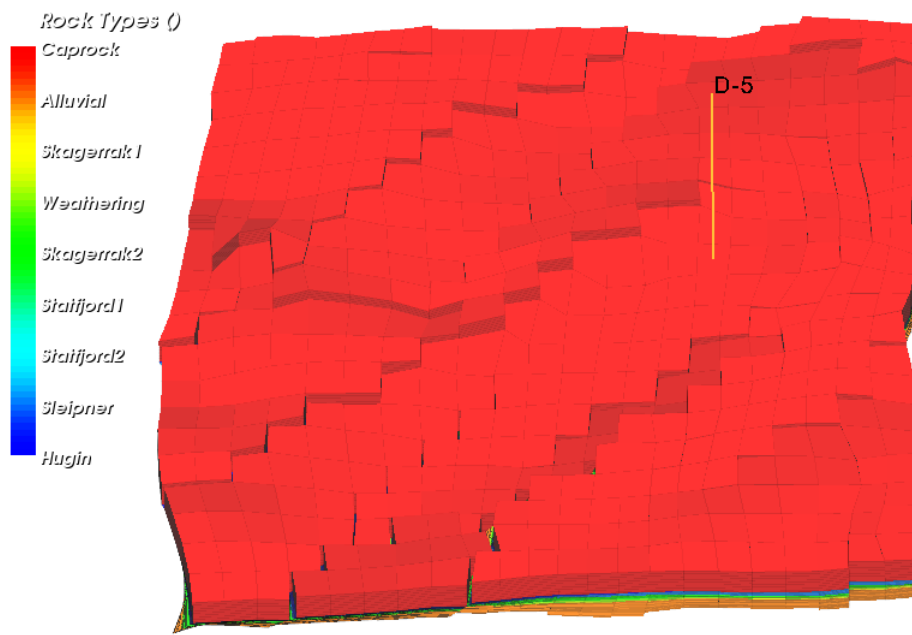


Figure 47: Sector model for injection well D-5, constant pressure BC.

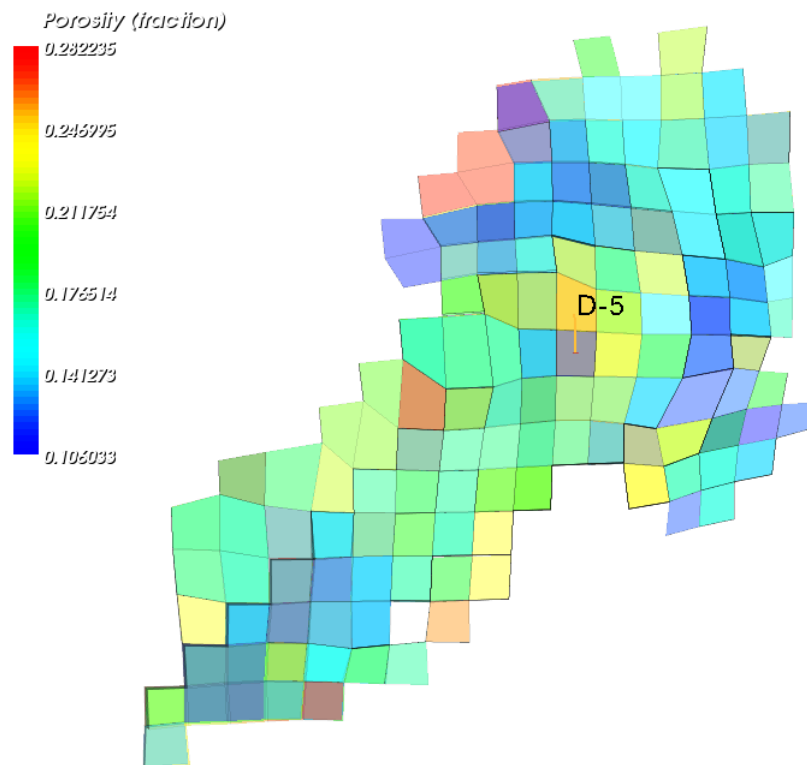


Figure 48: Sector model for injection well D-5, time-varying BC.

D Water viscosity

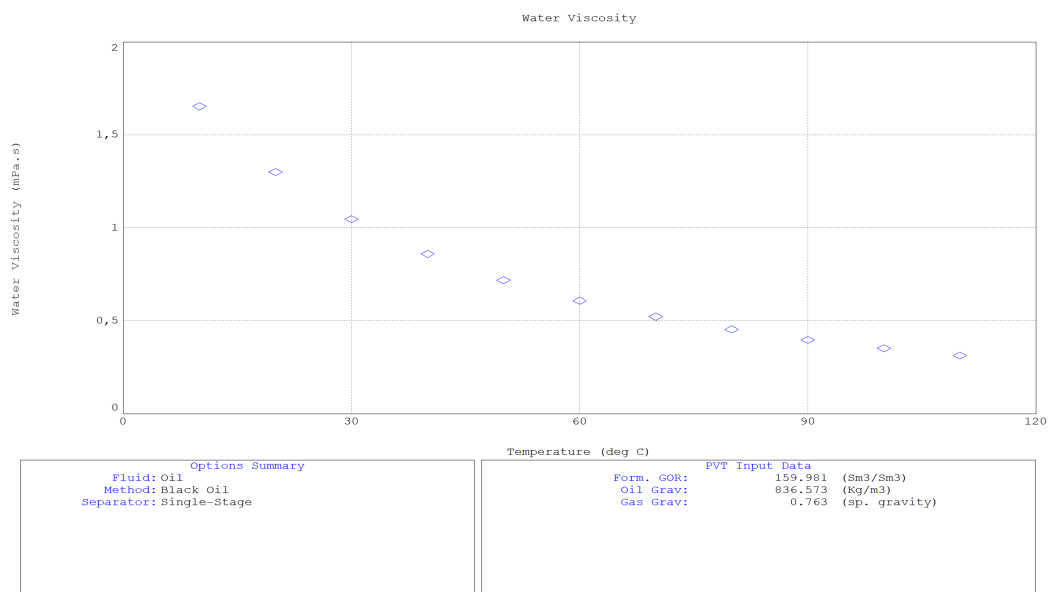


Figure 49: Water viscosity as a function of temperature, from thermal PVT table.

E Simple thermal fracture model

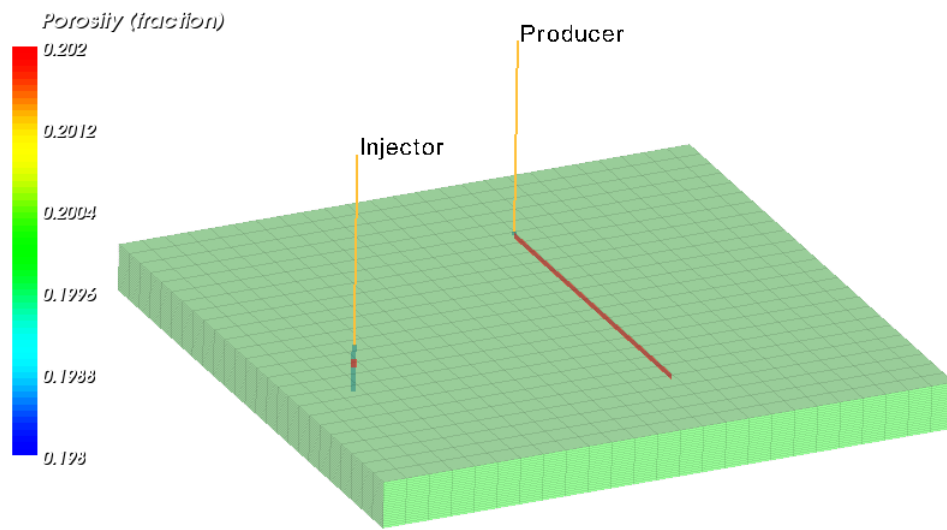


Figure 50: Simple thermal fracture model.

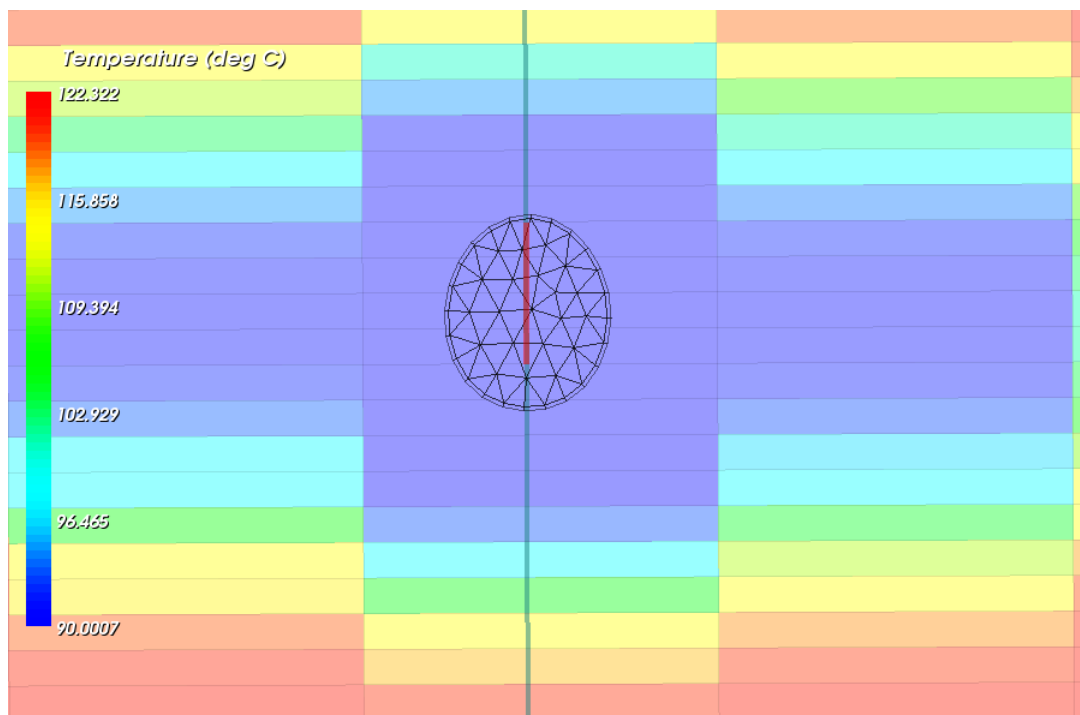


Figure 51: Cross-section simple thermal fracture model.

F Formulas/input data for thermo-elastic stress reduction calculation

	A	B	C
1	BHT	8	°C
2	Tres	98	°C
3	at	=0.00001	1/°C
4	v	0.3	-
5	E	1160301.95	psi
6	dT	=B2-B1	°C
7	At	=B3*(B5/(1-B4))	psi/°C
8	Δ Stress	=B7*B6	psi
9	Δ Stress reduction	=B8/14.2	Bar
10	Shmin	=(2505+68.3)*0.159	Barg
11	New Shmin	=B10-B9	Barg



 **NTNU**

Norwegian University of
Science and Technology